Investigation of an atypical protoporphyric family in South Africa

CE Haumann

Abstract

Affected members of the family investigated in this dissertation presented with photosensitivity and raised red cell protoporphyrin concentrations, indicative of protoporphyria. Further examination of this family revealed features that were atypical of erythropoietic protoporphyria. These included a highly penetrant disease, disease severity as expressed by more prevalent hepatic complications, a preponderance of protoporphyrin in its zinc chelated form, a therapeutic response to iron supplementation, and an absence of mutations in the *ferrochelatase* gene or haplotype markers associated with erythropoietic protoporphyria. We have reviewed clinical data from this family, established a ferrochelatase enzyme assay in our laboratory, and shown normal ferrochelatase enzyme activity in affected subjects. This is consistent with the atypical features observed, and suggested the presence of a disease locus distinct from *ferrochelatase*. Whilst this study was in progress, a collaborative effort between colleagues in Wales and France, and our laboratory, led to the discovery of mutations in exon 11 of the X chromosome erythroid specific *5-aminolevulinate synthase 2* gene as being disease-causing in our family (c.1706-1709 delAGTG) and other families abroad. A resultant gain of *5*-aminolevulinate synthase 2 function leads to increased flux of the haem biosynthetic pathway and culminates in this form of protoporphyria. In this work we performed direct sequencing of *5-aminolevulinate synthase 2* exon 11 as a means of mutational analysis. These data, in conjunction with knowledge of the X-linked inheritance pattern, have allowed us to offer appropriate genetic counselling and prediction of genetic risk to family members. Furthermore, as there was reason to justify iron supplementation as a partial treatment strategy, we present data showing red cell protoporphyrin fluctuations and ultimate reduction during intravenous iron supplementation of 1 family member. Results suggest that iron supplementation is a promising and rational treatment strategy in this particular form of porphyria.

Investigation of an atypical protoporphyric family in South Africa

by

Student: Carel Eduard Haumann

Student number: HMNCAR001

SUBMITTED TO THE UNIVERSITY OF CAPE TOWN

In partial fulfilment of the requirements for the degree

MMed in Clinical Pathology

Faculty of Health Sciences

UNIVERSITY OF CAPE TOWN

Date of submission: **August 2010**

Supervisor: **Prof PN Meissner, Division of Medical Biochemistry, UCT**

Co-Supervisors: **Prof TS Pillay, Division of Chemical Pathology, UCT**

Dr AV Corrigall, Department of Medicine, UCT

Dr PA Berman, Division of Chemical Pathology, UCT

DECLARATION

I, Carel Eduard Haumann, hereby declare that the work on which this dissertation is based is my original work (except where acknowledgements indicate otherwise) and that neither the whole work nor any part of it has been, is being, or is to be submitted for another degree in this or any other university.

I empower the university to reproduce for the purpose of research either the whole or any portion of the contents in any manner whatsoever.

Signature: ……

Date: ……9 August 2010……

Acknowledgements

This dissertation is dedicated to family EPP8. Thank you for your patience and encouragement.

I thank my supervisor Prof PN Meissner for initiating this project, for superb direction and leadership along every step of the way, for a particularly appropriate sense of humour, and for the intellectual and physical infrastructure created over decades which has made this work possible.

I have been privileged to have 3 co-supervisors who have contributed enormously to this dissertation and to the events leading up to its initiation.

I have enjoyed the unwavering support of Prof TS Pillay. From my very first days in the Division of Chemical Pathology, when I could barely hold a pipette, you built my confidence systematically. Thank you for the academic thoughts you have shared with me, for helping me overcome every obstacle which presented itself, and for nurturing me.

Dr Anne Corrigall has become a very special friend and mentor. To work in such close proximity to, and under the guidance of someone of your calibre and experience, has been very precious. You have been completely selfless in your investment in me. I will carry the excitement we have shared in gaining new and uncharted territory with me. Thank you, for so very much….

Dr Peter Berman was the first to instil a sense of interest in porphyria in me, when I was in MBChB third year in 1997. Your ability to bring life and comprehension to devastatingly complex ideas is legendary. Many of your valuable ideas have found their way into this dissertation. Thank you for encouraging me, for finding my thoughts when they seemed to be slipping into an abyss, and for being a constant source of logical reasoning. The amplified effect of your teaching at the University of Cape Town is comparable to that of a PCR reaction.

I gratefully acknowledge the help and support of the following colleagues:

- The characterisation of EPP in South Africa by Ms Michelle Parker laid the foundation which this project could be built upon.
- Dr Mark Sonderup has been responsible for the care and management of patient EPP8.2 and other members of family EPP8. Thank for contextualising this project clinically, for allowing me to present data generated during the treatment of patient EPP8.2 and for reviewing clinical data presented in this dissertation.
- Dr Fierdoz Omar and Dr David Haarburger provided exceptionally valuable assistance, superb ideas and sustained encouragement. You have nourished me with your brilliance. To work with colleagues like you, is a rare privilege.
- Dr Craig Corcoran – thank you for being prepared to help me with the FECH mRNA RT PCR quantification.
- Ms Ingrid Baumgarten provided me with patient and expert tuition in the techniques of cell culture and performed the vast majority of the culture work.
- Mr Brandon Davidson performed all red cell porphyrin quantifications presented in this dissertation.
- Ms Mags Paul performed all the DNA extractions used in this dissertation.
- Dr Margie Shuttleworth focussed my attention on the morphological appearance of iron stores in the bone marrow, kindled my growing excitement about the wonders of iron metabolism, and reviewed the bone marrow of subject EPP8.2 with me.
- Ms Amina Adams and Ms Maggie Steenkamp provided a clean environment conducive to work in the Lennox Eales Porphyria Laboratory.
- Prof P Jacobs allowed me to view and photograph the bone marrow biopsy of subject EPP8.2.
- Ms Colleen Jackson assisted in the preparation of bone marrow biopsy specimens.
- Ms Glynnis Schutte helped obtain photographs of fluorocytes.

- Associate Prof H Wainwright and Dr Hue-Tsi Wu provided me with and interpreted images of liver histology from patient EPP8.2.
- Prof S Benningfield reviewed CT scan and TIPSS radiology from patient EPP8.2 with me.
- Dr Heleen Vreede helped in the management and administration of funding for this project.
- Dr Judy King played a major role in developing my academic thinking and writing abilities. She proof read this dissertation.

I am very grateful to have been able to use the infrastructure, equipment and reagents of the University of Cape Town/Medical Research Council Liver Centre and the Lennox Eales Porphyria Laboratories.

I thank the National Health Laborotary Service Research Trust for financial assistance.

My parents, Tielman and Ester Haumann, were the first to show me the joy, the beauty and the power of the unique human ability to ask “why?”

Marise, my sister, provided me with the computer and technical assistance used in the writing of this dissertation.

Sume en Cara ons het hierdie tesis beplan, gedoen en geskryf in ons leeukuil-dae. Julle is die ware skrywers van hierdie tesis.

You held my hand so tightly through all these years. Your presence and Your power is overwhelming.

Table of Contents

CHAPTER FOUR: Ferrochelatase enzyme assay

CHAPTER FIVE: ALAS2 and X-linked dominant protoporphyria

CHAPTER SIX: Iron treatment in XLDPP

CHAPTER SEVEN: Further discussion and recommendations based on all available data

CHAPTER EIGHT: Future studies, summary and final remarks

List of Figures

List of Tables

List of Abbreviations

A	adenine
ABC7	adenosine triphosphate binding cassette 7 transporter protein
Abs	absorbance

ALA	5-aminolevulinic acid
ALAS	5-aminolevulinate synthase protein
ALAS	5-aminolevulinate synthase gene
ALAS2	5-aminolevulinate synthase isoform 2 protein
ALAS2	5-aminolevulinate synthase isoform 2 gene
ASAT	X-linked sideroblastic anaemia and ataxia
bp	base pair(s)
C	cytosine
c	centi
c.	coding sequence
°C	degrees Celsius
CD	cluster of differentiation
cm	centimetre
conc	concentration
CPG	coproporphyrinogen
CT	computed tomography
C-terminus	carboxy-terminus
del	deletion
dl	decilitre
DMSO	dimethyl sulfoxide
DMT1	divalent metal transporter 1
DNA	deoxyribonucleic acid
dNTP	deoxyribonucleic acid triphosphate
EBVTL	Epstein Barr virus transformed lymphoblast(s)
EC	Enzyme Commission number
EDTA	ethylenediaminetetraacetic acid

EKLF	erythroid Kruppel-like factor
EPP	erythropoietic protoporphyria
FECH	ferrochelatase enzyme
FECH	ferrochelatase gene
FLVCR	feline leukaemia virus subgroup C receptor
Fe-S	iron-sulphur
fl	femtolitre
G	guanine
g	gram
xg	relative centrifugal force
GABA	γ-aminobutyric acid
G6PD	glucose 6 phosphate dehydrogenase
GSH	Groote Schuur Hospital
h	hour(s)
IMD	inherited metabolic disease
INH	isoniazid
INR	international normalised ratio
IRE	iron response element(s)
IRP1	iron regulatory protein 1
IRP2	iron regulatory protein 2
IRP(s)	iron regulatory protein(s)
k_{cat}	catalytic constant
K_M	Michaelis constant
L	litre
LRP	low density lipoprotein receptor-related protein
m	milli

mag	original magnification
ml	millilitre
min	minute(s)
mol	mole
MW	molecular weight
mRNA	messenger ribonucleic acid
n	nano
N	normal
NHLS	National Health Laboratory Service
nm	nanometre
nmol	nanomole
%	percentage
gram %	grams per 100ml (grams %)
p.	protein
PCR	polymerase chain reaction
PGC-1α	proliferator-activated receptor γ coactivator 1α
pH	-log[hydrogen ion]
PHA	phytohaemagglutinin
PP	protoporphyrin
RES	reticuloendothelial system
RFU	relative fluorescence units
rpm	revolutions per minute
RR	reference interval or range
RT PCR	reverse transcriptase polymerase chain reaction
SD	standard deviation
sec	second(s)

SNP	single nucleotide polymorphism
STAT	signal transducer and activator of transcription
T	thymine
TBE	tris, boric acid EDTA
TEMED	tetramethylethylenediamine
TIPSS	transjugular intrahepatic portosystemic shunt
TLC	thin layer chromatography
T_m	melting temperature
U	units
µ	micro
UCT	University of Cape Town
µl	microlitre
µm	µmetre
µmol	micromole
UPG	uroporphyrinogen
UTR	untranslated region
vs	versus
v/v	volume for volume
V_{max}	maximal enzyme velocity
WT	wild type
x	times
XLDPP	X-linked dominant protoporphyria
XLSA	X-linked sideroblastic anaemia
ZnPP	zinc protoporphyrin
Zn meso	zinc mesoporphyrin
~	approximately

CHAPTER ONE

Haem biosynthesis and the porphyrias

This dissertation investigates the clinical and pathological manifestations of a porphyria as encountered in a South African family. Porphyria, as a generic term, refers to a heterogeneous spectrum of clinical syndromes resulting from the accumulation of substrate proximal to enzyme defects in the haem biosynthetic pathway (Anderson et al 2000).

It is thus appropriate to give a brief overview of porphyrins, haem biosynthesis and the disorders resulting from defects therein. Aspects most relevant to later chapters will be afforded emphasis.

Porphyrins

Porphyrins consist of four monopyrrole rings joined by methylene bridges, forming tetrapyrroles (Figure 1). Porphyrinogens are the hexahydro-reduced form. Porphyrins are capable of metal chelation in the centre of the nitrogen ring – in the case of ferrous iron incorporation, haem results (Deacon et al 2008). Magnesium and cobalt chelation achieves the formation of chlorophyll and a component of vitamin B12, respectively. Tetrapyrroles are the most abundant natural pigments, creating the visual perception of red blood and green grass (Heinemann et al 2008). Examples of essential functions haem fulfils include oxygen transport, mitochondrial respiration, nitric oxide sensing and drug, fatty acid, gluconeogenic and peroxide metabolism.

Different peripheral substituents occupying positions labelled 1 to 8 (Figure 1) in the form of 2 to 3 carbon side chains, with or without carboxyl groups, lend unique chemical and biological properties to tetrapyrroles. Their position and composition are shown in Figure 2. Importantly, solubility decreases with decreasing numbers of carboxyl groups. Variation of the distribution of the side chains allows isomer formation, designated by means of Roman numerals – numbers assigned in sequence of discovery (Israels and Israels 2002).

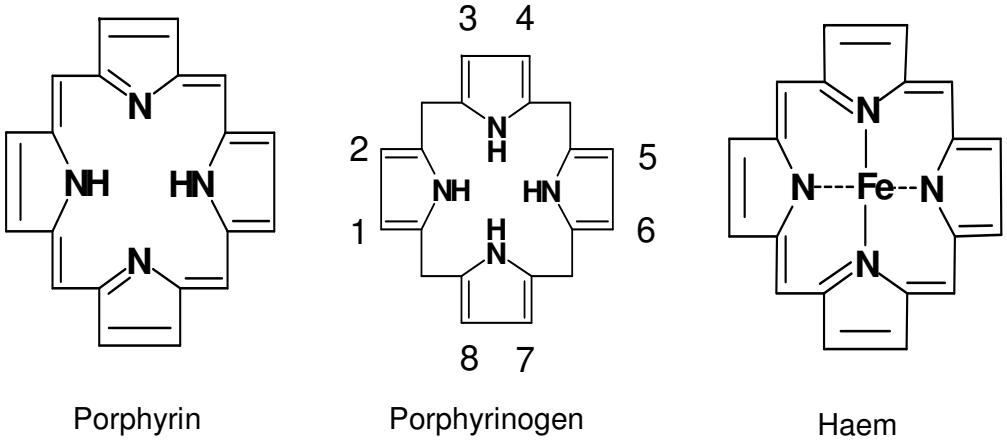

Figure 1: Fundamental tetrapyrrole structure. Note that the porphyrin ring has 11 double bonds while that of porphyrinogen has 8.

Fluoresence as a chemical property is important in the study of porphyrins. A molecule may be raised to an excited energy state by the absorption of radiant energy. Fluorescence occurs when decay from this excited state to the ground state occurs, in part by energy transfer to surrounding molecules as radiation. Fluorescence always occurs at a longer, lower energy wavelength than that which was absorbed (Mathews and van Holde 1990).

Porphyrins absorb light powerfully around 400 nm (the Soret band). This results in an appealing orange-red fluorescence in the range from about 550 to 650 nm. Peak fluorescence wavelength is influenced by metal chelation and peripheral side chain composition. This property of photoreactivity is in part responsible for the photocutaneous lesions observed in the porphyrias. Iron chelation virtually abolishes fluorescence while zinc shifts peak emission to a shorter wavelength and decreases peak intensity. Porphyrinogens, lacking conjugated double bonds within the ring, do not fluoresce. They do however undergo spontaneous oxidation to porphyrins *in vitro* (Deacon et al 2008).

Haem biosynthesis

The 8 step biosynthesis of the remarkably complex haem ring in mammals, commencing in the mitochondrial matrix with two relatively simple compounds - glycine and succinyl CoA, is shown diagrammatically in Figure 2.

The first reaction, catalysed by the enzyme 5-aminolevulinate synthase (ALAS) (Enzyme Commission number [EC] 2.3.1.37), using pyridoxal phosphate (vitamin B6) as co-factor, results in the formation of 5-aminolevulinic acid (ALA). Importantly, 2 isoenzymes coded by 2 distinct genes for ALAS exist: a ubiquitous 'housekeeping' isoenzyme is carried on chromosome 3 and referred to as *ALAS1* (also as *ALASN*). An erythroid specific enzyme referred to as *ALAS2* (also as *ALASE* or *eALAS*) is encoded on the X chromosome (Bishop et al 1981, 1990). These 2 forms of ALAS allow the differential regulation of haem synthesis as required by the 2 primary sites of haem biosynthesis. Indeed, approximately 80% of haem synthesis occurs in the bone marrow and about 15% in the liver. Interestingly, ALAS2 shows interaction with succinyl CoA synthase within the mitochondrial matrix of normoblasts, from which one of its substrates is derived (Furuyama and Sassa 2000). In general, regardless of the specific site of haem synthesis, ALAS may be considered the main rate-limiting step and sets the rate of flux through the pathway (Bloomer 1991, Philips and Kushner 2005).

The second reaction occurs in the cytosol during which 2 molecules of ALA condense to form a monopyrrole, porphobilinogen (PBG). Two molecules of water are eliminated. This is catalysed by the enzyme ALA dehydratase (EC 4.2.1.24) and requires zinc as co-factor.

.

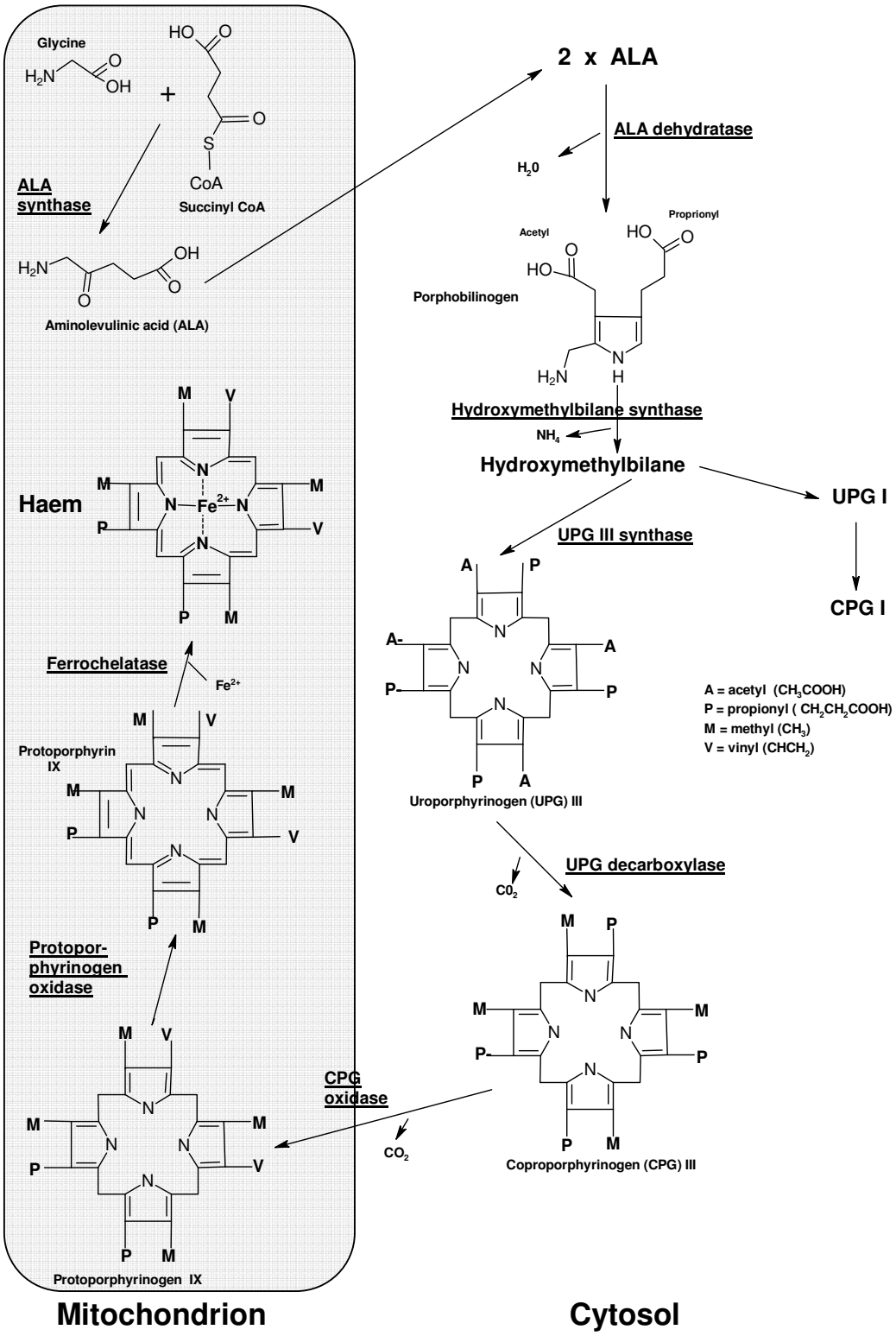

Figure 2: Diagram of the haem biosynthetic pathway. Enzymes are numbered 1 - 8 (adapted from Deacon et al 2008).

In the next step, hydroxymethylbilane synthase, (EC 2.5.1.61) (also known as PBG deaminase) catalyses the condensation of 4 molecules of PBG with the release of 4 molecules of ammonia to form hydroxymethylbilane – a linear tetrapyrrole.

During the fourth reaction, uroporphyrinogen (UPG) III synthase (EC 4.2.1.75) is responsible for closing the tetrapyrrole ring and catalysing isomerisation to UPG III, containing 8 carboxyl groups on the side chains. Non-enzymatic cyclisation to the I isomer may occur.

Sequential decarboxylation by UPG decarboxylase (EC 4.1.1.37) through 7, 6 and 5 carboxyl groups occur to generate the 4 carboxyl coproporphyrinogen (CPG) III. The remainder of the pathway, including the final haem-producing reaction, occurs within the mitochondrion.

The sixth reaction consists of the oxidative decarboxylation of CPG III to form the dicarboxylic protoporphyrinogen IX via the enzyme CPG oxidase (EC 1.3.3.3).

The penultimate step involves the enzymatic oxidation of protoporphyrinogen IX to protoporphyrin (PP) IX by protoporphyrinogen oxidase (EC 1.3.3.4). Only dicarboxylic porphyrins of the IX series are biologically active (Deacon et al 2008). For the purposes of this dissertation all protoporphyrins discussed will be assumed to be IX isomers.

Ferrochelatase (FECH) (EC 4.99.1.1) catalyses the final reaction which uses ferrous iron and PP to produce haem. This enzyme is capable of using other divalent metals (e.g. zinc) and dicarboxylic porphyrins (e.g. mesoporphyrin) as substrates (Deacon et al 2008). This may be exploited *in vitro* during FECH enzyme assay (Li et al 1987).

Substrate competition between iron and zinc during FECH-mediated PP chelation means that zinc PP (ZnPP) serves as a sensitive marker of intra-mitochondrial iron deficiency. Trace amounts of ZnPP are normally formed during haem biosynthesis, but during systemic iron deficiency, ZnPP accumulates in erythrocytes (Langer et al 1972).

Similarly, during diverse states of *de facto* intra-mitochondrial iron deficiency, as occurs in lead poisoning (Lamola et al 1974), the anaemia of chronic disorders (Hastka et al 1993), and during accelerated (especially in haemolytic anaemia) or ineffective erythropoiesis (Finch 1994), ZnPP may increase.

Regulation of haem biosynthesis

ALAS1 is capable of responding to fluctuating hepatocyte haem requirements imposed by cellular metabolic pathways. Haem itself, through a number of mechanisms, exerts negative feedback on ALAS1 by inhibiting *ALAS1* transcription and import into the mitochondrial matrix (Lathrop and Timko 1993). In addition, a number of other factors such as drugs, starvation and hormonal changes, are capable of inducing ALAS1. These mechanisms are not well defined. However, it has been suggested that fasting stimulates gluconeogenesis and fatty acid oxidation via induction of peroxisome proliferator-activated receptor γ coactivator 1α (PGC-1α). This effect is antagonised by glucose and insulin (Handschin et al 2005), and is the basis by which both fasting and glucose may play a role in the regulation of porphyrin biosynthesis.

In contrast, *ALAS2* transcription is stimulated via erythroid transcription factors binding to the promoter region in response to a variety of physiological stimuli. The zinc finger transcription factor GATA-1 (named after the guanine, adenine, thymine, adenine sequence it binds) has at least 2 *ALAS2*-associated binding sites (Surinya et al 1997) while erythroid Kruppel-like factor (EKLF) has 1 (Miller and Bieker 1993). These factors serve to coordinate haem synthesis relative to the normoblast maturational stage and state of globin expression (Nuez et al 1995, Marinkovic et al 2007).

Similar to ALAS1 regulation, ALAS2 import into the mitochondrial matrix is inhibited by haem (Lathrop and Timko 1993). However, the physiological

implications of this effect are probably of less importance than in the case of ALAS1 (see later under 'Ferrochelatase, haem and iron synergy').

Potential toxicity of PP accumulation demands that during erythropoiesis ALAS2 activity is capable of matching PP production to iron availability. It is believed that appropriate iron delivery to developing normoblasts is achieved through translational induction of ALAS2 by means of iron regulatory proteins 1 (IRP1) and 2 (IRP2). In this seemingly elegant system (for a summary see Table 2), intracellular iron deficiency activates iron regulatory proteins (IRPs). IRPs are then able to bind to iron response elements (IRE) on mRNA transcripts of ALAS2 (Cox et al 1991), ferritin (Theil 1998), the divalent metal transporter 1 (DMT1) (Israels and Israels 2002) and the transferrin receptor 1 (Klausner et al 1993).

In the case of ALAS2 and ferritin, the IRE is located in 5' untranslated region (UTR) of the mRNA transcript. Binding of the IRP to the IRE results in inhibition of translation, signalling a decrease in haem synthesis and iron storage until iron availability is restored. This contrasts with the binding of IRPs to the transferrin receptor 1 and DMT1 mRNA IRE which occurs in the 3' UTR and serves to mediate transcript stability, and hence translation followed by transferrin-bound iron uptake and import into the developing normoblast.

IRP1 and IRP2 are homologous proteins. Data generated from murine knock out models suggest IRP2 has greater biological utility than IRP1 (Cooperman et al 2005). IRP1 has an iron-sulphur (Fe-S) cluster which appears to allow iron sensing. Abundant iron leads to cluster assembly, inhibiting its IRE binding capabilities and converting IRP1 to a cytosolic aconitase enzyme. The intermediary metabolic role of the mitochondrial aconitase isoform in the Krebs cycle is well known. In contrast, the function of citrate isomerisation to isocitrate in the cytosol of mammals and its relationship with iron status is poorly understood (Pitula et al 2004).

IRP2 does not posses a Fe-S cluster. Instead, intracellular concentrations are a function of the rate of IRP2 degradation. Oxidation-induced

ubiquitination leads to degradation by the proteosome system. IRP2 is oxidised upon haem binding to its haem regulatory motif (Ishikawa et al 2005). In addition, intracellular iron activates ubiquitination of IRP2 (Guo et al 1995).

Schranzhofer et al (2006) challenge the applicability of the abovementioned 'standard' model of translational control of erythropoiesis during the final accelerated haemoglobinisation phase with its concomitant increased iron demand. If the IRP dependent system were able to sense increasing iron concentrations, transferrin receptor expression would be down-regulated, acquired iron lost to ferritin and iron availability for haem synthesis compromised. The "kiss and run" hypothesis (Ponka 1997) offers a partial explanation. During terminal erythropoiesis, iron present in vesicles acquired by receptor-mediated endocytosis is capable of being targeted directly to the mitochondrion without increasing cytosolic iron concentrations. Schranzhofer et al (2006) postulate that increased mitochondrial iron import would have a similar effect and that during maximal haemoglobinisation, ALAS2 mRNA increases disproportionately to IRPs thus obviating any requirement for cytosolic IRP concentrations to decrease in order to enhance ALAS2 translation.

In contrast to the basic tenets of the theory used to explain the regulation by the IRP system, and despite the postulate that ALAS2 expression may not be dependent on iron signaling through the IRP system (Schranzhofer et al 2006), it has been shown that iron is capable of increasing haem synthesis through the IRP system during iron-deficient states. However, during iron-replete states, additional iron does not stimulate haem synthesis (Ishikawa et al 2005). This may serve to prevent excess haem synthesis in genetic disorders of iron overload, and account for the rapid reticulocyte response commonly observed during the reversal of iron-deficient states.

Further coordination of erythroid mass, haem synthesis and iron metabolism in defending oxygen delivery is attained by erythropoietin-induced IRP1 activation, leading to increased normoblast transferrin receptor expression (Weiss 1997). Secretion of erythropoietin is under control of the von Hippel-Lindau / hypoxia-inducible transcription factor pathway, which is capable of sensing oxygen tension via an oxygen-requiring, iron-dependent, prolyl hyroxylase system (Elbert and Brunn 1999). This system contributes to the regulation of iron absorption and availability via inhibition of hepcidin and upregulation of ferroportin (Peyssonnaux et al 2007). Ultimately, *ALAS2* transcription is also regulated by the activation, and enhanced transcription of, *GATA-1* by erythropoietin through the Janus kinase 2 and signal transducer and activator of transcription (STAT) pathways (Dalyot et al 1993, Zhao et al 2006). Erythropoietin and GATA-1 are powerful survival stimuli to normoblasts (Israels and Israels 2002).

The porphyrias

The porphyrias result from partial deficiencies of specific enzymes in the haem biosynthetic pathway (Anderson et al 2000).

Precursor accumulation has the potential to cause an acute porphyric attack. Conversely, porphyrinogen or PP (tetrapyrrole) accumulation correlates with photosensitivity, a less acute symptom. These are the two cardinal syndromes in the porphyrias. Precursor and proximal, more water-soluble tetrapyrroles are excreted in the urine. More distal, less water-soluble tetrapyrroles are excreted via bile and hence the stool. In the erythropoietic porphyrias, porphyrin accumulation is primarily within erythrocytes (Deacon et al 2008).

The acute attack of porphyria represents a medical emergency in which confident laboratory diagnosis or exclusion is essential to direct appropriate treatment (Anderson et al 2000). There are several theories (Meyer et al

1998) relating to the pathogenesis of the acute attack. One such hypothesis states that ALA (or a related metabolic product) may act as a neurotoxin (Solis et al 2004). Such an effect may relate to the structural resemblance of ALA to neurotransmitters such as γ-aminobutyric acid (GABA). Furthermore, succinylacetone, which accumulates in hereditary tyrosinaemia type I, resembles ALA and is capable of competitive inhibition of ALA dehydratase. Lead is another well known and potent inhibitor of ALA dehydratase (Sassa 2006). These toxins share an ability to induce a crisis very similar to the acute porphyric attack.

Interestingly, not all the cutaneous porphyrias exhibit identical skin involvement. The photosensitivity in erythropoietic protoporphyria typically manifests as an acute photoreaction accompanied by burning and pruritis within minutes of sun exposure. This, in time, may lead to subtle but typical chronic changes such as waxy skin thickening and mild grooving, particularly over the dorsal surfaces of the knuckles and the bridge of the nose. This is in contrast with the typical blisters, pigmentary changes and scarring in sun exposed areas seen in variegate porphyria and porphyria cutanea tarda. The underlying pathology is thought to be due to circulating or skin-entrapped photoreactive porphyrins which are excited by light in the Soret band (Smith et al 1990). Conventional non-porphryric sunburn occurs after exposure to light of a wavelength around 300 nm.

Transfer of energy from porphyrin to oxygen molecules occur with subsequent generation of reactive oxygen species and lipid peroxidation. Complement activation and degranulation of mast cells ensue, leading to an acute inflammatory cascade. Fibroblast response leads to scarring (Lim 1989).

X-linked sideroblastic anaemia (XLSA) results in anaemia and iron overload and is due to loss of function mutations in the first enzyme of haem biosynthesis in erythroid cells, *ALAS2* (Sadlon et al 1999). As would be expected, porphyrin accumulation and porphyria does not result. Mututions in *ALAS1* have not been described.

A brief outline of the porphyrias and other related disorders associated with haem biosynthesis is shown in Table 1.

Table 1: Summary of the disorders resulting from enzymatic defects in the haem biosynthetic pathway (modified from Sassa 2006)

Enzyme defect	Disorder	Main clinical effects	Aetiology
ALA synthase 2	X-linked sideroblastic anaemia	Anaemia	X-linked recessive
ALA dehydratase	ALA dehydratase deficiency porphyria	Acute attack	Autosomal recessive (enzyme may be inhibited by lead and succinylacetone)
Porphobilinogen deaminase	Acute intermittent porphyria	Acute attack	Autosomal dominant
Uroporphyrinogen III synthase	Congenital erythropoietic porphyria	Severe photosensitivity, haemolytic anaemia	Autosomal recessive
Uroporphyrinogen III decarboxylase	Porphyria cutanea tarda	Skin disease (scarring)	Acquired (majority) or autosomal dominant
Coproporphyrinogen oxidase	Hereditary coproporphyria	Skin disease, acute attack	Autosomal dominant
Protoporphyrinogen oxidase	Variegate porphyria	Skin disease, acute attack	Autosomal dominant
Ferrochelatase	Erythropoietic protoporphyria	Skin disease, liver disease	Autosomal pseudodominant (majority) – see text

Erythropoietic protoporphyria

As the family of interest in this dissertation presented with a biochemical picture of atypical erythropoietic protoporphyria (EPP), EPP will be discussed in more detail.

EPP results from a partial deficiency of FECH. Autosomal dominant inheritance, usually with a primary *FECH* mutation in *trans* to a low-expression IVS3-48C polymorphism, is most common (Gouya et al 2002). This form of inheritance, although not strictly autosomal dominant, is referred to as 'autosomal dominant' or 'autosomal pseudodominant'. The IVS3-48C polymorphism increases the use of an aberrant splice site. Approximately 3% of cases are due to true autosomal recessive inheritance (Gouya et al 2006). Acquired EPP has been reported in the setting of haematological malignancy and cytogenetic *FECH* deletions associated with clonal expansion of *FECH* deficient bone marrow cells (Aplin et al 2001, Bharati et al 2006, Goodwin et al 2006).

The biochemical hallmark of EPP is raised red cell PP which tends to be in the free (i.e. no bound metal) form – due to an inability of the FECH enzyme to metabolise substrate. Causes of raised ZnPP (see page 23-24), are generally related to decreased iron availability as opposed to FECH deficiencies *per se*.

Unique clinical features of EPP include the acute nature of the photosensitivity, disease onset in infancy, and the possibility of liver disease developing as a direct result of the porphyria (Todd 1994).

Manifest liver disease is a relatively rare complication, occurring in approximately 3% of EPP patients (Anstey and Hift 2007). Free PP (but not ZnPP) is capable of diffusing out of red cells, with reticulocytes containing proportionally more PP than mature red cells (Piomelli 1975). PP is excreted into bile by the liver and undergoes extensive enterohepatic circulation due to its lipophilic nature. Increasing PP concentrations may lead to PP insolubility,

cholestasis and cholelithiasis. Hepatocyte injury is manifest with inflammation which may eventually lead to cirrhosis (Poh-Fitzpatrick 1986). In the terminal phase of EPP-related liver disease, increasing cholestasis impairs hepatic PP excretion. Oxidative stress-induced haemolysis occurs with increasing PP concentrations, driving erythropoiesis and increasing PP load presented to the liver - propagating a cycle of clinical deterioration (Key et al 1992, Anstey and Hift 2008).

The precise pathogenesis of hepatopathy in EPP is not fully understood, but an autosomal recessive inheritance pattern, a family history of EPP-related liver disease and additional non-EPP related liver insults (e.g. ethanolic or viral injury) are risk factors or associations for hepatic complications (Nordmann 1992, Anstey and Hift 2008).

Major structural *FECH* alterations have been associated with developing hepatopathy but on the other hand the liver disease may simply be a function of particularly marked PP accumulation (Bloomer et al 1998). One case report describes aggravation of EPP disease severity leading to hepatopathy as a consequence of hypermethylation of the *FECH* promoter (Onaga et al 2004).

While photosensitivity may be painful, distressing or disrupt an affected individual's lifestyle (Todd 1994), liver disease may be fatal. An understanding of the factors culminating in liver disease represents (one of) the holy grail(s) of EPP-related research.

Ferrochelatase, haem and iron synergy

Ponka (1999) indicates that erythroid iron acquisition and metabolism is often neglected when haem biosynthesis is considered. He complains of *"….heme pathway schemes, which, with overwhelming majority, show iron 'mysteriously' appearing in mitochondria, always ready to be grasped by ferrochelatase".*

Iron is absorbed into developing erythroid cells by receptor-mediated endocytosis of the iron-transferrin complex bound to the transferrin receptor. The endosome is acidified leading to release of iron from transferrin. Transport across the endosomal membrane is effected by DMT1 - the same transporter which is responsible for moving iron across the apical border of the enterocyte in the gut (Ponka et al 1998).

Haem deficiency, signalling though the IRP2 system, serves as a potent stimulant to transferrin-mediated iron uptake by erythroid cells (Ishikawa et al 2005). In an experiment investigating product (haem) inhibition during haem synthesis, it was found that iron presented to reticulocytes as a lipophilic conjugate, negates any inhibitory effect of haem. When transferrin is used as an iron carrier (rather than the lipophilic conjugate), inhibition does occur, and radiolabelled glycine is incorporated into PP but not into haem (Ponka et al 1973). This is consistent with failure of iron delivery to erythroid cells when excess haem is present (Ponka and Schulman 1985).

The power of erythron iron acquisition (such as would be required for physiological haem production) is illustrated by a simple calculation. Assume normal diferric transferrin iron of ~ 3 µmol/L (only diferric transferrin can deliver iron effectively to the transferrin receptor) (Ponka 1998) and a normal whole blood haemoglobin of ~ 15 g/dL = 150 g/L. At a haematocrit of 50%, red cell haemoglobin = 300 g/L. The molecular weight of a haemoglobin monomer is ~ 15 000. Thus red cell haemoglobin monomer concentration = 0.02 mol/L = 20 mmol/L. Each monomer chelates one iron atom, thus a ~ 7000 fold difference between serum and erythron iron concentrations exists.

Mammalian FECH is nuclear encoded. After synthesis in the cytosol it is targeted to the inner mitochondrial membrane via a leader sequence where it functions as a homodimer (Karr and Dailey 1988). FECH contains a Fe-S complex near its carboxy (C)-terminus. The Fe-S cluster is not involved in binding iron as substrate for FECH catalysis (Ferreira 1999). Instead, the Fe-S cluster serves to facilitate FECH dimerisation (Dailey et al 2000). Furthermore, it enables intracellular iron concentrations to influence FECH expression, suggesting an iron-sensing capability, and serving to coordinate FECH activity and substrate availability (Taketani et al 2000).

A recent report described decreased erythroid FECH activity and intracellular FECH concentrations during intracellular iron deficiency, in genetic disorders of Fe-S assembly and during oxidative stress (Crooks et al 2010).

Haem is reported to inhibit FECH activity in a non-competitive manner (Dailey and Fleming 1983). This may function physiologically as a negative feedback system on FECH activity.

X-linked sideroblastic anaemia and ataxia (ASAT), resulting from a mutation in the adenosine triphosphate binding cassette 7 transporter (ABC7), is characterised by elevated free PP concentrations (Allikmets et al 1999). This disorder is a different entitity from the more well-known XLSA previously mentioned. Taketani et al (2003) propose that ABC7 is involved in the formation and maintenance of the FECH Fe-S cluster. In addition, ABC7 exports Fe-S clusters for use by other cytosolic proteins.

Mitochondrial iron import in erythroid tissue is achieved by a transporter termed mitoferrin (Shaw et al 2006_a). Mitoferrin forms a complex with FECH, which may facilitate the coordination of mitochondrial iron import and haem biosynthesis (Chen et al 2010). It has been proposed that aberrant splicing of mitoferrin mRNA may be capable of producing a rare variant form of protoporphyria (Shaw et al 2006_b).

Although haem deficiency is not necessarily part of the porphyria syndrome, a mild anaemia with hypochromic and microcytic features is frequently found in EPP. This suggests that a mild defect in haem production might exist in erythroid tissue in EPP. Iron parameters, in the absence of other factors such as blood loss, are normal (Holme et al 2007) and bone marrow iron store assessment reveals stainable normoblast iron. However, ring sideroblasts have been reported in human EPP (Rademakers et al 1993). Interestingly, ring sideroblasts were not present in the murine EPP model (Lyoumi et al 2007).

It is of note that the only vehicles for iron export from mitochondria are haem and Fe-S clusters (Huang et al 2009).

It may be useful to conclude this discussion of the relevance of iron metabolism to the haem biosynthetic pathway with a summary (Table 2).

Table 2: Relative and simplified physiological changes in normoblast effector proteins associated with varying intracellular iron concentrations

Effector protein	Iron-deficient normoblast	Iron-replete normoblast
IRP	Increase	Decrease
Transferrin receptor 1	Increase	Decrease
DMT1	Increase	Decrease
Ferritin	Decrease	Increase
ALAS2	Decrease	Increase
FECH	Decrease	Increase

Laboratory testing in erythropoietic protoporphyria

As this dissertation focuses on an atypical EPP family, and initially in establishing a diagnosis, it is appropriate to review conventional approaches in establishing such.

Biochemical testing for EPP focuses on detection of elevated concentrations of PP in the blood. For example, biochemical diagnosis of EPP can be made by plasma fluorescence scanning with excitation at 405 nm. A characteristic emission peak occurs at 632 nm, assisting in the differentiation of EPP from other cutaneous porphyrias such as variegate porphyria (emission peak at 625 nm) and porphyria cutanea tarda (emission peak at 618 nm) (Poh-Fitzpatrick 1980, Deacon and Elder 2001).

Quantitative analysis may be performed on extracted porphyrin esters or porphyrin acids. This may be followed by a variety of chromatographic

methodologies with fluorescence detection including high performance liquid chromatography (Deacon et al 2008). These methods have the potential to quantify other porphyrins in addition to PP (Day et al 1978). Alternatively, PP may be quantified fluorometrically against a standard (Deacon and Elder 2001), or even qualitatively by simple visual inspection of a red cell methanol extract under ultraviolet light. However, although commonly performed, the latter method is insensitive and should only be used if preferred methodologies are not available. Acidic reagents or extraction media used in the above methods dissociate zinc from ZnPP, thus converting ZnPP to free PP and measuring total PP. When attempting to measure the 2 individual PP species, non-acidic reagents such as acetone should be used.

Qualitative determination of the relative contributions of ZnPP and free PP to total PP concentrations may be performed by simple inspection of a fluorescence emission spectrum, typically with excitation at 420 nm. ZnPP has a main emission peak at 588 nm while that of free PP lies at 632 nm. Two caveats apply – ZnPP has less specific fluorescence than free PP and ZnPP has a subsidiary emission peak at 636 nm, thus boosting the apparent fluorescence of the free PP peak at 632 nm (Hart and Piomelli 1981). The finding of a dominant peak at 588 nm tends to rule against EPP (because of probable elevated ZnPP) while a single peak at 632 nm is highly suggestive of EPP (Deacon and Elder 2001). In order to obtain ZnPP as a percentage of total PP by emission fluorescence measurement an equation has been developed (Hart and Piomelli 1981). This involves fluorescence measurement at 588 nm and 618 nm (the isosbestic point – where equal concentrations of ZnPP and free PP will exhibit identical fluorescence intensity).

Fluorocytes are red cells packed with PP, endowing them with fluorescence. This may be visualised with a microscope equipped with a light source capable of excitation in the Soret band (Rimington and Cripps 1965).

Due to the insolubility of PP, and because PP does not cause secondary inhibition of porphobilinogen deaminase as may occur in variegate porphyria (Meissner et al 1991), urine precursors and porphyrins are not elevated in EPP. This is a consideration in the formulation of a differential diagnosis.

Stool porphyrin analysis may show the presence of PP (reflecting degraded red cells) but false positives from bacterially degraded haem, gastrointestinal haemorrhage, and other factors may occur.

Considering the inherited nature of EPP, it follows that genetic testing may be appropriate and may be conducted using standard molecular biology techniques. However, it must be noted that the majority of the mutations in the *FECH* gene causing EPP are heterogeneous (Rufenacht et al 1998) and testing must be individualised for most families. This being said, DNA-based testing is a particularly efficient way of diagnosis in families where the mutation causing the porphyria is already known, or a degree of homogeneity may be expected. Indeed, due to the unique history of the early South African immigrant population, founder mutations often predominate. Among patients affected by EPP in South Africa, the 757_761delAGAAG five base pair deletion in exon 7 of *FECH* is a particularly common disease-causing mutation (Parker et al 2008). This deletion causes a frameshift mutation, resulting in a truncated FECH protein. As found elsewhere (Gouya et al 2006), the IVS3-48C EPP low-expression polymorphism is common in South Africa among patients with EPP and in control groups (Parker et al 2008). Thus, in EPP families, testing the unaffected parent for the IVS3-48C polymorphism has clinical utility in predicting clinical disease expression in the progeny (Deacon et al 2008).

Due to varying disease penetrance, DNA-based results should be interpreted within the clinical context. Furthermore, porphyrin biochemistry should be considered as essential in the diagnosis and monitoring of disease progression.

CHAPTER TWO

Development of the project aims and objectives

Family EPP8

The family of interest (family EPP8) in this dissertation was identified during a study conducted by the Lennox Eales Porphyria Laboratories of the University of Cape Town (UCT) from 2004 to 2007 (Parker et al 2008).

In that study, single-stranded conformational polymorphism analysis, direct sequencing of abnormalities, restriction digestion to screen for specific mutations, and haplotyping were used to genotype *FECH* in a South African cohort of EPP and control subjects. The family investigated and characterised further in the present dissertation was designated 'family EPP8'.

Although initially assumed to have EPP, Parker et al (2008) noted several atypical features which served to distinguish family EPP8 from other patients with EPP in that study.

Strikingly, mutations in the *FECH* gene were not detected. Haplotype analysis revealed that the porphyria in this family did not segregate with haplotype markers associated with EPP. Clinically manifested disease transmission from parent to child occurred between generations II and III (Figure 3, Chapter 3). This contrasts with conventional EPP inheritance, where the unique requirement for the IVS3-48C allele to be in *trans* to the primary mutation, causes generations to be 'skipped'. Unusually, photosensitivity was highly penetrant and hepatopathy was severe with 2 out of 6 affected subjects manifesting severe liver disease. One of these had died of hepatic complications many years previously, while another deteriorated during the course of this study. Biochemical testing showed a preponderance of ZnPP, as opposed to free PP usually found in EPP. Finally, iron treatment was noted anecdotally to decrease photosensitivity.

Discussion with investigators in Wales (University of Cardiff) and France (Centre Francais des Porphyries), revealed a very similar if not identical

disease entity in some atypical EPP patients in those countries. International collaboration was established. Several hypotheses emerged and aspects of these formed the basis of the investigation described here. The present study was conducted at Groote Schuur Hospital (GSH), Cape Town in 2008 to 2009.

Initial aims and objectives were proposed and pursued. Additional aims and objectives were formulated in principle, and developed as the project proceeded, guided by emerging and evolving information. In addition, this study and dissertation should best be considered as a part component of a more comprehensive investigation (and in some aspects, collaborative).

Initial aims

1. Characterise the clinical and biochemical features of porphyria found in family EPP8.
2. Investigate FECH activity in family EPP8.

Initial objectives

1. Following ethics approval, establish clinical contact with family EPP8. Collect additional clinical information and blood samples. Collate and review all available clinical and biochemical data.
2. Transform subject and control lymphocytes with Epstein Barr Virus (EBV) to generate immortalised lymphoblast cell lines as tissue medium for FECH enzyme assay.

3. Establish a FECH enzyme assay locally (not previously performed in South Africa) using a published method. Measure EBV transformed lymphoblast (EBVTL) FECH activity in subjects and controls.

Supplementary aims

1. In the case of abnormal FECH activity, establish level and nature of defect.
2. In the case of normal FECH activity, explore alternative gene loci and/or explanations. However, it should be noted that finding an alternative gene locus and/or disease mechanism may be beyond the scope of a MMed project.
3. Develop and implement rational treatment strategies based on study findings and relevant to this particular family. This would be in addition to a consideration of the existing guidelines for the management of EPP.

Supplementary objectives

1. Abnormal FECH activity with normal genotyping would suggest the utility of the following investigations:
    a. Measurement of FECH mRNA concentrations to investigate epigenetic disease mechanisms (e.g. hypermethylation of the *FECH* promoter as described by Onaga et al 2004). Quantitative reverse transcriptase polymerase chain reaction (RT PCR) of FECH mRNA could be used to measure relative *FECH* transcription in subjects and controls against a reference 'housekeeping' gene such as beta-actin.

b. Quantification of FECH protein expression by Western blot analysis.

2. Normal FECH activity would imply that an alternative locus or mechanism is the cause of the disease. Iron transporters would be suitable alternative candidate genes. Potentially, other genes or proteins in the haem biosynthetic pathway, either synthetic or regulatory, may be involved in the pathogenesis of the porphyria in family EPP8.
3. Potentially explore novel treatment strategies based on knowledge gained of the molecular pathogenesis of the porphyria.
4. Report back to family EPP8 on findings of this project and offer appropriate counselling and assessment of risk based on clinical, biochemical and (if established) genetic information.

CHAPTER THREE

Review of clinical data from family EPP8

This chapter provides clinical information from family EPP8, to illustrate the background to the investigations described in Chapters 4 - 6.

Family EPP8

The family is of Jewish descent, generation I having arrived in South Africa from Poland in 1927.

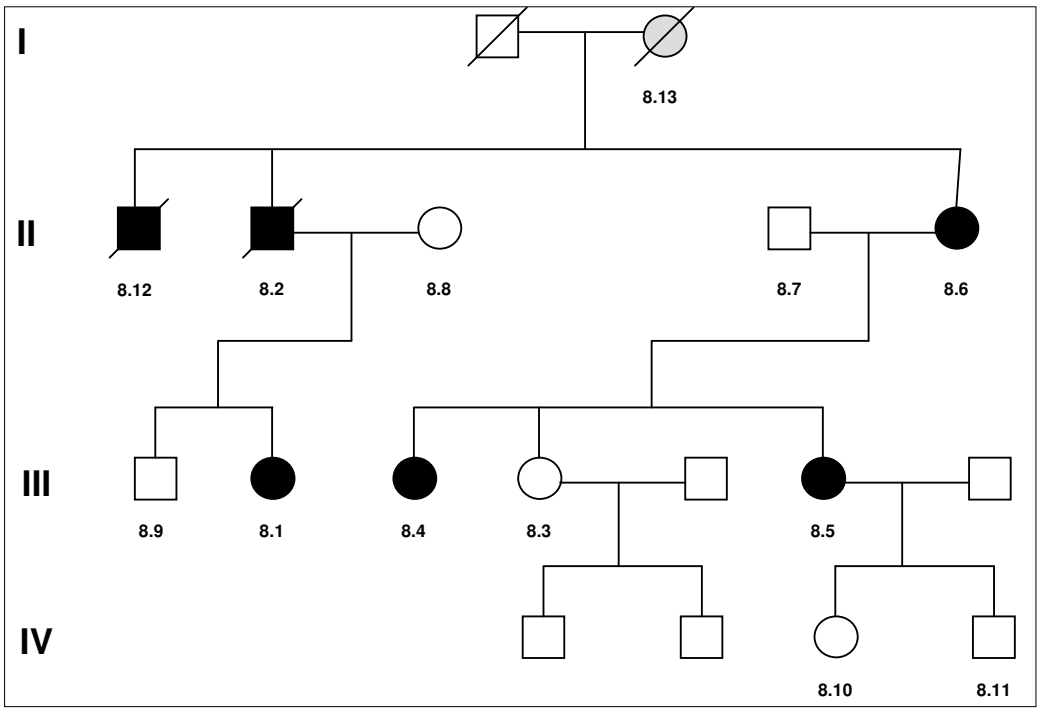

Figure 3: Genogram of family EPP8 showing 4 generations. Squares represent males and circles, females. A strike through represents a deceased individual - 1972 and 2008 for subjects EPP8.12 and EPP8.2, respectively. A filled symbol implies disease manifestation while a shaded symbol refers to uncertain disease manifestation. An unfilled symbol implies an asymptomatic state. Asymptomatic subjects who were not investigated are not numbered.

Eales et al (1978) gives a detailed account of the clinical presentation of patient EPP8.12. At the age of 29 (1971), his liver disease was investigated and a liver biopsy showed cirrhosis. He, along with his 2 siblings, was

diagnosed with EPP. Although all 3 siblings reported photosensitivity typical of EPP since early childhood (5 – 6 years of age), subject EPP8.12 was unique in the scarring and severity of his skin symptoms. In 1972 he presented to GSH with liver failure. Despite all available therapy, he died of massive haemorrhage from oesophageal varices secondary to portal hypertension.

Although the genogram in Figure 3 shows clear evidence of an inherited disease coupled with a high degree of penetrance in generation II and III, the exact mechanism of inheritance is not apparent. In 1971, subject EPP8.13 had raised faecal porphyrins and was thought to be a carrier. She remained completely asymptomatic and was described as being “able to sit in the sun for hours”.

Subject EPP8.2 was noted to have a firm hepatosplenomegaly and underwent open liver biopsy in 1975. This resulted in post operative haemorrhage requiring intensive care admission. Histology showed early bridging fibrosis and PP pigment. Subject EPP8.6 was also found to have hepatosplenomegaly, albeit less than in her brother. She did not have a liver biopsy. At the time, thrombocytopenia was noted in subjects EPP8.12 and EPP8.2 (23 and 89 x 10^9/ L, respectively).

The presence of glucose 6 phosphate dehydrogenase (G6PD) deficiency in this family was established by Eales et al (1978). In that study, subjects EPP8.12 and his brother EPP8.2 were shown to have deficient G6PD activity. Their sister, subject EPP8.6, manifested as a G6PD deficiency carrier, consistent with X-linked recessive transmission.

Contact was re-established with family EPP8 during the study on EPP in South Africa (Parker et al 2008). Red cell PP concentration was measured in 2005 and again in 2008/9 in available subjects (Table 3 and Appendix C). The results, in conjunction with symptoms (photosensitivity and avoidance of sun exposure, e.g. wearing of gloves while driving), were used to define the syndrome of EPP. The preponderance of ZnPP in family EPP8, in contrast to the free PP observed in typical EPP, was also noted (Appendix D) and an example is shown in Figure 4.

Table 3: Red cell PP concentration (conc) in family EPP8 (normal red cell PP < 2000 nmol/L)

Subject	Conc 2005 (nmol/L)	Conc 2008/9 (nmol/L)	Photosensitivity
EPP8.1	5644	24 083	Moderate
EPP8.2	11 083	72 042	Severe
EPP8.3	Not measured	970	None
EPP8.4	9343	48 750	Severe
EPP8.5	8138	Not measured	Mild
EPP8.6	27 285	10 140	Moderate
EPP8.7	195	Not measured	None
EPP8.8	97	Not measured	None
EPP8.9	95	Not measured	None
EPP8.10	Not measured	813	None
EPP8.11	Not measured	572	None

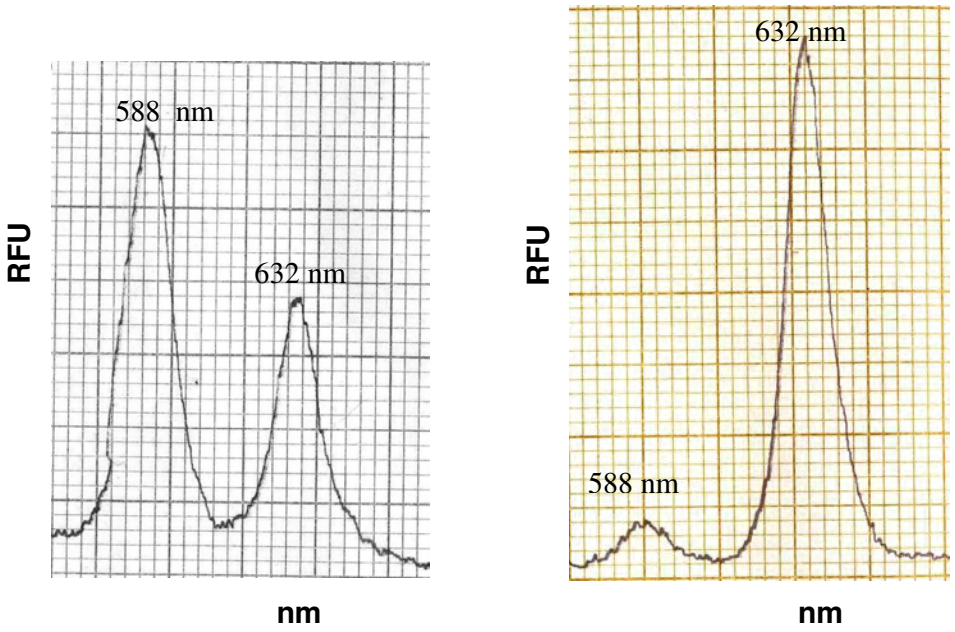

Figure 4: Fluorescence emission scans of red cell porphyrin extracts with excitation at 420 nm. Relative fluorescence units (RFU) are plotted vertically against emission wavelength. On the left is the spectrum obtained from subject EPP8.1 with prominent ZnPP peak at 588 nm. On the right, note the dominant peak at 632 nm seen in an unrelated patient with typical EPP, indicative of predominantly free PP. Courtesy of Ms M Parker, Hatter Institute, UCT.

In addition, routine biochemical and haematological parameters were measured in symptomatic subjects (Table 4).

Table 4: Age**,** biochemistry and haematology results from selected members of family EPP8 taken at baseline investigation in 2008/9. Reference ranges are indicated in brackets.

Subject	**EPP8.1**	**EPP8.2**	**EPP8.4**	**EPP8.5**	**EPP8.6**
Age	25	63	39	45	68
Haemoglobin (10.5-13.5 g/dl: females, 13.0-17.0 g/dl: males)	12.1	11.0	12.1	13.9	12.3
Mean red cell volume (81-96 fl)	95	96	79	86	79
White cell count (4.0-10.0 x10^9/L)	6.0	4.9	5.9	5.8	3.9
Platelets (140-420 x 10^9/L)	172	38	127	158	63
Albumin (37-52 g/L)	43	43	38	47	46
Total bilirubin (2-20 µmol/L)	38	38	11	12	15
Alkaline phosphatase (40-120 U/L)	43	89	34	62	45
Gamma glutamyl transferase (5-43 U/L)	41	244	20	18	28
Alanine amino transferase (10-32 U/L)	21	152	33	20	26
Asparate amino transferase (10-32 U/L)	19	179	32	20	26
International normalised ratio (INR)	0.9	1.3	0.9	1.0	1.0
Iron (10-30 µmol/L)	11	14	5	18	12
Transferrin (2.0-3.6 g/L)	3.2	2.9	3.0	2.7	2.5
Transferrin sats (20-50%)	14	19	7	27	18
Ferritin (30-400 µg/L)	59	28	8	111	80

Subject EPP8.2

Subject EPP8.2 manifested with accelerated disease during 2008, leading to intensive investigation which yielded information which will be presented here to illustrate the progression of his disease. It should be noted that much of the biochemistry and pathology described here for subject EPP8.2 may reflect the porphyria against a background of decompensated liver disease, which may be different to that observed in a patient with normal liver function.

Presenting features and investigation

Subject EPP8.2 was able to lead a productive and relatively asymptomatic life until the middle of 2007 when he noted increasing photosensitivity and right upper quadrant pain. At his initial evaluation at GSH in December 2007 he was found to have mild hyperkeratosis of the hands and face, hepatosplenomegaly and modest ascites. Blood results were as presented in Table 4. His peripheral blood contained fluorocytes (Figure 5). Previously, in November 2007, a bone marrow biopsy had been performed at another centre in view of ongoing thrombocytopenia and had excluded a myelodysplastic syndrome. Increased megakaryocytes were present (Figure 6), compatible with peripheral consumption, due to e.g. hypersplenism secondary to portal hypertension. Iron stores were decreased (Figures 7a and 7b).

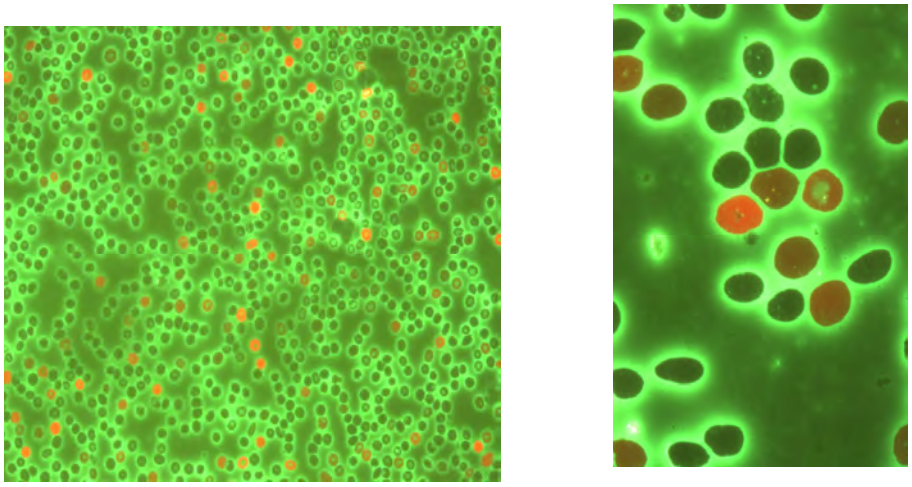

Figure 5: Fluorocytes (red) are visible on an unstained peripheral slide of patient EPP8.2 at 100x original magnification (mag) on the left and 500x mag on the right. Excitation wavelength ~ 400nm with an Olympus BX41 fluorescence microscope. Photograph taken with the help of Ms G Schutte, Cytogenetics, National Health Laboratory Service (NHLS) GSH.

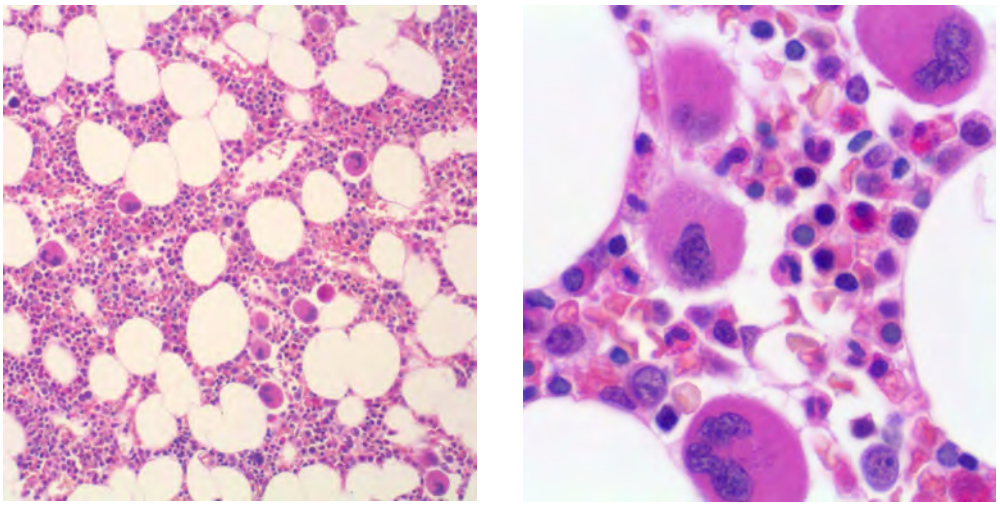

Figure 6: Haematoxylin and eosin stained section of a bone marrow biopsy from patient EPP8.2 shows increased megakaryocytes (100x mag) on the left, and at 500x mag on the right. The tissue was provided by and photographed with the permission of Prof P Jacobs (Constantiaberg Medi-Clinic, University of Stellenbosch and Tygerberg Hospital).

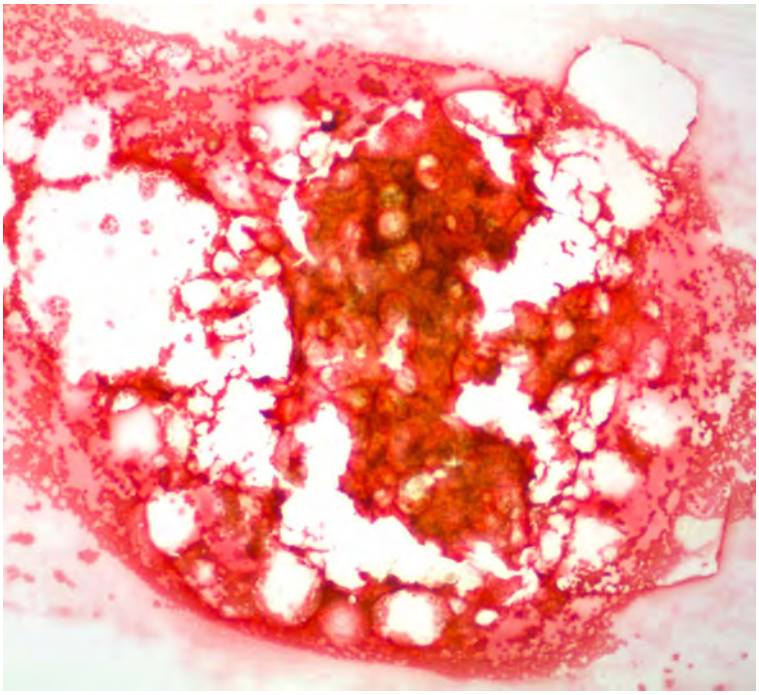

Figure 7a: Prussian blue staining of a particle obtained during bone marrow aspiration of patient EPP8.2 (100x mag). Note decreased iron stores. A normal control showing stainable iron is not shown here. The tissue was provided by and photographed with the permission of Prof P Jacobs (Constantiaberg Medi-Clinic, University of Stellenbosch and Tygerberg Hospital).

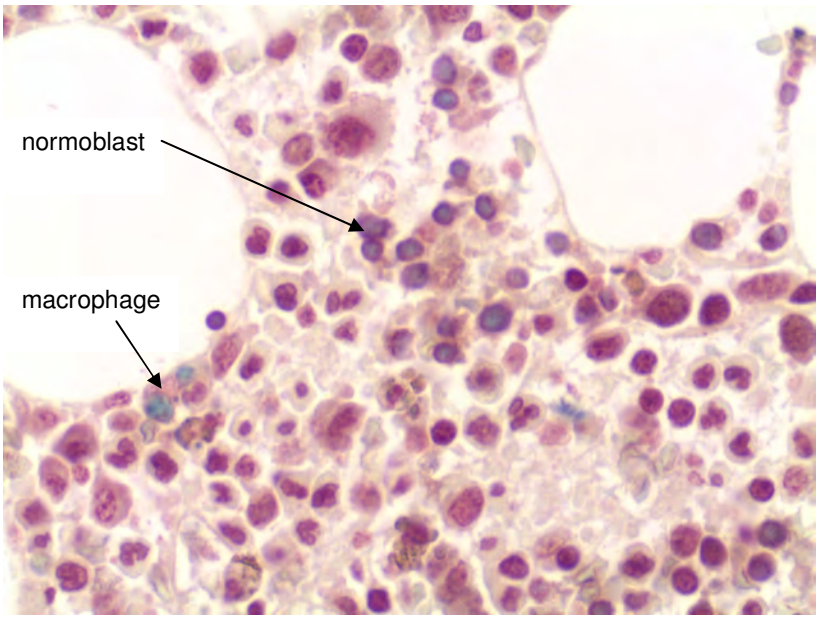

Figure 7b: Prussian blue staining of bone marrow trephine biopsies from a normal control (above) and from patient EPP8.2 (below) is shown (both at 500x mag). Note the presence of iron in the normal control biopsy but decreased stainable iron in the biopsy from patient EPP8.2. The tissue from patient EPP8.2 was provided by and photographed with the permission of Prof P Jacobs (Constantiaberg Medi-Clinic, University of Stellenbosch and Tygerberg Hospital).

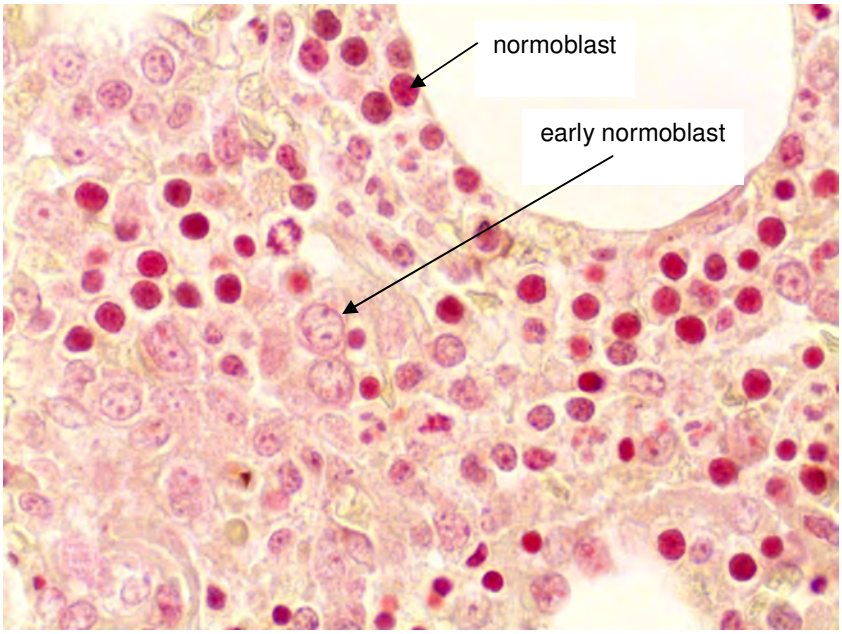

The precise cause of the iron deficiency was not apparent and a gastroscopy did not reveal oesophageal varices. Thrombocytopenia may have been contributory.

An abdominal computed tomography (CT) scan was performed in order to investigate ongoing abdominal pain (Figure 8). The gallbladder appeared abnormal. Chronic cholecystitis was diagnosed and it is likely that calculi were composed of PP. He later developed several episodes of cholangitis requiring admission and treatment with intravenous antibiotics.

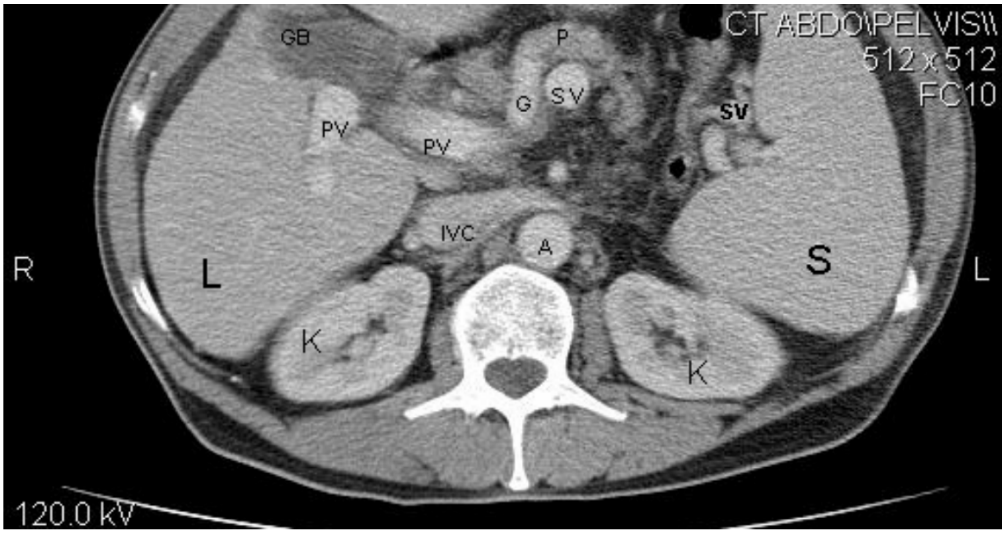

Figure 8: Transverse abdominal CT scan with intravenous contrast of patient EPP8.2 showing features of portal hypertension. Note the splenomegaly, the dilated portal and splenic veins, and the abnormal gallbladder. Ascites is not apparent, as the images were taken after paracentesis. (L = liver, S = spleen, K = kidney, A = aorta, IVC = inferior vena cava, PV = portal vein, SV = splenic vein, G = left gastric vein, P = pancreatic neck vein). Courtesy of Prof S Benningfield, Department of Radiology, UCT and GSH.

Treatment and progression of patient EPP8.2

Ongoing standard treatment of protoporphyric liver disease included treatment with oral ursodeoxycholic acid, cholestyramine, intravenous haem arginate and iron (see Chapter 6). A more definitive management plan directed at the predominant problem of portal hypertension and liver cirrhosis was proposed. The plan included the following sequential procedures:

1. Reduction in portal pressure by transjugular intrahepatic portosystemic shunt (TIPSS) insertion (Figure 9)
2. Cholecystectomy to remove a possible source of sepsis
3. Liver transplantation.

TIPPS insertion on 16 July 2008 caused a dramatic but temporary improvement in symptomatology, as evidenced by a marked decrease in ascites, a reduction in abdominal discomfort, and a subjective sense of recovery.

A liver biopsy (Figure 10) was performed at the time of TIPPS insertion and confirmed severe, long-standing PP induced liver damage.

Hyperammonaemia (Figure 11) and encephalopathy, known complications of TIPSS insertion, were not clinically significant problems.

Ascites, previously requiring the drainage of 3 - 7 litres of peritoneal fluid every 2 weeks, no longer required paracentesis. The patient was able to resume employment.

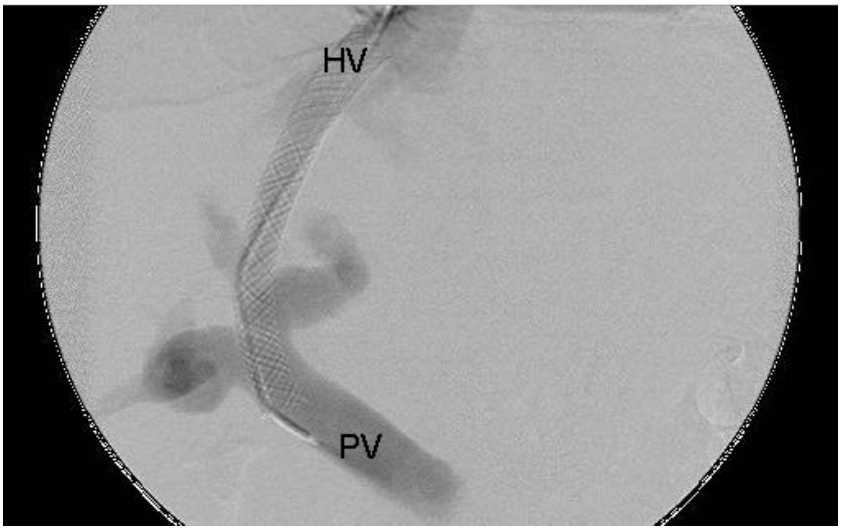

Figure 9: Image produced during fluoroscopically guided TIPSS placement in patient EPP8.2. The stent traverses the hepatic vein (HV), the liver parenchyma and the portal vein (PV). A catheter is temporarily located within the stent. Courtesy of Prof S Benningfield, Department of Radiology, UCT and GSH.

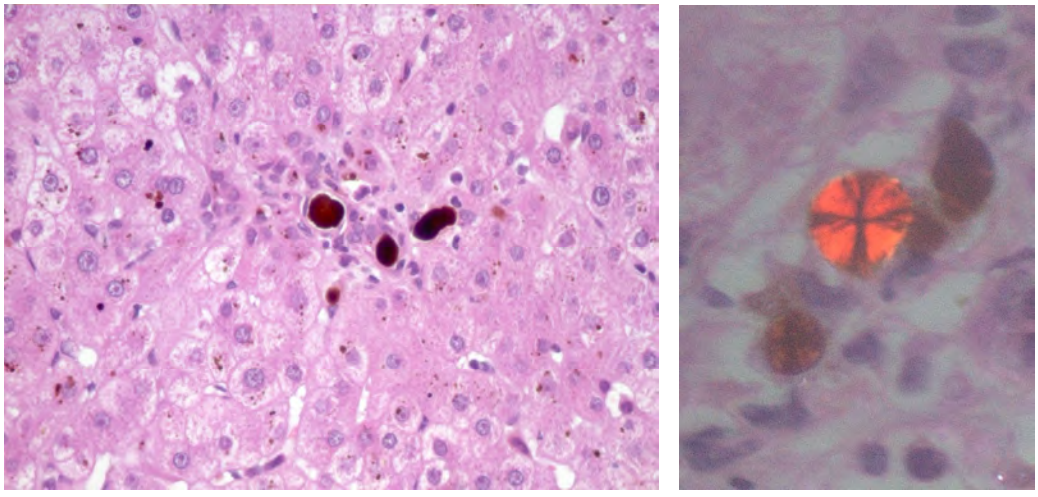

Figure 10: Haematoxylin and eosin stained section of liver tissue from patient EPP8.2. On the left (500x mag), ballooning degeneration of hepatocytes and plugging of bile ducts by mahogany coloured pigment casts are seen. Smaller quantities of pigment are visible within hepatocytes. On the right (1000x mag), polarizing microscopy shows yellow to red birefringence of PP with a Maltese cross appearance. Courtesy of Dr HT Wu and Associate Prof H Wainwright, Division of Anatomical Pathology, UCT and NHLS GSH.

On 21 August 2008 the patient was admitted to the intensive care unit in a critically ill state with renal and respiratory failure. After 11 hours of incubation, a blood culture specimen taken on admission yielded gram negative bacilli which were identified as extended spectrum beta lactamase producing *Klebsiella pneumonia* organisms.

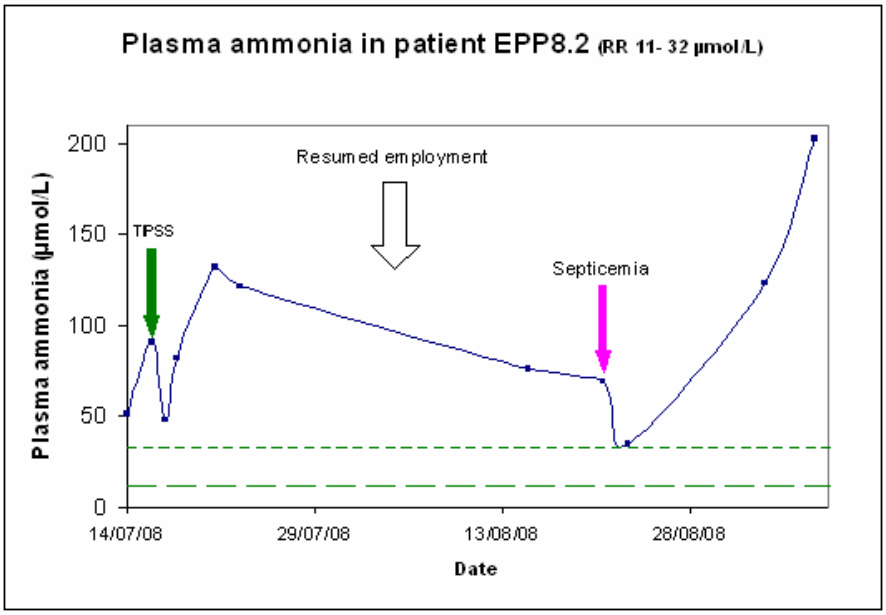

Figure 11: Changes in plasma ammonia concentration in patient EPP8.2 over time. Baseline plasma ammonia remains elevated. Concentrations rise modestly, and then stabilise following TIPSS insertion. During septicemia and multi organ failure, ammonia concentrations rise precipitously as a consequence of impaired liver function. Upper and lower limits of the reference interval are shown as green stippled lines.

During the final phase of his illness, his PP fluorescence shifted from a bi-peaked fluorescence emission scan associated with the atypical porphyria as encountered in family EPP8 (Figure 4, left), to a pattern more typical of that associated with EPP (resembling Figure 4, right), containing ~ 90% free PP.

It is thought that the septic focus, from where the septicaemia originated, was the diseased gallbladder, or alternatively the TIPSS. Leucopenia (Figure 12), predominantly a neutropenia, may have resulted from direct myelosupression secondary to sepsis.

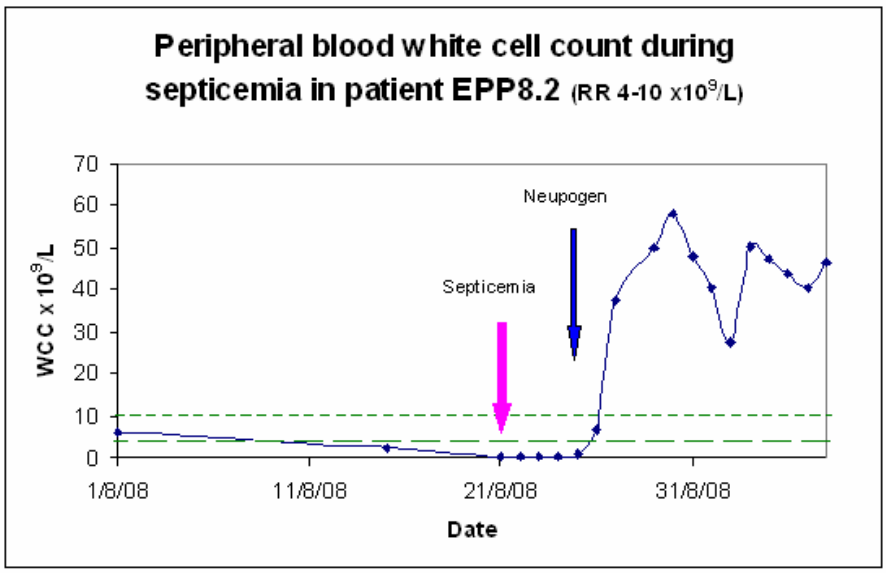

Figure 12: Changes in peripheral blood white cell count over time during septicemia in patient EPP8.2. Initial marked leucopenia during septicemia changes to leucocytosis with filgrastim (Neupogen; recombinant human granulocyte colony stimulating factor) treatment. Upper and lower limits of the reference interval are shown as green stippled lines.

Despite all available supportive management in an intensive care setting, including appropriate antibiotics, ventilation and haemodialysis, patient EPP8.2 died from multi-organ failure secondary to overwhelming sepsis.

An autopsy was not performed.

CHAPTER FOUR

Ferrochelatase enzyme assay

As outlined in Chapter 2, determining FECH enzyme activity in family EPP8 was an important first step in establishing a diagnosis and elucidating a pathogenic mechanism. Indeed, a divergence in proposed investigation objectives was dependent on this measurement - normal activity would suggest that an alternative disease locus should be sought; in the case of decreased activity, further investigation of the *FECH* gene would be undertaken.

Introduction

In vivo, FECH catalyses the chelation of ferrous iron by PP to form haem (Figure 2). Zinc may act as an alternative substrate to form ZnPP. *In vitro*, FECH is capable of using alternative dicarboxylic porphyrins such as mesoporphyrin or deuteroporphyrin as substrates. As indicated in Chapter 1, PP and ZnPP fluoresce, but haem does not – this is therefore the basis for many FECH enzyme assays. Only iron in its ferrous (reduced/Fe^{2+}) state can act as substrate for FECH, necessitating anaerobic assay conditions. Zinc as substrate is not prone to oxidation, and enzyme activity for zinc chelation may be measured aerobically.

FECH activity has been measured using a variety of techniques. Porra and Jones (1963) used the pyridine haemochromogen procedure to measure FECH activity. This assay is said to be less sensitive than fluorometric methods (Li et al 1987).

Sassa et al (1982) measured PP substrate disappearance by fluorimetry during incubation for 24 hr as a measure of FECH activity. Further information was gained by including either iron chelation or supplementation. However, a large excess of porphyrin is used during the incubation and this is reported to result in poor sensitivity (Li et al 1987).

In another technique, radiolabelled iron $^{59}Fe^{2+}$ as substrate provides greater sensitivity. Difficulties have been encountered during the separation of free $^{59}Fe^{2+}$ from the ^{59}Fe labelled haem at the end of the reaction (Bloomer and Morton 1982).

The FECH assay described and used in this dissertation was a direct fluorometric measurement of FECH-catalysed zinc mesoporphyrin (Zn meso) product formation, using mesoporphyrin and zinc as substrates. This method was based primarily on the assay described by Gouya et al (2006). Earlier work was an additional source of information (Li et al 1987, Rossi et al 1988).

In our assay, EBVTL served as a tissue source of FECH. Li et al (1987) originally used homogenated rat liver as tissue. Rossi et al (1988) and Gouya et al (2006) used lymphocytes isolated from peripheral blood.

As our objective was to establish a FECH assay and utilise it in the measurement of FECH activity in the subjects of interest, a description of the assay, together with pertinent results and discussion on the optimisation thereof is included in the following sections.

Materials and methods

Following ethics approval (Appendix A), consenting subjects were provided with information regarding the study (Appendix B). Fifteen ml of heparinised blood was collected from 5 affected subjects - EPP8.1, EPP8.2, EPP8.4, EPP8.5 and EPP8.6.

In addition, samples were obtained from 10 non-EPP controls (clinically and/or biochemically not affected by EPP).

One subject known (identified by Parker et al 2008) to have clinical and biochemical EPP was included as a positive control. This control subject

reported typical EPP-related photosensitivity and had a raised red cell PP of 5160 nmol/L (normal < 2000 nmol/L). Additionally, EPP was confirmed by *FECH* genotyping (Parker et al 2008), which had shown the presence of the IVS3-48C polymorphism in intron 3 and a 757_761delAGAAG 5 base pair deletion in exon 7, which is a known EPP-associated mutation.

EBVTL as an assay source of FECH

B lymphocytes were transformed with EBV as described in Appendix E. EBV, though capable of infecting other cell types, has a specific tropism for B lymphocytes (Bird et al 1981). EBV particles were derived from the B95-8 marmoset monkey cell line (Miller and Lipman 1973). *In vitro*, unchecked by an immune system, EBV drives EBVTL to proliferate by sustained expression of viral proteins (Thorley-Lawson 2001).

It is interesting to reflect on the biology of *in vitro* EBV transformation. Following B lymphocyte infection via the cluster of differentiation (CD)21 receptor (the viral ligand being glycoprotein 350) (Fingeroth et al 1984), EBV establishes a so called 'latent' infection. Viral DNA exists in episomal form within the nuclei of infected cells. Latency contrasts with lytic replication, which rarely occurs in human B lymphocytes *in vitro*. However, latency is a misleading term in so far as viral activity is concerned. Typically, all 9 viral 'latency' proteins are expressed in EBVTL (Thorley-Lawson 2001).

Latency proteins include the EBV nuclear antigen and latent membrane type. Examples of how EBVTL proliferation is stimulated include:

- The resemblance of latent membrane protein 1 to a constitutively active CD40 receptor, culminating in increased nuclear factor kappa beta expression and EBVTL survival
- The ability of latent membrane protein 2 to mimic an intact B cell receptor, so rescuing EBVTL from apoptosis
- EBV nuclear antigen 1 facilitated propagation of viral DNA to the EBVTL progeny

It was decided to use EBVTL (Figure 13) as a source of material for the following reasons:

1. EBVTL, once established in culture, provide a renewable source of cells, allowing enzyme assays to be performed on multiple occasions. This was especially desirable during the initial phase of setting up the FECH assay.
2. EBVTL also provide a renewable source of nucleic acids. DNA extracted directly from peripheral blood is stable and provides sufficient template for multiple assays. RNA, however, is unstable and large quantities are required per assay.
3. EBVTL can be stored under liquid nitrogen for almost indefinite periods of time, allowing future studies to be undertaken.
4. The use of EBVTL as a source of cellular material for measuring enzymes in the haem biosynthetic pathway has previously been validated (Meissner et al 1986, 1991) and EBVTL have been used to measure FECH activity (Gouya et al 2002, Risheg et al 2003).
5. EBTVL culture is regularly performed in the Inherited Metabolic Disease laboratory (Division of Chemical Pathology, UCT and NHLS GSH) for routine diagnostic enzyme assays (i.e. other than FECH).
6. The same quantity of lymphocytes required for a single FECH assay is used for lymphocyte transformation. Thus, for the same level of inconvenience to the blood-donating subject, increased utility is obtained.

Two out of 5 EBVTL cell lines from affected members of family EPP8 were lost during culture due to unknown reasons. Possibilities include failure of the initial EBV infection to become established, bacterial infection, and excess/inadequate media. Repeat blood sampling was not possible. EBVTL cell lines from subjects EPP8.1, EPP8.2, EPP 8.5, 10 normal controls and 1

positive control were established. The fact that 2 cell lines were not established was considered acceptable, in the light of results obtained in the successful cell lines.

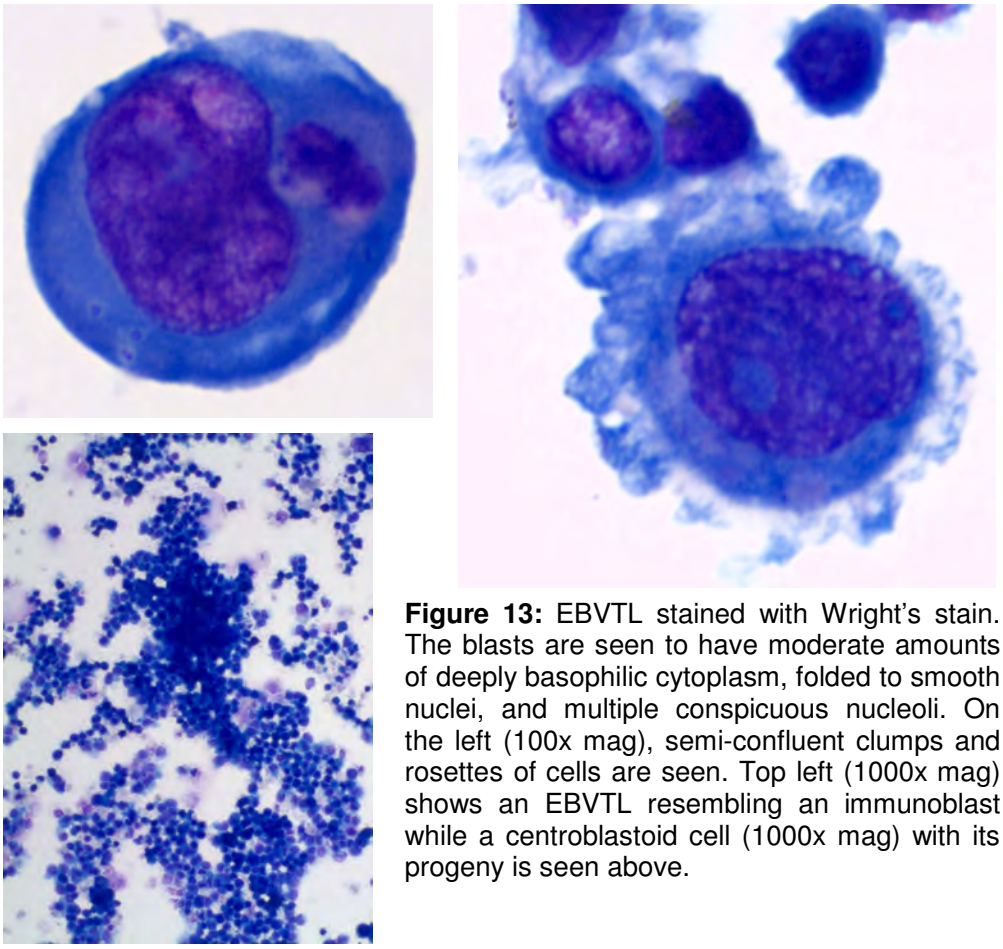

Figure 13: EBVTL stained with Wright's stain. The blasts are seen to have moderate amounts of deeply basophilic cytoplasm, folded to smooth nuclei, and multiple conspicuous nucleoli. On the left (100x mag), semi-confluent clumps and rosettes of cells are seen. Top left (1000x mag) shows an EBVTL resembling an immunoblast while a centroblastoid cell (1000x mag) with its progeny is seen above.

After confirming cellular viability by phase contrast microscopy and the trypan blue exclusion test (Appendix E), EBVTL in culture medium were washed isotonically. This served to remove culture medium-derived protein and any impurities (with potential for fluorescence) which may be included in the medium. Sonication followed, solubilising the mitochondrial FECH (Appendix G). Sonicated protein concentration was determined by the Bradford method (Appendix F), and the samples were diluted appropriately to achieve comparable protein concentrations each time the assay was performed.

FECH enzyme principle

FECH activity was expressed as a rate as Zn meso (product) formation per h per mg of protein at 37 °C. The details of the FECH enzyme assay are described in Appendix G. Mesoporphyrin is a more suitable substrate to use than PP, because it is more soluble and stable than PP. In addition, mesoporphyrin has a lower Michaelis constant (K_M) and a higher maximal FECH activity is recorded, compared to PP as substrate (Li et al 1987). The mesoporphyrin substrate is prepared from the dihydrochloride salt (Figure 14).

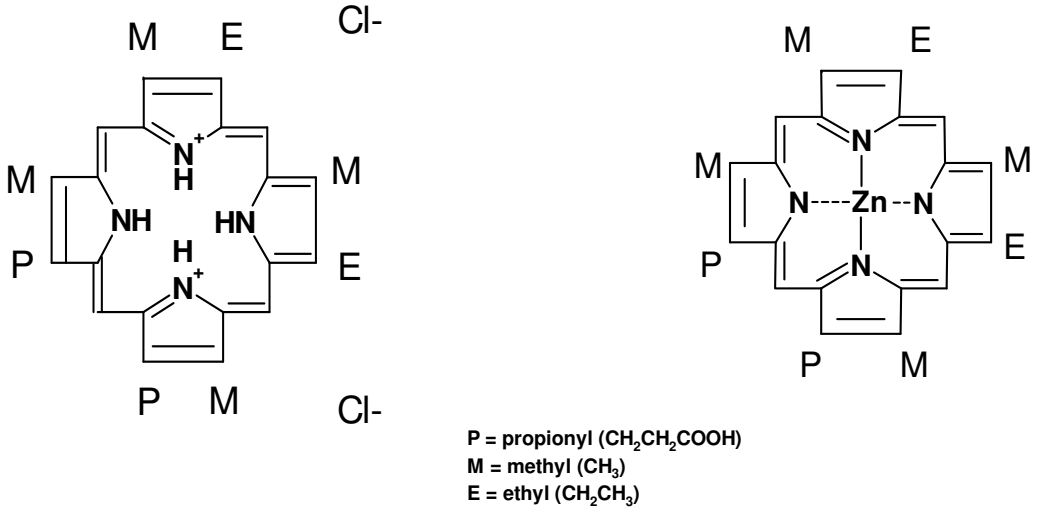

Figure 14: Mesoporhyrin dihydrochloride on the left and Zn meso on the right. The side groups represented by P, M and E are indicated. In the case of PP, the ethyl group is replaced by a vinyl group.

Zn chelation by mesoporphyrin, which occurs both enzymatically and non-enzymaticallly, shifts the fluorescence emission maximum to a shorter wavelength (Figures 15 and 16) and the excitation maximum to a longer wavelength (Figure 17). Zn meso is thus readily distinguishable from its free form. Therefore, after termination of the reaction, Zn meso (present in nmol concentrations) may be measured at an excitation wavelength of 410 nm and an emission wavelength of 580 nm with relatively little interference from free mesoporphyrin (present in µmol concentrations) (Figure 18).

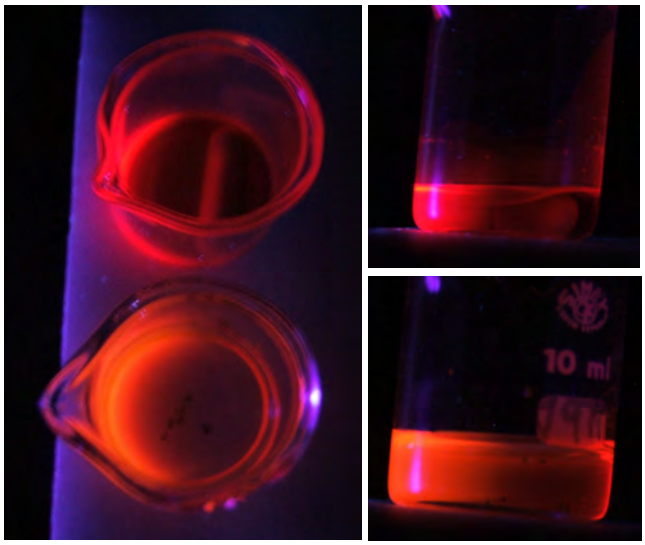

Figure 15: Under ultraviolet irradiation, mesoporphyrin (top, with magnetic stirrer) and Zn meso (bottom) fluoresce at an emission maxima of 620 nm and 577 nm, respectively. The more orange hue of the Zn meso fluorescence can only just be appreciated on this photograph.

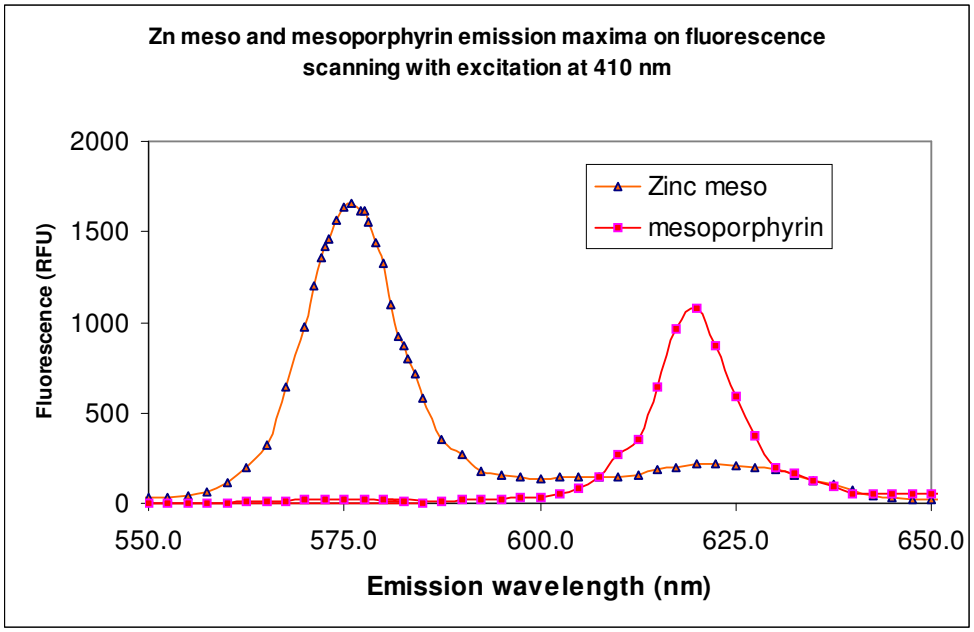

Figure 16: Equimolar concentrations (500 nmol/L) of Zn meso and mesoporphyrin show peak fluorescence at 577 nm and 620 nm, respectively. Both compounds are excited at 410 nm, and the Zn meso fluoresces more intensely here than mesoporphyrin, because excitation is occurring at its excitation maximum.

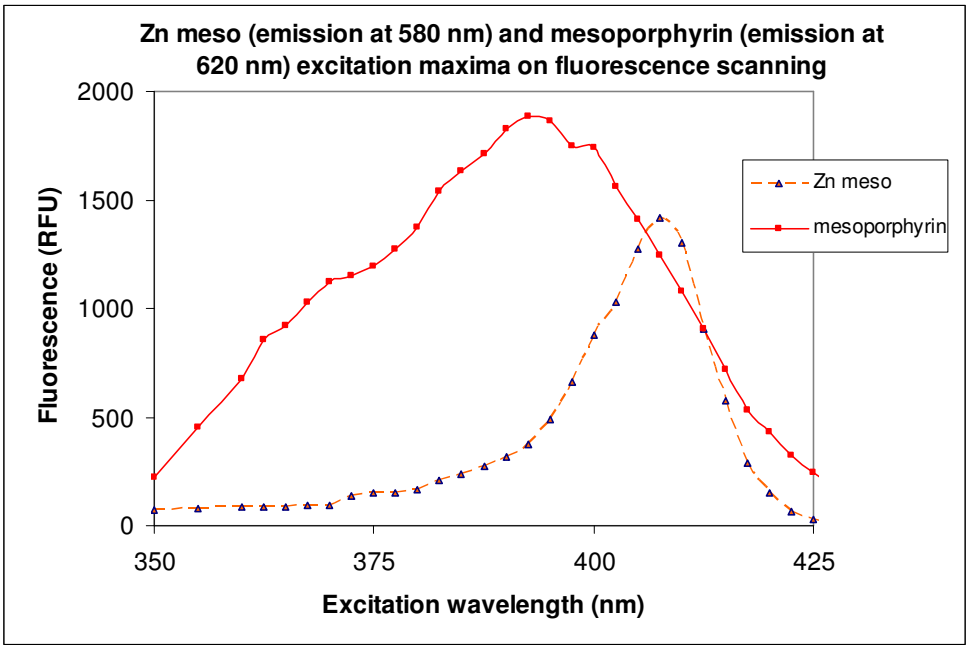

Figure 17: Fluorescence is measured in a range of excitation wavelengths. The mesoporhyrin excitation maximum is at 393 nm and the Zn meso maximum at 408 nm (equimolar concentration of 500 nmol/L). Free mesoporphyrin has a higher specific fluorescence than Zn meso.

After FECH is allowed to react with its substrates for 1 h during the enzyme assay, the fluorescence generated by a blank (with buffer replacing EBVTL sonicate), is subtracted from sample fluorescence. Enzymatic Zn meso formation is quantified using a Zn meso standard curve in which fluorescence is related to a known concentration of Zn meso. An emission wavelength of 580 nm (rather than 577 nm) was chosen to maintain agreement with published methods (Li et al 1987, Rossi et al 1988, Gouya et al 2006). The blank and reaction fluorescence is compared to that of the mesoporphyrin substrate and Zn meso standard in Figure 18.

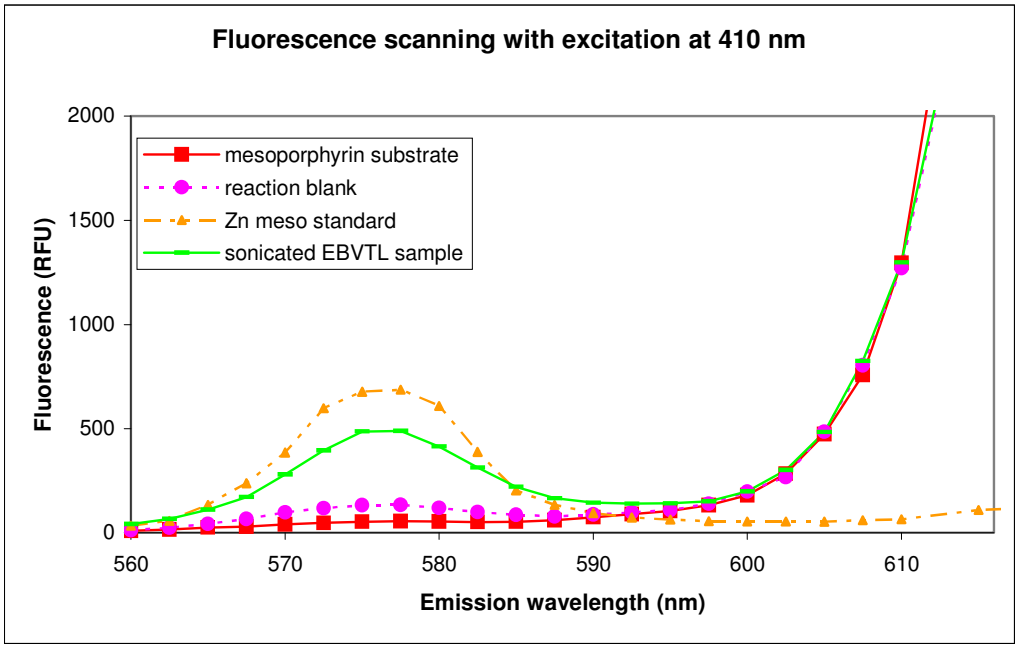

Figure 18: Comparison of emission spectra of 4 assay-relevant mixtures. Note how the blank fluorescence at 580 nm is composed of a small mesoporphyrin tail and some Zn meso formed by autochelation. The sonicated EBVTL sample was scanned after 1 h of incubation with substrate.The Zn meso standard contains 180 nmol/L Zn meso.

FECH assay variables and optimisation

In order to ensure that the FECH assay was fully optimised and that maximal enzyme velocity was being measured, selected methodological variables were investigated.

a) Method of cell lysis to solubilise FECH

Whereas it is vital that FECH be released from mitochondria for assay, excessive sonication may thermally denature enzymes. Homogenisation is an alternative method of enzyme solubilisation, but is more tedious. Gouya et al (2006) used homogenisation while Rossi et al (1988) used sonication. Hence FECH activity was compared over varying sonication times (20 sec x1, 20 sec x2, 20 sec x3: in all cases at 3 watt), with homogenisation, and with sonication at 15 one sec bursts of 30% output.

b) Comparison of FECH activity: lymphocytes and EBVTL

In theory, EBVTL and peripheral lymphocytes may exhibit differing FECH activities. Using zinc and mesoporphyrin as substrates to measure FECH activity, Gouya et al (2002) showed similar results when using EBVTL and lymphocytes as tissue sources.

However, as most authors (Rossi et al 1988, Gouya et al 2006) describe the use of lymphocytes to measure FECH activity, some form of comparison was necessary. EBVTL and peripheral lymphocytes from the same study subject were not available and could not be directly compared. However, peripheral lymphocytes were isolated (Appendix E) from 1 clinically normal subject and FECH activity was measured as an indication of lymphocyte FECH activity under our assay conditions.

c) Accuracy of the Bradford protein assay

The accuracy of the protein assay was assessed by measuring protein concentration in internal quality control material (U1 and U2 – Bio-Rad QC)

with assigned concentrations, using the Bradford method (Appendix F). This served to investigate the accuracy of the protein determination used in the determination of FECH activity over the concentration range experienced in our assay material.

d) Palmitic acid activation of FECH

The assay includes palmitic acid. Fatty acids (primarily palmitic acid) are known to activate FECH, which is useful in optimising assay conditions. The mechanism has not been elucidated but may involve the creation of a suitable micro-environment for catalytic activity. Taketani and Tokunaga (1981) hypothesise that it is due to the carboxyl groups of the palmitic acid which aid the approach of the porphyrin molecule to the catalytic site of FECH, perhaps by keeping porphyrins in solution. Addition of a detergent such as Triton X-100 is essential to dissolve palmitic acid. Varying palmitic acid concentrations in the final reaction mixture have been used: 0.70 mmol/L - reported as optimal (Li et al 1987), 0.89 mmol/L – reported as optimal (Rossi et al 1988) and 0.76 mmol/L (Gouya et al 2006). Thus the FECH activity at varying palmitic acid concentrations was measured to determine optimal activity in our laboratory.

e) Optimum pH used for FECH reaction

An experiment was performed to compare a pH of 7.6 in the FECH enzyme assay as used by Gouya et al (2006) with the pH of 8 used by Rossi et al (1988).

f) Volume of stopping solution used to terminate reaction

The volume of dimethyl sulfoxide (DMSO) / methanol solution needed to terminate enzyme activity, and the need to transfer 1 ml of supernatant into the fluorimetry cell (Appendix G) were factors which prompted the determination of an optimum stopping solution volume. By adjusting volumes of Zn meso standard, sonication/incubation buffer and stopping solution, a

constant Zn meso concentration could be maintained while increasing the volume (and % volume contribution) of stopping solution to the final mixture which is transferred into the fluorimetry cell.

g) FECH interassay variability

Reasonable reproducibility of EBVTL enzyme activity over time is essential for assay validity. However, fluxes in the growth and viability state of the EBVTL culture may occur and thus may influence activity. Hence, FECH activity from the same culture was assayed in 4 EBVTL cell lines over a 2 month period in order to establish reproducibility.

FECH assay of study subjects and controls

After assay optimisation, EBVTL FECH activity was determined for 10 normal control subjects, 1 genotyped EPP positive control and 3 study subjects (see "FECH enzyme principle" above and Appendix G).

Data analysis

FECH activity measurements (Table 7) were performed in triplicate to increase the precision of the results and the mean calculated.

Data generated were plotted, and graphs constructed using Microsoft *Excel.*

Statistical comparison of FECH enzyme data of 10 normal controls and 3 study subjects from the family EPP8 was conducted using Statsoft *Statistica*.

Results

FECH assay variables and optimisation

a&b) Homogenisation vs sonication yields comparable results, but as higher activities are obtained with shorter periods of sonication time, it is important to minimise rather than maximise the sonication period. Activity for lympocytes is similar to that of EBVTL (Table 5).

Table 5: FECH assay variables

Sample	Method	FECH activity (nmol/h/mg protein at 37°C)
Comparison of homogenisation and sonication		
Control 4	Homogenisation	1.07
Control 4	Sonication 3W x20 sec x3	1.10
Comparison of sonication time		
EPP8.2	Sonication 3W x20 sec x1	1.37
EPP8.2	Sonication 3W x20 sec x2	1.20
EPP8.2	Sonication 3W x20 sec x3	1.21
EPP8.2	Sonication 15 one sec bursts of 30 % output	1.40
Lymphocytes as tissue medium		
Control Lymphocytes	Routine assay (Appendix G)	1.32

c) Protein measurement of internal quality control material by the Bradford method showed values within 2 SD of the assigned mean – and thus considered acceptable (Table 6).

Table 6: Bradford protein assay accuracy			
Sample	**Assigned conc (mg/L)**	**Assigned conc SD (mg/L)**	**Measured conc (mg/L)**
U1 Bio-Rad QC	172	14	151
U2 Bio-Rad QC	616	49	591

d) FECH activity in a range of palmitic acid concentrations shows optimum activation at 0.76 mmol/L (Figure 19).

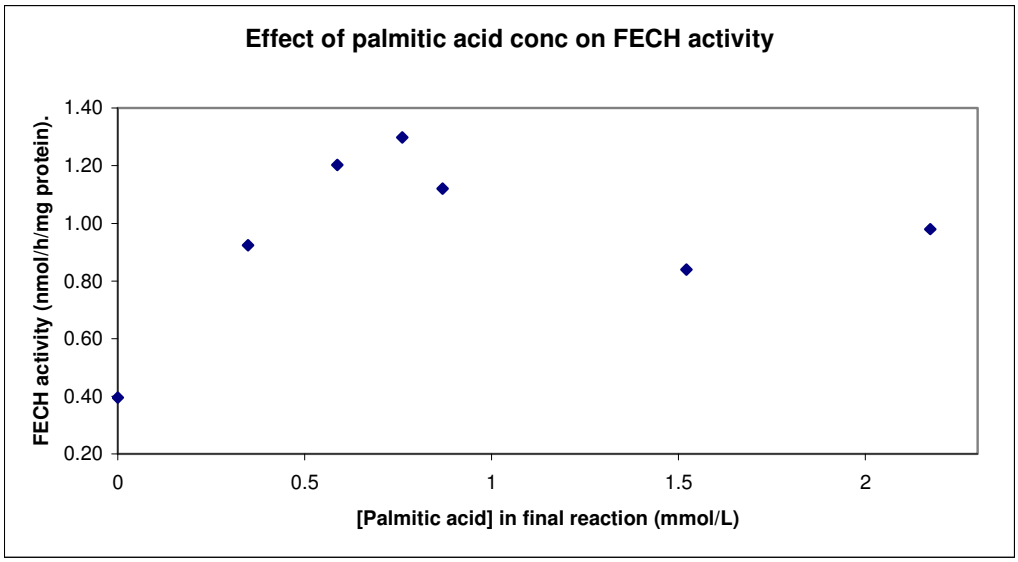

Figure 19: FECH activity as a function of varying palmitic acid concentration. (Data points obtained from a single experiment). EBVTL from control 6 has been used as a source of FECH.

e) A pH of 7.6 was considered optimum for FECH, based on the typical pH ranges reported (Rossi et al 1988, Gouya et al 2006). No difference in activity over a pH 7.6 – 8.0 range was noted (data not shown).

f) An experiment to determine variation of fluorescence as a function of the % volume contributed to the final assay mixture by the stopping solution, showed an 8% variation, with no particular trend. This was considered within experimental error. A range of stopping solution volumes could be used, but 1000 µl was established as the most convenient.

g) Assay reproducibility was assessed on at least 3 occasions during a 2 month time period in 4 EBVTL cell lines (2 controls, 2 subjects) and found to be reproducible with a coefficient of variation of 12% (data not shown).

The final optimised assay conditions which were employed (Appendix G) in order to establish FECH activity in family EPP8 were similar to that used by Gouya et al (2006) – the only distinct difference being that sonicated EBVTL rather than homogenised lymphocytes were used.

Experimental FECH results

FECH enzyme activities in normal controls, the genotyped EPP positive control and affected subjects from family EPP8 are shown in Table 7. No significant differences between FECH activities in the normal controls and in members of family EPP8 are apparent.

Table 7: FECH activity in controls and family EPP8 subjects

Sample	**FECH activity (nmol/h/mg protein at 37°C)**
Normal control 1	1.14
Normal control 2	1.34
Normal control 3	1.26
Normal control 4	1.14
Normal control 5	1.24
Normal control 6	1.11
Normal control 7	1.23
Normal control 8	1.09
Normal control 9	1.58
Normal control 10	1.38
Normal control mean ± standard deviation = 1.25 ± 0.15 (nmol/h/mg protein at 37 ° C)	
Genotyped positive EPP control	0.23
EPP8.1	1.15
EPP8.2	1.49
EPP8.5	1.08

Discussion

The FECH activity assay, (Gouya et al 2006), was suitable for measuring FECH activity from EBVTL. The assay required very little modification, was optimised as described above and was capable of detecting significant aberrations in FECH activity from lymphocyte-derived material.

The mean normal FECH activities previously reported were 3.25 (Rossi et al 1988) and 4.83 (Gouya et al 2006) nmol/h/mg protein at 37 °C, respectively. This corresponded to a 2.6 and 3.9 fold higher mean FECH activity measurement than that recorded here (1.25 nmol/h/mg protein at 37 °C). A significant interlaboratory bias, which ultimately could not be explained, was present. However, the use of a standard curve to quantify Zn meso concentration suggests that general 'laboratory' variation such as instrumentation used, was not causative. Similarly, although Zn meso fluorescence was measured at an emission wavelength of 580 nm and not at its peak (577 nm), standard and sample fluorescence should be affected equally, resulting in accurate measurement. The FECH assay was fully optimised, true maximal FECH velocity was being measured, and protein measurement was accurate and representative of functional FECH.

One positive EPP control was investigated in order to validate the assay as a means with which to diagnose FECH-deficient EPP. This positive control was known to carry the *FECH* IVS3-48C polymorphism and 757_761delAGAAG mutation. FECH activity was significantly decreased compared to the normal control group (18%, expressed as a percentage of the normal mean). This is consistent with the 10 – 30% range for FECH activity in autosomal dominant EPP (Gouya et al 2006). Based on this result we were satisfied that the assay was capable of functioning as a diagnostic tool. Due to time-constraints and the lack of easily available tissue, it was not considered necessary to add further EPP patients to a positive control cohort.

Importantly, subjects EPP8.1, EPP8.2 and EPP8.5 did not have significantly different FECH activities when compared to the control group ($p = 0.735$,

Mann-Whitney U-test). Thus, it was apparent that a reduction in FECH activity was not the likely primary cause of the porphyria in these patients. This is consistent with the other atypical findings discussed in Chapters 2 and 3. These findings, together with those of Parker et al (2008) in which no DNA variant in the *FECH* gene was noted in this family, were strongly suggestive of a disease locus distinct from *FECH*.

Conclusion

1. A FECH enzyme activity assay was successfully established in our laboratory. It was reproducible, optimal and was capable of distinguishing between normal and FECH-deficient EPP subjects. The assay may thus be used to aid in the diagnosis or exclusion of EPP.
2. Three subjects from family EPP8, with clinical and biochemical evidence of protoporphyria, were found to have FECH activity within the normal range.
3. This result supports the suggestion that the disease locus in family EPP8 is distinct from *FECH*.

CHAPTER FIVE

ALAS2 and X-linked dominant protoporphyria

Introduction

As set out in the section entitled 'Additional aims and objectives' (Chapter 2), in the light of no apparent FECH involvement in the disease, the objective was redirected to search for non-FECH genes/loci/disease mechanisms in order to explain the protoporphryria observed in family EPP8.

In Chapter 2 we indicated that international collaboration had been established in 2007 with researchers in Wales (University of Cardiff) and France (Centre Francais des Porphyries). They had noted and investigated atypical EPP patients with a porphyric syndrome very similar, if not identical, to those found in family EPP8.

At the time of conducting FECH activity measurements which the previous chapter has detailed, a seminal discovery was made – an alternative disease-causing locus was identified. Mutations in the erythroid specific *5-aminolevulinate synthase* (*ALAS2*) gene were present in affected members of family EPP8 and 7 other families abroad and resulted in a gain of function in ALAS2 (Whatley et al 2008).

The realisation that a mutation in the first enzyme in the haem biosynthetic pathway was porphyria-causing, brought about a paradigm shift in the investigations described in the remainder of this dissertation; allowing the additional aims and objectives outlined in Chapter 2, to be developed.

With the alternative disease locus identified, and with the lack of evidence for *FECH* mutations (Parker et al 2008) or FECH enzyme dysfunction in family EPP8 (see above), it was decided unnecessary to further investigate FECH at RNA or protein level.

ALAS2 and X-linked dominant protoporphyria

In the international collaboration 8 families exhibiting features of an atypical protoporphyria syndrome were identified – this included our family EPP8 (Whatley et al 2008). Examination of family pedigrees revealed an X-linked inheritance pattern. Using a candidate gene approach, 2 disease-causing frameshift mutations in *ALAS2* exon 11 were found: coding sequence (c.)1706-1709 delAGTG in family EPP8 and 5 other families; and c.1699-1700 delAT in 2 families. Expression of the *ALAS2* mutations in a prokaryotic system showed that both ALAS2 activity and porphyrin synthesis were markedly increased. The atypical protoporphyria syndrome resulting from a gain of function mutation in *ALAS2*, was named X-linked dominant protoporphyria (XLDPP). The dominant inheritance pattern and almost 100% penetrance observed, was caused by this gain in ALAS2 function.

Although mutational analysis of *ALAS2* exon 11 in family EPP8 was performed by Whatley et al (2008), samples from subjects EPP8.3, EPP 8.10 and EPP 8.11 had not been available at that study. The need to offer DNA based diagnoses to these 3 subjects, and any other patients who might warrant investigation for XLDPP, prompted us to establish a method for *ALAS2* exon 11 mutational analysis in our laboratory.

The *ALAS2* gene

The reaction catalysed by ALAS2, its regulation in erythroid tissue, and the importance thereof in establishing flux through the haem biosynthetic pathway, have been detailed in Chapter 1.

The human *ALAS2* gene is ~ 23 000 base pairs (bp) in size (Ensembl Human Geneview) and a diagram depicting its organisation is presented in Figure 20. The coding sequence consists of 1761 bp for 587 amino acids. The *ALAS2* promoter includes GATA-1 and EKLF binding sites. Intronic enhancer sequences with the ability to bind GATA-1 are found in introns 1 and 8 (Sadlon et al 1999).

Exon 2, the first coding exon, contains the mitochondrial signal sequence which is cleaved during translocation into the mitochondrial matrix. Alternative splicing causes the exclusion of exon 4 to yield an mRNA isoform which constitutes ~ 40% of total ALAS2 mRNA. This isoform produces a functional enzyme, with mildly reduced catalytic activity. Other minor isoforms are also described, yielding truncated and probably non-functional ALAS2 (Cox et al 2003).

Mutations in *ALAS2* are numbered and named using the coding sequence numbers, commencing with the ATG start codon in exon 2. *ALAS2* exons 5 - 10 encode the catalytic domain and numerous loss of function mutations have been reported, resulting in XLSA (Sadlon et al 1999). Earlier work has suggested that the catalytic domain would include exon 11 (Cox et al 1991, Sadlon et al 1999, Cox et al 2004), but this could not be proved by crystallography. The only crystal structure available for ALAS (Astner et al 2005) is a bacterial (*Rhodobacter capsulatus*) ALAS which does not include exon 11. Intriguingly, a loss of function missense mutation in exon 11 (S568G), in very close proximity to the 2 gain of function XLDPP mutations, has been reported (Harigae at al 1999). In the light of the exon 11 mutations described in XLDPP, the suggestion is that the C-terminus appears, in some way, to modulate enzyme activity (Whatley et al 2008).

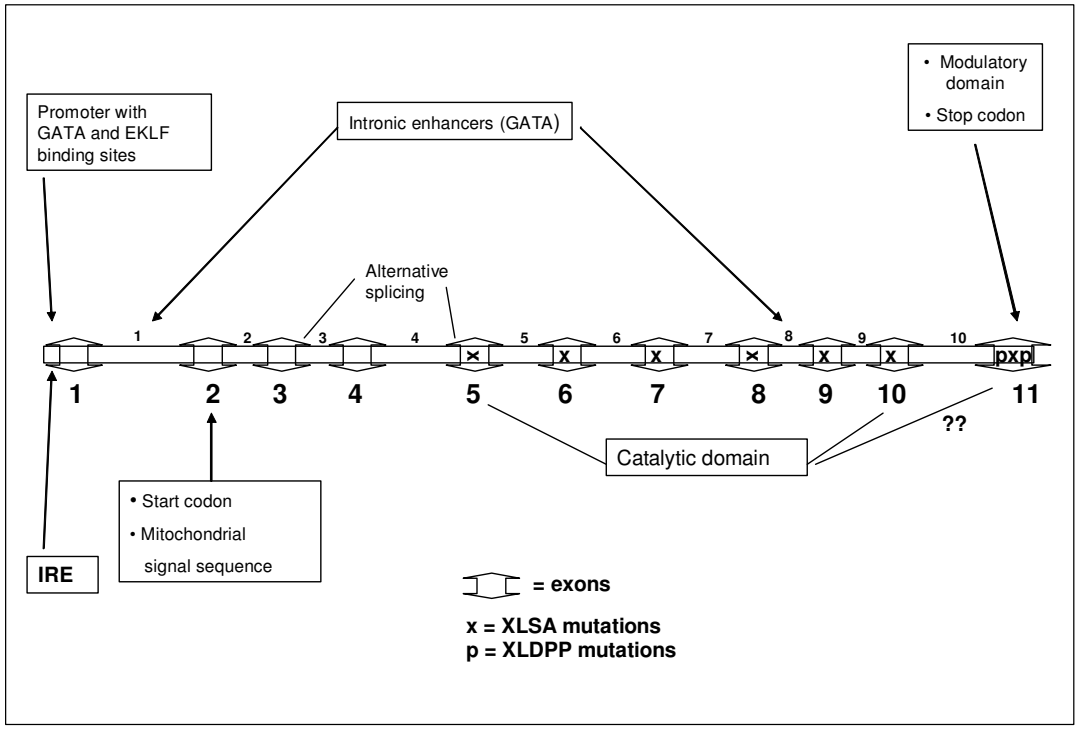

Figure 20: Human *ALAS2* gene organisation showing the promoter, containing binding sites for erythroid transcription factors (GATA, EKLF). An iron response element (IRE) is located in the 5' UTR. Also shown are 11 exons, 10 introns, other relevant sequences (discussed in text) and mutations causing XLSA in exons 5 – 11 (adapted from Sadlon et al 1999). Mutations in exon 11 causing XLDPP are indicated. Question marks refer to postulated catalytic modulation by the C-terminal domain located in exon 11 (Whatley et al 2008).

Materials and Methods

DNA was extracted from EDTA blood samples (Appendix H). Subjects EPP8.8 and EPP8.7 (non-related spouses of affected family members) were included as family controls and used as wild type (WT) DNA.

The genomic *ALAS2* sequence was accessed on Ensembl Human Geneview: Ensembl number 00000330807; sequence = ALAS2-006 (http://www.ensembl.org).

The mRNA *ALAS2* sequence was accessed on Genbank: Accession number NM000032.4; non splice variant sequence = isoform a (http://www.ncbi.nlm.nih.gov).

A 417 bp fragment from exon 11 was chosen for amplification by PCR (Appendix J) to enable inspection of the entire exon and flanking introns. Figure 21 illustrates the *ALAS2* exon 11 region, relevant mutations and sequences of interest.

cacggcacacacagaagcaaacagtaggctacttctggccctgaggtatcttgaagggttgaggggg

atcaatatcttggctcatctgtactgtgacagatttggaagatctagtctaacccatttttccctccctcccctaccacct

tcagAGAAGCTGCTGCTGGCTTGGACTGCGGTGGGGCTGCCCCTCCAGGATGT

GTCTGTGGCTGCCTGCAATTTCTGTCGCCGTCCTGTACACTTTGAGCTC**AT**G

AGTG**AGTG**GGAACGTTCCTACTTCGGGAACATGGGGCCCCAGTATGTCA

CCACCTATGCC**TGA**GAAGCCAGCTGCC**TAG**GATTCACACCCCACCTGCGC

TTCACTTGGGTCCAGGCCTACTCCTGTCTTCTGCTTTGTTGTGTGCCTCTAGCT

GAATTGAGCCTAAAAATAAAGCACAAACCACAGCAtgtgaagccttttattggacagggaaca

gacaagtgcattctgactccctcagacaagtggcagatctatgaggtaaccataggtcacttgttggtcaccattccatt

ttaccaacagggaaacagaatgagaaagaggaaggaaatgcccaaaaa

Figure 21: *ALAS2* exon 11 WT sequence (upper case) and flanking introns (lower case). The numbered exon 11 sequence commences with the boxed A base (c.1601). Complementary intronic sequences to forward and reverse primers for the 417bp fragment amplification are underlined and in blue. The 4 bp AGTG deletion relevant to family EPP8 is indicated in red and boxed. The other XLDPP causing AT deletion is doubly underlined and indicated in red. The S568G mutation in codon 568 (AGT) is dotted and causes XLSA (Harigae et al 1999). The *ALAS2* WT stop codon (TGA) is indicated in green and underlined; preceded by the final coding C base (boxed, c.1761). The alternative distal stop codon (TAG) created by the c.1706-1709 delAGTG mutation is shown in green. The premature stop codon (TGA) created by the c.1699-1700 delAT mutation is indicated in pink - located immediately before and shares the first base of the boxed AGTG region.

Primer sequences used for the PCR were as follows (design discussed in Appendix I):

- Forward: 5' – ctt ggc tca tct gta ctg tg – 3'
- Reverse: 5' – gga gtc aga atg cac ttg tc – 3'

A temperature gradient PCR (discussed in Appendix I) was run to determine the optimal annealing temperature empirically.

Polyacrylamide gel electrophoresis (PAGE) was used to confirm amplification of the desired 417bp fragment (Appendix K). Whilst agarose gel electrophoresis would be an easier alternative to PAGE to be used as a checking gel, we elected to use PAGE because of personal and laboratory preference.

Direct sequencing of the 417 bp fragment was used to identify any sequence variation. Restriction digestion based analysis was not performed because the c.1706-1709 delAGTG mutation does not create or abolish a restriction site (as verified with NEBcutter V2.0, New England Biolabs, http://tools.neb.com/NEBcutter2/index.php). Prior to sequencing, amplicons were purified (Appendix L) and prepared as per the requirements of the University of Stellenbosch Central Sequencing Facility (Appendix M).

Results

Figure 22 shows PAGE of a temperature gradient PCR. An annealing temperature of 52 °C was selected. Amplification and PAGE of DNA from family EPP8 is shown in Figure 23. Heteroduplexes were observed in affected female subjects.

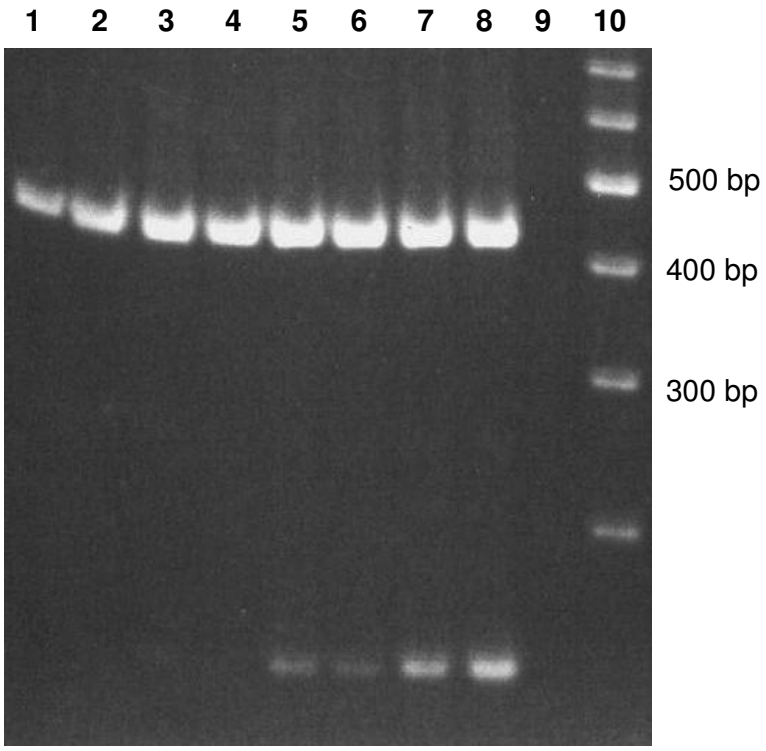

Figure 22: PAGE (6%) of gradient PCR, *ALAS2* exon 11 using control DNA. Non-specific product formation ~ 150bp in size is seen in lanes 5 – 8. Optimum amplicon formation was identified in lane 3.

Lane 1: 56 ℃

Lane 2: 54 ℃

Lane 3: 52 ℃

Lane 4: 50 ℃

Lane 5: 48 ℃

Lane 6: 46 ℃

Lane 7: 44 ℃

Lane 8: 42 ℃

Lane 9: Blank

Lane 10: 100bp DNA ladder

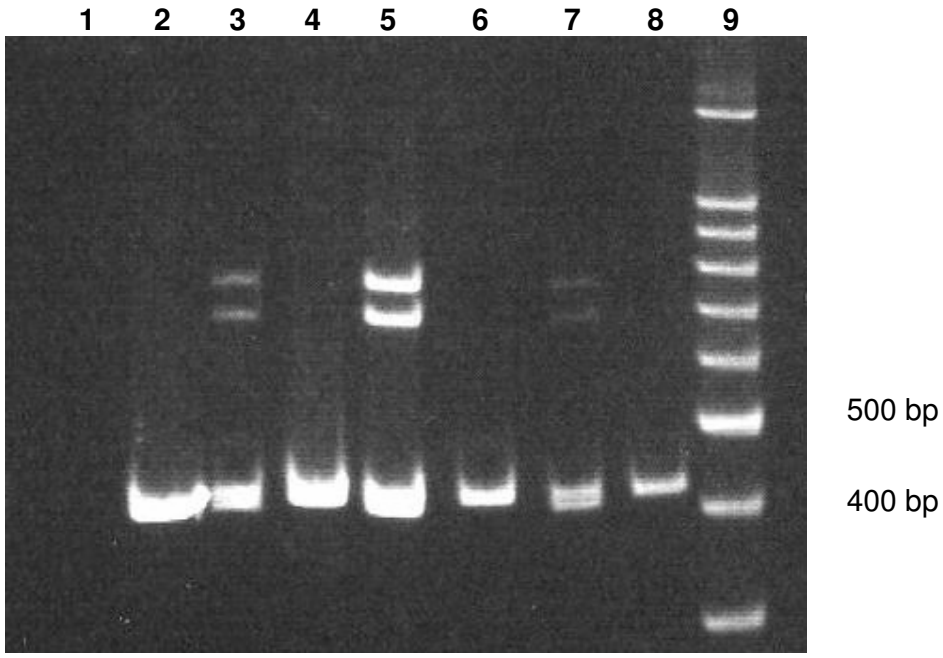

Figure 23: PAGE (6%) confirms amplification of the 417 bp product from members of family EPP8 and controls. Two different heteroduplexes migrating at ~700 /780 bp positions are seen in lanes 3, 5 and 7. Separation of 2 bands migrating at ~ 415 bp can only just be visualised in lane 7.

Lane 1: Blank

Lane 2: Subject EPP8.2 (affected male)

Lane 3: Subject EPP8.6 (affected female)

Lane 4: Subject EPP8.7 (family control, male)

Lane 5: Subject EPP8.5 (affected female)

Lane 6: Subject EPP8.9 (unaffected male)

Lane 7: Subject EPP8.1 (affected female)

Lane 8: Subject EPP8.8 (family control, female)

Lane 9: 100 bp DNA ladder

Figures 24 – 26 shows partial sequencing results from a family control and subjects affected by the c.1706-1709 delAGTG mutation. The results of *ALAS2* exon 11 mutational analysis of family EPP8 correlated with clinical/biochemical data, are presented in Table 8.

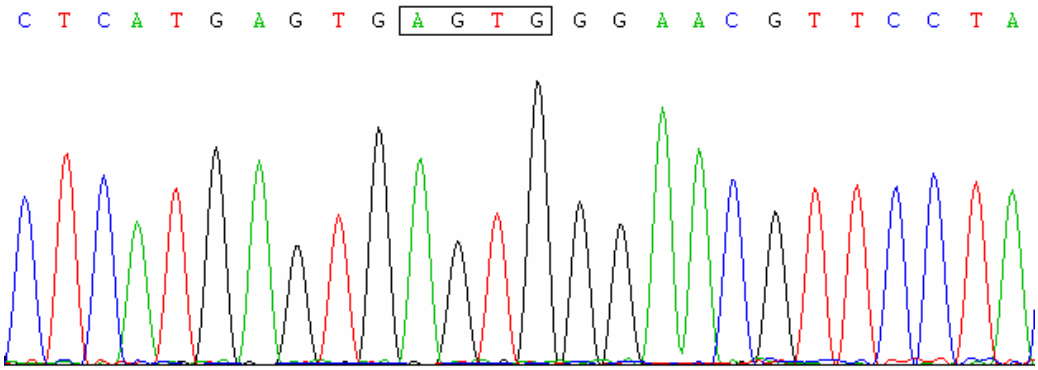

Figure 24: Partial direct sequence of WT *ALAS2* exon 11 using forward primer. The 4 bp which are deleted in c.1706-1709 delAGTG, have been boxed.

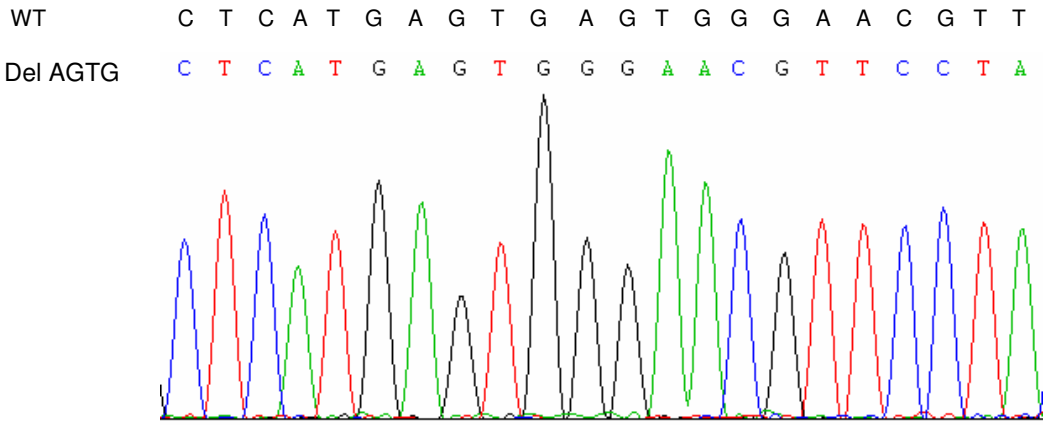

Figure 25: Partial direct sequence of c.1706-1709 delAGTG *ALAS2* exon 11 using forward primer in subject EPP8.2 (affected male). The WT sequence is shown above the mutant for comparison.

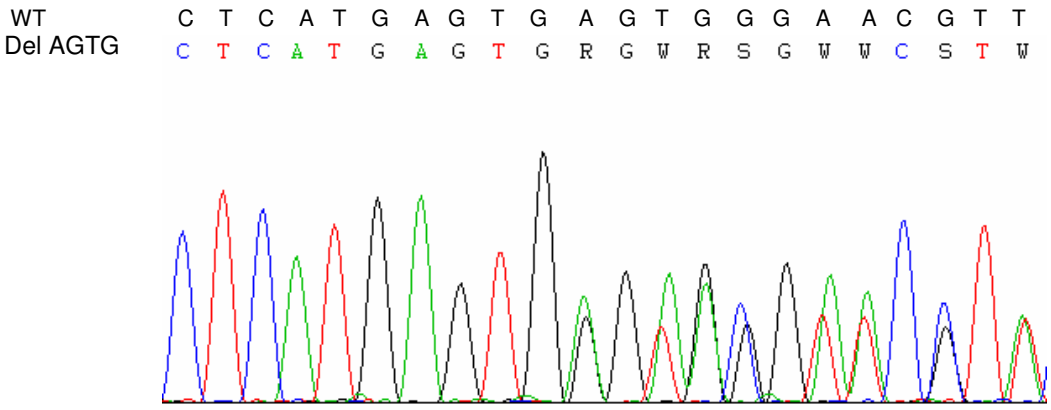

Figure26: Partial direct sequence of c.1706-1709 delAGTG *ALAS2* exon 11 using forward primer in subject EPP8.5 (affected female).The WT sequence is shown above the mutant for comparison.

Table 8: *ALAS2* exon 11 mutational analysis results

Subject	Protoporphyric phenotype	Mutational Status
EPP8.1	Affected	c.1706-1709 delAGTG
EPP8.2	Affected	c.1706-1709 delAGTG
EPP8.3	Unaffected	WT
EPP8.4	Affected	c.1706-1709 delAGTG
EPP8.5	Affected	c.1706-1709 delAGTG
EPP8.6	Affected	c.1706-1709 delAGTG
EPP8.7	Family control	WT
EPP8.8	Family control	WT
EPP8.9	Unaffected	WT
EPP8.10	Unaffected	WT
EPP8.11	Unaffected	WT
EPP8.12	Affected	Not available (deceased)
EPP8.13	Asymptomatic	

Discussion

Exon 11 PCR analysis of the *ALAS2* gene was successfully performed as described.

Five family members had the c.1706-1709 delAGTG mutation, all of whom were clinically and biochemically affected. The molecular result was diagnostically useful, and allowed clinicians to understand and rationalise the disease better. This had significant implications for family EPP8, permitting clinical dialogue with family members. Issues discussed included the c.1706-1709 delAGTG mutation, postulated pathogenesis, mode of inheritance and assessment of genetic risk to future generations (Appendix N).

In subjects carrying the c.1706-1709 delAGTG mutation, interesting differences between male and female PAGE and sequencing results were seen. Males are hemizygous for genes on the X chromosome, while females may be homozygous or heterozygous. Thus, in the presence of a mutation on the X chromosome, heteroduplexes (on PAGE) and overlapping ddNTP signals (sequencing) is only seen in females. Heteroduplexes (Figure 23) are seen as 2 different bands, interpreted as 2 different double stranded DNA structures - sense and antisense WT, hybridised with its complementary delAGTG strand.

Furthermore, in heterozygous females, the 417 bp and 413 bp fragments can be seen as separate bands when resolution was improved by loading less DNA (Figure 23, lane 7). Other strategies may also be employed to improve resolution between fragments of differing size on PAGE (discussed in Appendix K), such as redesigning the PCR to generate a shorter fragment. In such manner detection of the c.1706-1709 delAGTG mutation without the need for sequencing may be possible, even in males – similar to the commonly employed amplicon size discriminatory technique used as a diagnostic method for the ΔF508 cystic fibrosis mutation. However, because the region of interest contains at least 3 different mutations in very close proximity, the utility of sequencing would remain.

ALAS2 exon 11 mutational analysis of family EPP8 was in keeping with their phenotypic presentation. That is, we only observed clinical and biochemical evidence of protoporphyria in mutation-positive subjects (Table 8). Although not normalised for factors such as iron status, it was interesting to note that the red cell PP determinations obtained at the time of this investigation (Table 3 in Chapter 3) seemed to indicate that the highest concentrations correlated with the most severe reported skin disease.

The c.1706-1709 delAGTG mutation is predicted to cause a frame shift in 24 codons distal to the 4 bp mutation (p.E569GfsX24), resulting in the extension of ALAS2 by 4 amino acids. In contrast, the c. 1699-1700 delAT mutation leads to a frameshift mutation in 2 codons (p.M567EfsX2) and a truncation of ALAS2 (Whatley et al 2008). It is interesting that a single bp substitution in this same region (S568G) reportedly causes a loss of function in ALAS2, manifesting as XLSA (Harigae et al 1999). This mutation is located between the 2 XLDPP-causing mutations, as depicted in Figure 21. It is surprising that mutations in such close proximity, can have diametrically opposite effects.

The exact mechanism by which the XLDPP mutations increase ALAS2 activity, has not been determined. Iron as substrate has been postulated to become rate-limiting, leading to PP accumulation (Whatley et al 2008). This is discussed in the next chapter, in the light of iron treatment in subject EPP8.2.

Conclusion

1. This study confirmed the presence of the c.1706-1709 delAGTG mutation in family EPP8. Furthermore, additional subjects not available to the initial published investigation (Whatley et al 2008) confirmed the mutation to be disease-associated.
2. DNA based detection of c.1706-1709 delAGTG was extremely useful in the investigation of porphyria in subjects from family EPP8 and allowed better understanding of the disease, with concomitant benefit to the patients and their family.

CHAPTER SIX

Iron treatment in XLDPP

Better knowledge of the molecular pathogenesis in XLDPP allowed the investigation of potential treatment in the form of iron supplementation, and is described here. Hence, this section of the study was aimed at exploring the effect of iron supplementation on PP metabolism and thereby assisting our understanding of the condition. The data are presented with the kind permission of the clinician responsible for the care of subject EPP8.2, Dr M Sonderup (Department of Medicine, UCT and GSH) (Sonderup et al 2009).

Introduction

Bone marrow biopsy (November 2007, Chapter 3) of patient EPP8.2, showed decreased iron stores. Serum iron biochemistry (December 2007, at initial GSH evaluation, Chapter 3) was difficult to interpret in view of an acute phase response and hepatic damage, but was suggestive of iron deficiency. There was no obvious recent cause of iron loss (e.g. haemorrhage), iron supplementation or blood transfusion preceding this documentation of iron deficiency.

It was postulated that in XLDPP iron availability becomes rate limiting for FECH activity because of increased flux of the haem biosynthetic pathway due to increased ALAS2 activity (Whatley et al 2008). In light of evolving information which became available at the time of the discovery of the *ALAS2* mutations, it was considered mandatory to ensure that subject EPP8.2 was iron replete.

Prior to the intravenous iron replacement discussed in this chapter, iron stores were supplemented by way of blood transfusions in April 2008. This was necessary because of haemorrhage related to a gall bladder/liver fine needle aspirate biopsy in the context of portal hypertension. Sepsis and the anaemia of chronic disorders may have contributed to the anaemia.

Anaemia or iron overload have not been associated with the syndrome of XLDPP, apart from a single patient who developed iron deficiency anaemia as a consequence of bleeding from a gastric ulcer (Whatley et al 2008). In

that patient, a decline (though not a normalisation) in red cell free PP concentrations paralleled treatment and resolution of iron deficiency anaemia with oral iron supplementation.

Although the mean haemoglobin concentration and red cell volume was normal in XLDPP patients, iron studies were in keeping with iron deficiency - particularly in male subjects (Whatley et al 2008). Mean serum ferritin and transferrin saturation were decreased, while soluble transferrin receptor concentration was increased. These results were significant ($p < 0.05$) when compared to those obtained from unaffected relatives. Similar serum iron parameters have been recorded in subjects from family EPP8, e.g. subject EPP8.4 (Table 4). As stated in Chapter 3, the ability of intravenous iron to decrease photosensitivity temporarily (sustained subjective symptom relief for up to 4 months in subject EPP8.6, and 1 year in subject EPP8.1), was noted by affected subjects from family EPP8. This was confirmed by treating clinicians. Interestingly, patients insisted that oral iron treatment did not achieve an effect similar to that of the intravenous form. Indeed, before knowledge of the c.1706-1709 delAGTG mutations in *ALAS2* was available, response to iron constituted one of the atypical features in family EPP8. Iron treatment described here was part of the overall and complex management of patient EPP8.2, as described in Chapter 3.

Method

Two hundred mg elemental iron was infused intravenously on 4 occasions into patient EPP8.2. The first 3 of these infusions were clustered together over a period of 5 days at the end of May to the beginning of June 2008. Serum iron biochemistry (using routine automated methods) and red cell PP concentrations (Appendix C) were measured over the ensuing 2 months to assess response.

Intravenous iron was in the form of *Venofer,* an iron sucrose complex with a MW of 34 000 – 60 000. This complex is taken up by the reticuloendothelial

system (RES) and dissociated into iron and sucrose, resulting in a relatively short half life of 6 hr (www.venofer.com).

Results

Data generated during iron treatment of patient EPP8.2 are displayed in the following series of figures (Figures 27 – 31).

Figure 27 documents the rapid increase in serum iron concentrations following iron administration. Figure 28 shows a modest reduction in serum transferrin concentrations. This results in a marked increase in serum transferrin saturation with iron treatment, as seen in Figure 29. The increase in iron stores is reflected in the increase in serum ferritin (Figure 30).

Red cell PP response during iron treatment is presented in Figure 31. After an initial dramatic increase, PP concentrations decrease during iron treatment, but do not reach the reference interval.

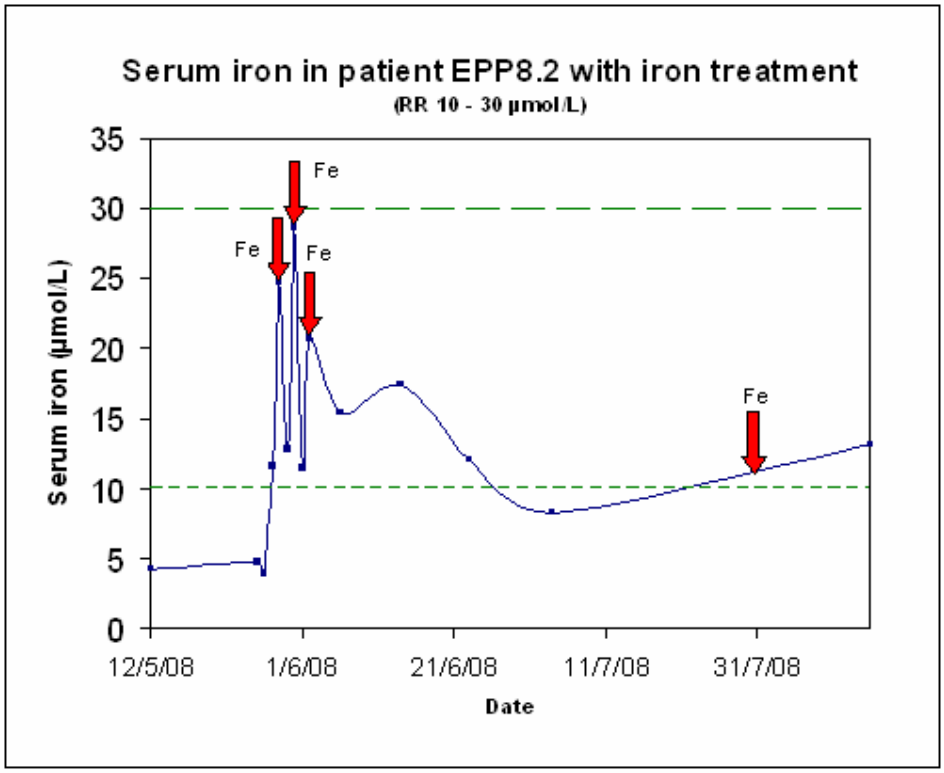

Figure 27: Effect of parenteral iron treatment (red arrows) on serum iron concentration over time. Data courtesy of Dr M Sonderup (Department of Medicine, UCT and GSH). Upper and lower limit of reference intervals are shown as green stippled lines.

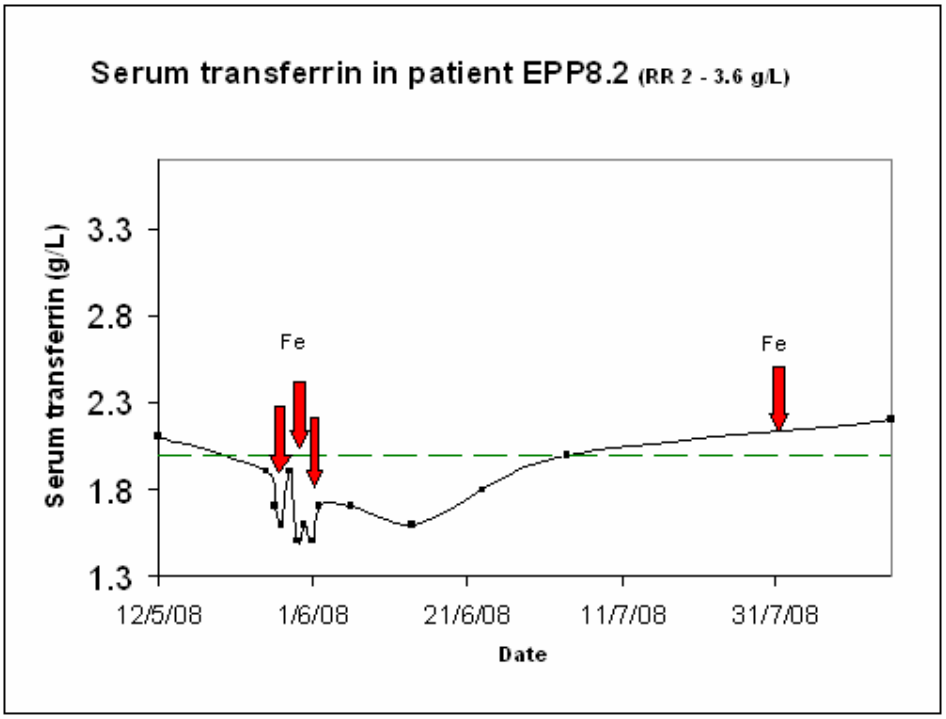

Figure 28: Effect of parenteral iron treatment (red arrows) on serum transferrin concentration over time. Serum transferrin concentration remains low, in keeping with a negative acute phase response, during iron treatment. Data courtesy of Dr M Sonderup (Department of Medicine, UCT and GSH). Lower limit of reference interval shown as green stippled line.

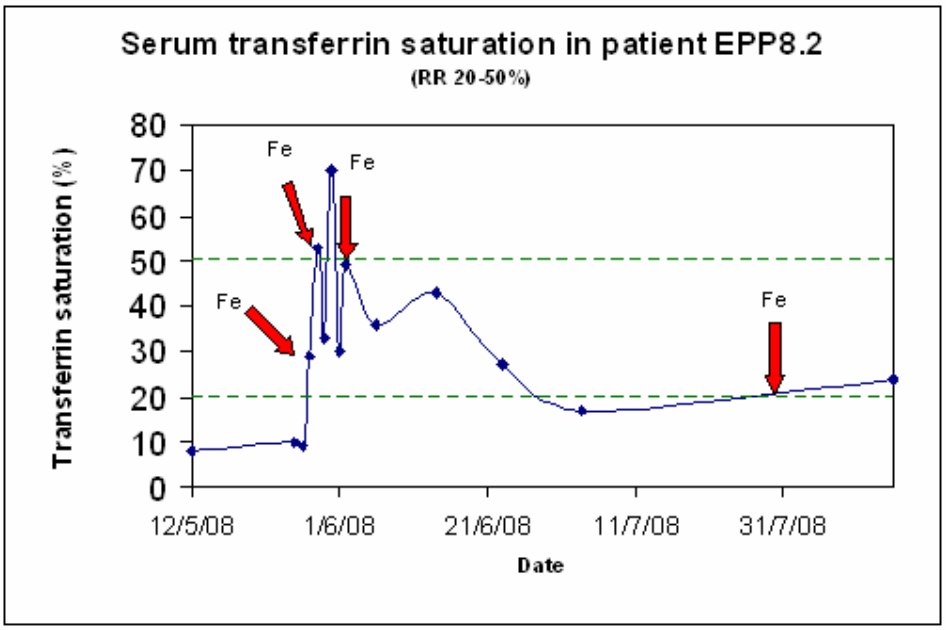

Figure 29: Effect of parenteral iron treatment (red arrows) on % serum transferrin saturation over time. Serum transferrin saturation increases during iron treatment. Data courtesy of Dr M Sonderup (Department of Medicine, UCT and GSH). Upper and lower limits of reference intervals shown as green stippled lines.

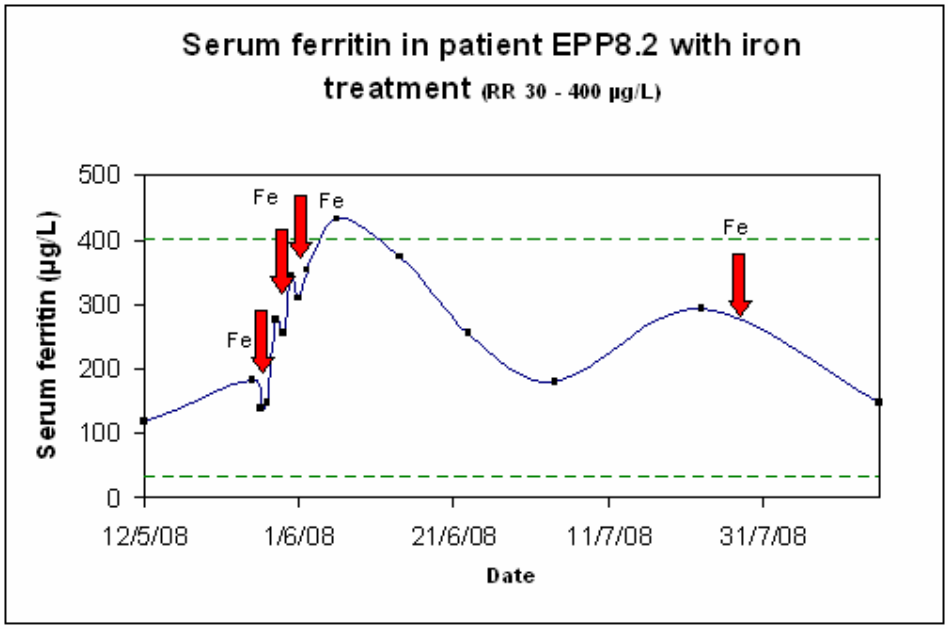

Figure 30: Effect of parenteral iron treatment (red arrows) on serum ferritin concentration over time. Serum ferritin concentration increases during iron treatment. Data courtesy of Dr M Sonderup (Department of Medicine, UCT and GSH). Upper and lower limits of reference intervals shown as green stippled lines.

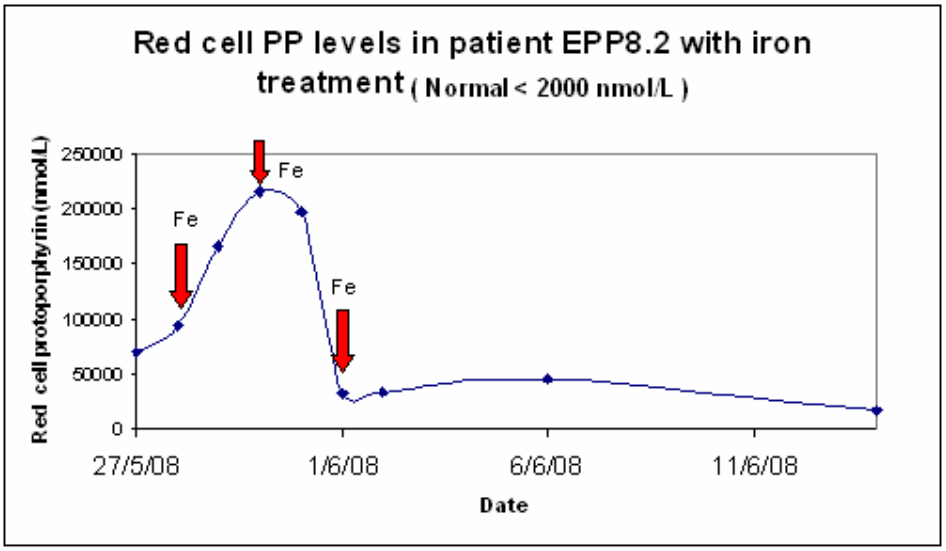

Figure 31: Effect of parenteral iron treatment (red arrows) on red cell PP concentration over time. PP increases dramatically, and then decreases, during iron treatment. Data courtesy of Dr M Sonderup (Department of Medicine, UCT and GSH).

Discussion

The observation that iron treatment increases, and then decreases serum PP concentrations, was somewhat surprising. Importantly, this flux in PP was recorded in a state of probable iron deficiency.

In XLDPP (even in the absence of iron deficiency), if iron delivery to FECH within the mitochondrion was insufficient to match PP production, iron supplementation would constitute a rational treatment strategy by decreasing PP accumulation.

It may be postulated that the initial rise in red cell PP was a consequence of increased ALAS2 translation due to signalling though the IRP system. Increased normoblast cytosolic iron would decrease IRP 1 and 2 levels, leading to ALAS2 mRNA stabilisation. This effect would occur in a state of iron deficiency, in keeping with the observations of Ishikawa et al (2005), and account for the relatively brief period of ALAS2 induction. It may be that the initial increase in red cell PP described here, would not be seen if subject EPP8.2 had been systemically iron replete.

Iron treatment may decrease PP concentrations in XLDPP by allowing accumulated PP to be metabolised to haem, due to the restoration of matching iron and PP substrate proportions. Increased iron concentrations, capable of saturating FECH activity, would achieve this effect in XLDPP even in the absence of systemic iron deficiency.

Another mechanism by which iron treatment may decrease PP concentrations in XLDPP, and specifically during iron deficiency, would be a reduction in *ALAS2* transcription, as a consequence of restoration of normal haemoglobin oxygen carrying capability. Anaemia due to any cause, acting through erythroid transcription factors, may be expected to increase *ALAS2* transcription (Nuez et al 1995, Marinkovic et al 2007), but in general XLDPP subjects do not exhibit anaemia (Whatley et al 2008). However, in the case of subject EPP8.2, anaemia was present (Hb = 10.9g/dl) when iron treatment

was given - although the origin of this was, as previously mentioned, probably a result of haemorrhage, sepsis and the anaemia of chronic disorders. Subjects EPP8.6 and EPP8.4 reportedly had associated anaemic episodes (haemoglobin of 8 and 10 g/dl, respectively) with their porphyria, but an unrelated factor (e.g. heavy menses) cannot be excluded. The increased photosensitivity they describe whilst anaemic, and the resolution of the anaemia and photosensitivity with intravenous iron treatment, does not establish XLDPP as the basis for the anaemia.

Iron and ferritin concentrations remain elevated for ~ 3 weeks after the iron infusions (Figures 27 and 30) in subject EPP8.2. Intravenous iron is taken up directly by the bone marrow reticuloendothelial system (RES) and stored as ferritin, in contrast to oral iron supplementation, which is siphoned off by the liver before entering the systemic circulation. Macrophage “nurse cells” frequently exist in proximity to normoblasts, supplying them directly with iron (Leimberg et al 2008). Potentially, iron concentrations remain elevated within the bone marrow micro environment for longer than serum iron studies would indicate. Thus, supra-physiological iron concentrations achieved during iron treatment would be expected to increase the total RES iron delivery capability.

Serum transferrin concentrations show a reduction after iron treatment (Figure 28), interpreted as a hepatic response to increased serum iron concentrations. Note that the transferrin concentration prior to iron treatment was borderline low, possibly secondary to hepatic disease and as an acute phase response. As another possible confounding factor, it is interesting to note that Lyoumi et al (2007), using a murine model, showed an increase in serum transferrin as a direct result of raised PP concentrations.

Increased flux of the haem biosynthetic pathway in XLDPP, suggests an increase in haem formation. The fate of this haem has not been determined (Whatley et al 2008), but deserves consideration. Normally, erythroid haem may be incorporated into haemoglobin, possibly exported from normoblast as free haem by the feline leukemia virus subgroup C receptor (FLVCR) (Keel et al 2008), or be broken down within the normoblast by haem oxygenase. Breakdown of haem yields inorganic iron, carbon monoxide and biliverdin.

Free haem is bound to haemopexin in plasma. The haem-haemopexin complex is taken up by the low density lipoprotein receptor related protein (LRP) in the bone marrow and spleen RES (Hvidberg et al 2005). The LRP, also known as CD91, is more well-known for its role as receptor for lipoproteins. In a very similar system, free haemoglobin bound to haptoglobin can be taken by the CD163 receptor. In both cases haem is targeted for lysosomal degradation. These receptors are also expressed in other tissues, such as liver (Hvidberg et al 2005). The RES may also acquire haem by phagocytosis of senescent or abnormal red cells. Inorganic iron may be exported from macrophages via ferroportin. Intact haem may also leave macrophages via the FLVCR (Keel et al 2008).

In all cases, this system achieves recycling and conservation of iron stores. In view of this, it is perplexing that in XLDPP increased flux of the haem biosynthetic pathway results in failure of mitochondrial iron availability.

In XLDPP, biochemical iron parameters may be in keeping with iron deficiency although total body iron stores may be normal (arbitrarily called postulate A here). This would be expected to occur if an increased flux of the haem biosynthetic pathway led to increased erythron iron acquisition, haem synthesis and eventually catabolism by the RES. The rate-limiting step, leading to PP accumulation, could then be postulated as being RES processing or release of recycled iron for erythron uptake. Disorders in which RES iron release is decreased, such as the anaemia of chronic disorders (increased hepcidin causing ferroportin transporter degradation) or scurvy, would be expected to reduce RES iron release even further.

As mentioned in Chapter 1, excess haem has been shown to impair erythron iron uptake (Ponka and Schulman 1985). In these *in vitro* experiments exogenous haem was added to incubated reticulocytes. Excess haem production is expected to occur in XLDPP, and this haem may impair erythron iron acquisition. However, it may be that the haem concentrations achieved in the experiments of Ponka and Schulman, and those which occur in XLDPP, are of different orders of magnitude. Furthermore, endogenous haem in excess of globin requirements may be exported by the FLVCR, thereby preventing intracellular haem toxicity (Keel et al 2008). Although

haem is known to degrade IRP2 via oxidation-induced ubiquitination (Ishikawa at al 2005), and such reduction in IRP2 may impair erythroid transferrin receptor expression in response to intracellular iron deficiency, the effect of this system in XLDPP has not been determined. Decreased serum transferrin saturation prior to iron treatment (Table 4 and Figure 29) and increased soluble transferrin receptor concentrations (Whatley et al 2008, but not measured in family EPP8) suggest increased, although insufficient, uptake of available iron by erythroid cells. It is possible that the effect of increased haem (if indeed present in XLDPP) on normoblast IRP2 signalling and consequent transferrin receptor expression, is overshadowed by other mechanisms.

If XLDPP does not cause systemic iron deficiency, ongoing iron treatment would entail a risk of systemic iron overload with associated toxicity. This would imply that PP reduction after iron treatment is simply a non-steady state phenomenon and that eventually iron would be incarcerated in the RES.

If XLDPP does cause total body iron deficiency (arbitrarily called postulate B here) – and biochemical parameters do in fact reveal systemic iron deficiency - on-going iron treatment may be partially curative. Keel et al (2008) postulate that free haem may be secreted by the liver into bile via the FLVCR, and thus provide a route of net iron loss from the body. This would provide an explanation for the reduction in iron stores observed in patient EPP8.2 at initial evaluation, for which no clear aetiology has been advanced.

Although it is tempting to hypothesise that haem production is stimulated in XLDPP through iron administration, it is prudent to remain speculative on this issue, and likewise on the role that the above mechanisms may be playing.

Indeed, the disposal or use of iron after haem synthesis in XLDPP has not been determined (Whatley et al 2008). Pending further investigation, a reasonable compromise between postulate A and B explaining inadequate mitochondrial iron availability, is to conclude that some measure of increase in total body iron stores would be required to match increased PP production and compensate for any iron loss sustained. This would imply a restoration of

normal iron and PP proportions, albeit at increased concentrations, perhaps by raising actual *in vivo* FECH activity and PP clearance.

Conclusion

1. Iron supplementation does appear to alter porphyrin metabolism in XLDPP as evidenced by an initial increase in erythocyte PP concentration, followed by a more sustained decrease, after iron treatment.
2. Iron treatment of subject EPP8.2, though reducing PP concentrations temporarily, did not reverse the inexorable advance of an established liver disease process.
3. It is difficult to quantify the impact iron treatment had on the course of his disease. Multiple confounding variables caused by advanced liver disease, means that the findings discussed here cannot necessarily be extrapolated to other subjects with XLDPP.
4. Iron treatment, in this case, has helped develop our concept of XLDPP further.

CHAPTER SEVEN

Further discussion and recommendations based on all available data

"…..who are first will be last, and the last - first."

Matthew 19: 30, Bible International Version

It is ironic that a mutation in the first enzyme in the haem biosynthetic pathway results in dysfunction and substrate accumulation at the level of the last. The discovery of *ALAS2* as the disease locus in family EPP8 explains many of the perplexing and atypical features initially noted by Parker et al (2008) and our collaborators at the University of Cardiff and the Centre Francais des Porphyries. However, a variety of new and as yet unanswered questions emerge. The following discussion points are made on the basis of a more comprehensive view and understanding of family EPP8 as work progressed.

Features of XLDPP and Family EPP8

The preponderance of ZnPP in family EPP8 and XLDPP is understood to reflect a state of relative mitochondrial iron deficiency – zinc being used by FECH as an alternative to iron. It is interesting that during the final phase of his illness, subject EPP8.2 reverted to a dominant free PP peak. This may reflect exhaustion of zinc as alternative FECH substrate. Zinc deficiency may be predominantly within normoblasts due to significantly increased flux of the haem biosynthetic pathway, but serum zinc deficiency as associated with catabolic states may have been contributory (unfortunately serum zinc levels were not measured). Whatley et al (2008) noted a similar pattern in the XLDPP patient they described who had iron deficiency (ZnPP plateaued while free PP increased significantly).

While G6PD deficiency was not confirmed in our study it is interesting to note that such deficiency may have been of clinical relevance in the affected male subjects from family EPP8. Particularly during the final phase of his illness,

PP accumulation and sepsis in subject EPP8.2 may have created sufficient oxidant stress to have generated haemolysis. However, no clear morphological evidence of haemolysis was found on examination of peripheral blood at that time. Other parameters such as unconjugated bilirubin could not be interpreted in view of the liver disease. Haemolysis, even if low grade, would have stimulated erythropoiesis and induced transcription of *ALAS2* via erythroid transcription factors. It is unlikely that G6PD deficiency is of relevance to XLDPP in female subjects.

Allthough DNA from subject EPP8.13 was not available for testing, an X-linked inheritance pattern and the presence of affected sons establish her as bearing the c.1706-1709 delAGTG mutation. We therefore consider her the 'founding mother' of the condition in South Africa. Biochemical features in support of a diagnosis of protoporphyria in her is limited to raised faecal porphyrins (Eales et al 1978).

One of the features which distinguish XLDPP in family EPP8 from EPP is the high degree of disease penetrance. Indeed, Whatley et al (2008) describe "close to 100% penetrance" in XLDPP. However, some variation in the disease severity does occur as documented in Table 3. Subject EPP8.12 had a particularly fulminant disease with death at the age of 29. This is in contrast to apparent lack of phenotypic disease as noted in subject EPP8.13 and also in another obligate (but not confirmed) carrier described by Whatley et al (2008). Brancaleoni et al (2009) reported an asymptomatic XLDPP female with the *ALAS2* deletion in an Italian family.

Although XLDPP is inherited as an X-linked dominant condition, it would be anticipated that a gene dilution effect would cause affected females to exhibit decreased disease severity. Furthermore, in females skewed X inactivation may influence disease penetrance. Whatley et al (2008) did not record significant differences in PP concentrations between females and males, although liver disease was more prevalent in males. This is similar to liver pathology in family EPP8, where males have exhibited a more malignant disease course.

Liver disease in XLDPP, as in EPP, is considered secondary to accumulated PP toxicity (Poh-Fitzpatrick 1986, Whatley et al 2008). The exact factors leading to the development of liver disease in XLDPP, as in EPP, have not been clarified. Whatley et al (2008) note higher PP concentrations and a higher incidence of PP related liver disease in XLDPP than in EPP. It seems reasonable that PP induced liver disease is a function of mean PP concentrations over an affected individual's lifetime, perhaps like microvasculopathy and blood sugar concentrations in diabetes mellitus.

Ferrochelatase

FECH has been shown to be normal in family EPP8, both at gene (Parker et al 2008) and enzyme (Chapter 4 of this dissertation) level. This is in keeping with the findings Whatley et al (2008) present for the other families with XLDPP. PP accumulation is ascribed to relative intra mitochondrial deficiency of iron as substrate, exemplified by ZnPP accumulation. However, as noted in Chapter 1, it has been suggested that FECH is capable of sensing intracellular iron concentrations via the Fe-S cluster (Taketani et al 2000), haem is reported to inhibit FECH activity (Dailey and Fleming 1983), and that erythroid FECH enzyme activity is decreased during intracellular iron deprivation (Crooks et al 2010). This may account for a fraction of the free PP which occurs in XLDPP, due to a reduction of *in vivo* FECH velocity beyond what would be expected from substrate deficiency alone.

Gain in ALAS2 function

The exact nature of the changes brought about by the mutations in *ALAS2* causing XLDPP, have not been elucidated. As noted in Chapter 5, the c.1706-1709 delAGTG mutation is predicted to cause a frame shift in 24

codons and to extend ALAS2 by 4 amino acids (p.E569GfsX24). The c.1699-1700 delAT mutation is predicted to result in a frame shift in 2 codons and to truncate ALAS2 by 20 amino acids (p.M567EfsX2). In both cases a marked increase in ALAS2 activity and porphyrin production in a prokaryotic expression system occurred (Whatley et al 2008). The activity and porphyrinogenesis of the c. 1699-1700 delAT mutant is higher than that of by the c.1706-1709 delAGTG mutant.

The role of this highly conserved (Whatley et al 2008) C-terminal region in the regulation of ALAS2 activity is not known. It is possible that solving the crystal structure of human ALAS will help shed light in this regard.

In essence, gain of function mutations in *ALAS2* may either increase the amount of enzyme formed, or increase the catalytic activity of the enzyme either directly or indirectly. No kinetic data for XLDPP *ALAS2* mutants are available.

Enzyme formation may be regulated at the level of transcription (e.g. by promoter regulation), translation (e.g. by changes in the rate of translation or rate of mRNA degradation), or at the rate of ALAS2 enzyme degradation. If ALAS2 was subject to the same level of negative feedback regulation by haem as that which exists for ALAS1, haem overproduction in XLDPP would be expected to exert more effective control of ALAS2 activity.

The location of the XLDPP mutations in the C-terminus of *ALAS2*, suggest possible stabilisation of ALAS2 mRNA or increased ALAS2 translation as a possible mechanism. It may be postulated than the XLDPP mutations may disrupt sequence(s) necessary for mRNA recognition by RNAase enymes or microRNA species. If the S568G substitution (Harigae et al 1999) does not disrupt this postulated recognition sequence, it would help explain why the S568G mutation located between the XLDPP mutations, causes a loss in ALAS2 function. However, this proximity of loss and gain in function mutations, remain an enigmatic and fascinating observation.

MicroRNA characteristically binds in the 3' mRNA UTR and may facilitate mRNA degradation or inhibit translation (Chu and Rana 2007). MicroRNA

binding in an exon has not been described, and if the XLDPP mutations were targets for microRNA regulation, this would be very unusual.

ALAS2 c.1699-1709 is not a known target for microRNA regulation of ALAS2 (as verified on http://microrna.sanger.ac.uk/cgi-bin/targets/v5/detail_view.pl?transcript_id=ENST00000330807). At the time of writing, 7 microRNA species are known to target the ALAS2 mRNA 3' UTR region.

ALAS2 enzyme concentrations may be regulated by degradation velocity. Degradation of proteins is often mediated by the ubiquitin-proteosome system, in which ubiquitin tags proteins for further processing. An isopeptide bond forms between the C-terminus of ubiquitin and lysine residues on the ubiquitinated protein (Hurley et al 2006). Mutations may abolish an ubiquitination site, thereby increasing ALAS2 enzyme half life. However, neither the c.1706-1709 delAGTG nor the c.1699-1700 delAT mutations are predicted to abolish a lysine residue, making this mechanism an unlikely cause for the gain in ALAS2 function in XLDPP.

Haem catabolism

The degradation of haem by haem oxygenase is competitively inhibited by ZnPP (Maines 1981). The physiological effect of ZnPP in XLDPP is not known but one may speculate that the accumulation of ZnPP would increase haem concentrations beyond that conferred by increased haem synthesis.

At least 85% of mammalian CO is derived from haem degradation (Goldsmith and Landaw 1968). CO measurement allows the measurement of haem catabolism and haem oxygenase activity (Vreman and Stevenson 1988, Coceani et al 1997). This may be accomplished by carboxyhaemoglobin measurement in blood using co-oximetry (Mahoney et al 1993), or through CO measurement in expired air (Rodgers et al1994). It would be anticipated

that CO production in XLDPP would be elevated, assuming there was an increased production/accumulation of haem.

Recommendations

It is useful to state some of the initial clinical recommendations we have formulated in order to inform and assist future encounters with patients suspected of, or confirmed to be affected by XLDPP. We advise the following:

1. XLDPP should be considered in the differential diagnosis of all patients presenting with clinical or laboratory features suggestive of EPP. Clinical features which would suggest XLDPP include a highly penetrant inheritance pattern, prevalence of liver disease and a response to iron supplementation. Laboratory features suggestive of XLDPP are a prominent or dominant ZnPP peak on erythrocyte fluorescence emission scanning (a dominant free PP peak does not exclude XLDPP, as seen with subject EPP8.2) and an inability to demonstrate FECH mutations or enzyme dysfunction. The easiest way of confirming a diagnosis of XLDPP is by direct sequencing of *ALAS2* exon 11 (Chapter 5). Serum iron biochemistry showing borderline/possible iron deficiency may suggest XLDPP but is not discriminatory as some EPP patients, particularly women, may show low serum iron and transferrin saturation.
2. Routine follow up by a clinician experienced in hepatology and preferably porphyrinology. Clinical, biochemical and histological data should be obtained and interpreted in the light of disease evolution, bearing in mind that the life-threatening complications in XLDPP are likely to result from liver disease. We noted in patient EPP8.2 that serum liver function abnormalities tended to show a cholestatic pattern

(with raised bilirubin, alkaline phosphatase and gamma glutamyl transferase) rather than a predominant transaminitis.

3. Males should be monitored more closely as they are more likely to be affected by severe disease.
4. Other factors which may portend a poorer prognosis may include marked photosensitivity, a moderate (to marked) elevation in erythrocyte PP concentration (arbitralily defined here as erythrocyte PP concentration > 10 000 nmol/L), the manifestation of hepatic complications at an early age and thrombocytopenia.
5. Treatment or management strategies resulting in lowering PP concentrations should be considered. A sustained reduction in steady state PP concentration, even if relatively minor, is anticipated to decrease hepatic toxicity. The findings presented in the previous chapter suggest that iron supplementation in XLDPP may have a PP-lowering effect, but additional studies are required. Clearly, supplementation resulting in iron overload is detrimental, and iron toxicity, in excess of a reduction in PP toxicity, should be avoided. Landefeld et al (2009) describe a case of a child with XLDPP who developed liver siderosis during inadvertent blood transfusion-related iron overload, accompanied by a marked reduction in erythrocyte and liver PP. Thus frequent monitoring of serum iron studies during steady state condtions outside of the acute phase response (due to e.g. intercurrent illness) and in the absence of the confounding influence of active liver disease, may be extremely useful in guiding cautious and ongoing iron supplementation without causing iron overload.
6. Avoidance of sun exposure is obviously useful in reducing photosensitivity symptoms and clearly effective in family EPP8.
7. General hepato-protective measures such as vaccination against viral hepatitis and avoidance of toxins such as excessive ethanol intake or hepatotoxic drugs.

8. Ongoing genetic counselling is vital in ensuring all patients with XLDPP understand the mechanism of disease transmission and the risk to future generations.

CHAPTER EIGHT

Future studies, summary and concluding remarks

Future studies

Additional studies may be undertaken to clarify the pathophysiological changes associated with XLDPP. As family EPP8 are (mainly) resident in South Africa, a real clinical need exists for any additional information which may clarify the molecular pathogenesis further and assist in future management strategies. Prevention of liver disease is accepted as the primary goal of management.

ALAS2 is exclusively expressed in erythroid cells. This fact, and the need to prove pathogenicity, prompted Whatley et al (2008) to use a prokaryotic expression system. Therefore the EBVTL culture lines used for the FECH enzyme assay described in Chapter 4 will not be suitable for ALAS2 characterisation.

Other suitable enzyme sources for studying ALAS2 may be developed. This could include murine erythroleukemia cells into which the mutation has been introduced. An XLDPP animal (e.g. murine) model would offer a vast number of opportunities for *in vivo* experimentation.

ALAS2 characterisation in XLDPP

This may be accomplished at enzyme activity, quantitative protein and mRNA concentrations. Such an approach would be similar to that originally proposed for the investigation of FECH in this dissertation.

A prokaryotic expression system would be suitable for enzyme kinetic studies. K_M and k_{cat} could be determined for ALAS2 in WT and mutated states. A decrease in K_M would signify a higher binding affinity for the substrate while an increase in k_{cat} would suggest improved catalytic efficiency. Characterisation of various *ALAS2* C-terminal engineered mutants could provide insight into how some mutations result in gain of ALAS2 function while others, such as the S568G substitution, cause loss thereof.

ALAS2 quantification may be accomplished by Western blotting.

Relative gene expression of *ALAS2* could be studied by conducting quantitative RT PCR of ALAS2 mRNA against a reference gene. Increased mRNA would imply increased mRNA or decreased degradation. Normal ALAS2 mRNA quantitation may still be compatible with regulation by a microRNA mechanism, if the mutant effect occurred by promoting translation of mRNA.

Isoniazid (INH) is a known inhibitor of ALAS activity. The mechanism involves sequestering of pyridoxal in the hydrazone form, thereby preventing phosphorylation to the active pyridoxal phosphate (Mathews and van Holde 1990). Investigation of ALAS2 activity and porphyrin production in an *in vitro* or animal XLDPP system during INH supplementation, would offer interesting information. Due to the potential toxic effects of INH (including peripheral neuropathy, vasculopathy and rarely convulsions), it is highly unlikely that INH would ever constitute an appropriate therapeutic agent in XLDPP.

XLDPP penetrance in female subjects

Skewed or non-random X chromosome inactivation is often postulated as a cause for varying disease penetrance in females with X-linked diseases. As noted in Chapter 7, this is the likely explanation for the lack of symptoms in subject EPP8.13.

In female subjects with particularly severe or mild disease, this may be confirmed by a PCR reaction of the first exon of the human androgen receptor gene located on the X chromosome (Allen et al 1992). This gene contains a highly polymorphic trinucleotide repeat sequence (distinguishing the maternal and paternal alleles) and a restriction site in close proximity. The restriction site is methylated during X-inactivation, abolishing its recognition by a methylation-sensitive restriction enzyme. The PCR primers flank both the trinucleotide repeat sequence and the restriction site. Thus amplification will only occur if restriction digestion has not occurred, as expected from the inactivated allele. A random pattern of X inactivation is evidenced by PAGE visualisation of both the maternal and paternal

amplicons. If only one band is detected, or if there is a marked difference between the bands, this would be in keeping with skewed X inactivation.

Kubota et al (1999) developed an alternative method, which employs chemical modification of DNA by sodium bisulfite (converting all unmethylated - but not methylated - cytosine bases to uracil) and subsequent PCR of the human androgen receptor gene. This technique does not employ restriction enzymes (thus not vulnerable to incomplete restriction digestion) and uses 2 sets of primers – 1 for the methylated and the other for the unmethylated allele. The same polymorphic trinucelotide repeat utilised by Allen et al (1992) allows a ratio of the maternal allele to the paternal allele (for the methylated and unmethylated state), to be determined.

Investigation of a control cohort revealed that 11% of normal females showed a skewed X-inactivation pattern (Kubota et al 1999).

Haem catabolism

Measurement of carboxyhaemoglobin concentration in blood (or CO in breath) in subjects from family EPP8 would suggest increased haem breakdown. Confounding influences such as smoke inhalation needs to be considered.

Stool urobilinogen may be quantitated in order to investigate biliverdin formation by haem oxygenase.

Supplementation with ^{13}C glycine, quantified using mass spectrometry, would provide more direct evidence of increased haem synthesis and catabolism. An early (within days) peaked ^{13}C stool urobilinogen would be expected in XLDPP with a later (~ 120 days) peak from senescent red cell breakdown. Normal controls are also expected to show peaks with a smaller initial peak and a similar sized later peak. A family of 4 signals obtained would confirm the tetrapyrrole origin of the signal, depending on the number of labeled glycine residues per ring. Interference from PP is possible although quantitatively the more hydrophobic PP undergoes significant enterohepatic circulation (Anstey and Hift 2007).

Alternatively, ^{14}C glycine supplementation could be used in an animal model and stool radioactivity measured.

Serum haemopexin concentrations in XLDPP could be assayed. Decreased concentrations would suggest increased serum free haem concentrations. This would be in keeping with increased free haem export from erythroid cells in XLDPP.

Iron metabolism in XLDPP

Examination of bone marrow iron stores remains a valuable and arguably gold-standard measure of iron stores. An animal XLDPP model would facilitate such examination of marrow iron content.

During further iron supplementation of affected subjects from family EPP8 (should it be indicated), red cell PP concentrations should be measured, as it was for subject EPP8.2 (Chapter 6). It would also be interesting to consider monitoring ZnPP : free PP ratios. Simultaneous reticulocyte indices would add further information regarding erythroid response to iron in XLDPP.

Hepcidin measurement, aided by a recently characterised serum hepcidin immunoassay (Ganz et al 2008), may provide additional information regarding iron stores in XLDPP.

Supplementation with ^{59}Fe in an animal XLDPP model may reveal the fate of iron and where it is sequestered - if at all. The possibility of ongoing loss of iron as free haem via the bile in XLDPP, requires investigation. Measurement of stool ^{59}Fe radioactivity would be useful in defining whether free haem is lost and so causes iron deficiency.

Summary and concluding remarks

Details of the haem biosynthetic pathway and its regulation were reviewed in Chapter 1. In Chapter 2, the aim of the project was defined as a systematic inquiry into the molecular pathogenesis of an atypical protoporphyria in family EPP8. Exclusion of dysfunction of FECH at enzyme level was stated as an important initial objective. Relevant clinical details were elaborated in Chapter 3. The establishment of a FECH enzyme assay, which showed normal enzyme activity in affected subjects, was documented in Chapter 4. Chapter 5 discussed the discovery of the gain in *ALAS2* function which causes XLDPP. The finding of *ALAS2* as the alternative disease locus resulted from international collaboration. Mutational DNA analysis of family EPP8 allowed genetic counseling and prediction of genetic risk. In Chapter 6, a treatment strategy in the form of iron supplementation was investigated. Data of porphyrin fluctuations during iron supplementation and hypotheses regarding iron metabolism in XLDPP were proposed. Some of the insights and conundrums that have emerged from this project and the findings of Whatley et al (2008) were addressed in Chapter 7. In the present chapter, future studies which may be undertaken to investigate XLDPP further, have been hinted at.

A novel porphyria with unique features has been identified as being disease causing in family EPP8. Relative intra mitochondrial iron insufficiency in XLDPP, inadequate to match markedly increased PP synthesis, allows a possible explanation for many of the atypical features noted in Chapter 2.

Regardless of the exact mechanism by which *ALAS2* exon 11 mutations raise ALAS2 activity and perturb haem metabolism, the findings described here and by Whatley et al (2008), provide novel insights into how the haem biosynthetic enzyme and substrate systems, are regulated.

The unfolding of events and sequential discoveries documented in this dissertation, illustrates how in the general field of medicine, atypical disease features should never be ignored. The failure to identify a rational explanation for a disease manifestation should not preclude further exploration of the phenomenon. Whilst immediate resolution and explanation of unusual findings is part of conventional clinical and laboratory activities, in the case of XLDPP more extensive work was needed. Ongoing investigation resulted in the elucidation of the pathogenesis.

APPENDICES

APPENDIX A

Ethics Approval

UNIVERSITY OF CAPE TOWN

Health Sciences Faculty
Research Ethics Committee
Room E52-24 Groote Schuur Hospital Old Main Building
Observatory 7925
Telephone [021] 406 6338 • **Facsimile** [021] 406 6411
e-mail: lamees.emjedi@uct.ac.za

17 March 2008

REC REF: 408/2004

Dr C Haumann
Chemical Pathology

Dear Dr Haumann

PROJECT TITLE: EXTENSION OF ERYTHROPOETIC PROTOPORPHYRIA (EPP) STUDY

Thank you for your letter to the Research Ethics Committee dated 16 February 2008.

It is a pleasure to inform you that the Ethics Committee has approved the extension to the above-mentioned study.

Please supply an updated report on the study for ongoing approval.

Please note that the ongoing ethical conduct of the study remains the responsibility of the principal investigator.

Please quote the REC. REF in all your correspondence.

Yours sincerely

Ashley Healey

pp **PROFESSOR M BLOCKMAN**
CHAIRPERSON, HSF HUMAN ETHICS

APPENDIX B

Project information letter to family EPP8

UNIVERSITY OF CAPE TOWN

Lennox Eales Porphyria Laboratories
UCT/MRC Liver Research Centre
Dept. of Medicine
K-floor, Old GSH Building
Observatory
7925
Tel: 27-21-406 6206
Fax: 27-21-448 6815
Department of Chemical Pathology
Email: carel.haumann@uct.ac.za

14th March, 2008

Dear Sir/Madam

We would like to ask for your assistance in our investigation of Erythropoietic Protoporphyria (EPP). As you will be aware, EPP is caused by a decreased amount of Ferrochelatase enzyme. In the past you or members of your family, have been investigated for EPP. During Ms Parker's study, the DNA sequence of your Ferrochelatase gene was investigated.

In order to understand better how EPP in your family comes about, we aim to measure Ferrochelatase enzyme activity. In addition we plan to measure how Ferrochelatase enzyme is formed. This will form part of a thesis Dr Haumann will be writing.

For this we would need another blood sample. This will also provide us with an opportunity to discuss any questions you might have about EPP.

Our findings might help us understand EPP better.

Thank you very much for considering this request.

Yours sincerely

Dr Carel Haumann
Registrar
Clinical Pathology NHLS and UCT

A/Prof Peter Meissner
Head, Porphyria Laboratories and Director UCT/MRC Liver Centre
Dept of Medicine

APPENDIX C

Porphyrin quantitation by chromatography

(Day et al 1978, Hift et al 2004)

Principle

Porphyrins are extracted from red cells and then esterified to methyl derivatives in acidic conditions. This decreases the overall polarity while retaining their relative polarity as conferred by carboxyl side chains. After pH neutralisation (neutralising the charge on two of the four inner nitrogens), porphyrins are extracted into an organic solvent. Thin layer chromatography (TLC) distributes porphyrins between a polar solid phase and a non-polar mobile phase. The solid phase and the solvent compete for binding with the solute. The migration of porphyrins on the TLC plate is inversely proportional to the number of carboxyl groups, with uroporphyrin adhering to the solid phase closest to the application point, and PP travelling furthest. Fluorescence is quantified against standards. Incorporation of volume used allows the concentration to be calculated. The same technique, with minor modifications, may be used for red cell, plasma, urine and stool porphyrin quantification. Only the method used for red cell porphyrin quantification is described here.

Specimen

Whole blood protected from light. EDTA anticoagulated blood does not show loss of porphyrins for 8 days at room temperature and 8 weeks at 4 ℃ in the dark (Deacon et al 2008). Approximately 1.5 ml of whole blood is needed, depending on the haematocrit.

Equipment

- Boiling tube with stopper
- Separating flask
- Glass funnel
- Measuring cylinder 25 ml
- TLC plates (TLC aluminium sheets 20X20cm Silica Gel-60, without fluorescent indicator, Merck Chemicals)
- Hamilton microsyringe
- A selection of pipettes and tips
- Fluoroscanning photodensitometer TLD 100 (Vitatron)
- Integrator SP4290 (Spectra-Physics)
- Centrifuge

Reagents

- Sulphuric acid (H_2SO4)
- Methanol (CH_3OH)
- Chloroform ($CHCl_3$)
- Ammonia solution (NH_4OH)
- Anhydrous sodium sulphate (Na_2SO_4)
- Porphyrin methyl ester calibrator - equal concentrations of uroporphyrin, heptacarboxylic porphyrin, hexacarboxylic porphyrin, pentacarboxylic porphyrin, coproporphyrin and mesoporphyrin methyl esters (Frontier Scientific Porphyrin Products)
- Carbon tetrachloride (CCl_4)

- Dichloromethane (CH_2Cl_2)
- Ethyl acetate ($CH_3COOC_2H_5$)
- Ethyl propionate ($C_5H_{10}O_2$)
- n-Dodecan ($C_{12}H_{26}$)
- n-Hexadecan ($C_{16}H_{34}$)
- Reagent grade water (H_2O)

Method

1. Add 500 µl of packed red blood cells and 30 ml 5% sulphuric acid in methanol (v/v) to a boiling tube.
2. Close with a stopper, shake and leave to esterify overnight in the dark.
3. Rinse a separating flask with methanol:chloroform::50:50 (v/v) and add 60 ml 4% ammonia and 10 ml chloroform in a fume hood.
4. Centrifuge the esterified sample at 280 xg for 20 min and transfer the supernatant to the separating flask and seal.
5. Shake flask vigorously for 5 - 20 sec intervals, releasing gaseous build-up intermittently.
6. Fill the flask to ¾ its volume by adding ~ 150 ml H_20. Stir and allow the heavier chloroform organic phase to settle at the bottom of the flask.
7. Rinse a funnel with chloroform and place below the flask in a measuring cylinder.
8. Add ~ 2 g of anhydrous sodium sulphate to the funnel. This binds and removes any residual H_20.
9. Allow the chloroform to run through the funnel into the measuring cylinder. Repeat after adding 10 ml chloroform.
10. Note the volume of chloroform eluted. Spot 60 µl (the spotted volume may be decreased to remain within the linear part of the fluorescence

concentration curve if large quantities of porphyrins are anticipated) onto a TLC plate using a Hamilton microsyringe ~ 1 cm from the base of the plate and with 2 cm between lanes. Evaporate the chloroform to dryness with warm air, e.g. using a conventional hair-drier.

11. Reserve two lanes on each plate for porphyrin ester standards.
12. Run the TLC plate vertically in a chromatography tank containing 180 ml mobile-phase solvent (carbon tetrachloride:dichloromethane:ethyl acetate:ethyl propionate::2:2:1:1 (v/v)) for 40 min or until the solvent front reaches the top of the plate.
13. Dry the TLC plate and dip briefly in a fluorescence enhancing solution containing chloroform:n-dodecan:n-hexadecan::3:1:1 (v/v).
14. Dry and read the plate on a fluoroscanning photodensitometer connected to an integrator/recorder unit using two interference filters (excitation filter at 399 nm; emission filter at 620 nm).
15. This produces a trace showing the porphyrin ester position and fluorescence (graphically and a numerical value corresponding to the integrated value of each porphyrin peak).

Interpretation

Standards allow porphyrin species to be identified and quantitated by their position and fluorescence intensity, respectively. The pattern of porphyrin species identified, allows the likely type of porphyria to be inferred. Quantitative results are expressed in nmol/L. Red cell PP reference range = 1 – 2000 nmol/L red cell (not whole blood).

Calculation

The general equation $A_{sample}/A_{std} = (C_{sample} \times V_{sample}) / (C_{std} \times V_{std})$ is used where A = area of peak (analogous to absorbance), std = standard, C = concentration and V = volume. This is the equation from which the very well-known equation $C_1 \times V_1 = C_2 \times V_2$ is derived.

The sample was diluted by a factor (packed red cell volume) / (final chloroform volume). In order to calculate the initial red cell concentration this needs to be corrected for. Thus:

$$\text{Csample} = \frac{\text{Asample} \times \text{Cstd} \times \text{Vstd}}{\text{Astd} \times \text{Vsample}} \times \frac{\text{Vcholoroform}}{\text{Vred cells}}$$

APPENDIX D

Qualitative zinc and free protoporphyrin fluorescence scanning

(Piomelli et al 1975, Deacon and Elder 2001, modified by Parker et al 2008)

Principle

ZnPP and free PP have distinct fluorescence emission maxima at 588 nm and 632 nm, respectively. Emission fluorescence scanning may be used to determine which PP specie predominates. More specific information on the percentage contributed by the two species to the total PP pool may be calculated by additionally measuring fluorescence at the isosbestic point at 618 nm.

Specimen

Whole blood protected from light. EDTA is generally used as anticoagulant.

Approximately 60 ul of whole blood is required, depending on the haematocrit.

Equipment

- Glass tube
- Fluorescence spectrophotometer 650-10S (Hitachi Koki)
- Linear 1200 chart recorder (Spectrum Medical Industries)

- 150 Xenon Power Supply (Perkin-Elmer)
- Quartz cuvette (acetone will damage plastic)
- A selection of pipettes and tips
- Vortex mixer
- Centrifuge

Reagents

- 0.9% NaCl
- Acetone:H_2O::80:20 (v/v)

Method

1. Make a 1 in 10 dilution of 20 µl of packed red cells in a glass tube.
2. Add 5 ml of 80% acetone.
3. Vortex for 30 sec.
4. Centrifuge at 700 xg for 1 min.
5. Transfer 1 ml of the supernatant to a quartz cuvette for fluorimetry.
6. Perform an emission scan from 540 nm to 650 nm with excitation at 420 nm, sensitivity of 10, slit width 4.5 nm and a scan speed of 60 nm/min. If necessary, adjust sensitivity to include entire peak.
7. Record a profile of the scan on a chart recorder (chart speed: 3 cm/min) and the RFU at 588, 618 and 632 nm.

Interpretation

If the main peak is at 588 nm, EPP is unlikely. A dominant peak at 632 nm is highly suggestive of EPP.

Calculation

(derived empirically by Piomelli 1975)

$$\frac{\text{Concentration ZnPP}}{\text{Concentration total PP}} = \left\langle \frac{\text{RFU 588 nm}}{\text{RFU 618 nm} \times 3.3576} \right\rangle - 0.2534$$

APPENDIX E

Epstein-Barr virus lymphocyte transformation

(Miller and Lipman 1973, Bird et al 1981, van der Westhuyzen et al 1984, Thorley-Lawson 2001)

Principle

Lymphocytes are isolated from peripheral blood by centrifugation over a Ficoll-hypaque density gradient. EBV is introduced into the mixed lymphocyte suspension and B lymphocytes are infected, giving rise to an immortalised lymphoblastoid cell line. EBV particles are derived from the transformed marmoset monkey B95-8 cell line. Transformation is aided by T lymphocytes stimulation via phytohaemagglutinin (PHA). EBVTL are continued in culture, initially with antibiotic cover, and then later in duplicate without antibiotics, until sufficient cells are available for enzyme assay. Sterility is of utmost importance to prevent infection of the culture with *Mycoplasma* species and other organisms. The duplicate culture is conducted with separate media from 2 different manufacturers to decrease the risk of infection or culture failure. Cell growth is assessed by macroscopic and microscopic inspection. EBVTL may be seen microscopically as colonies of cells growing in clumps. An indicator in the medium may also help to assess growth by changing from pink to yellow as the pH declines with active cell metabolism. During culture, EBVTL require an appropriate cell concentration in culture medium. Both overdilution and overgrowth of EBVTL may result in culture failure, due to loss of culture conditioning and nutrient deficiency/metabolite excess, respectively.

Sample

10 ml of whole blood collected into heparinised tubes within 24 h (ideally) or up to 48 h after venesection. If 10 ml blood is not available, make an initial dilution with an equal volume of culture medium. Paediatric samples contain more lymphocytes and less blood is required (2 – 5 ml sufficient). A culture that is initiated with a suboptimal quantity of lymphocytes will be slower to grow initially. EDTA forms a precipitate with culture medium and is best avoided.

Equipment

- Tissue culture hood (Biological safety cabinet class II, Laminaire)
- Incubator (Queue)
- CO_2 supply
- Centrifuge
- Pipet-Aid pipettor with disposable, individually wrapped sterile 5 and 10ml pipettes
- 15 ml Conical tubes
- 50 ml Conical tubes
- 25 cm^2 Culture flasks
- 75 cm^2 Culture flasks
- 2 ml Cryotubes
- 0.22 µmetre (µm) filter discs
- Filter paper (Whatman number 1)
- Phase contrast microscope with green filter (Nikon TMS)
- Fluorescent microscope (Zeiss Axiophot)
- Nalgene freezing container

Reagents

- Marmoset B95-8 cell line stored at -180 °C under liquid nitrogen
- Dulbecco's modified Eagle's medium (Gibco) stored at 4 °C
- Dulbecco's modified Eagle's medium (Sigma) stored at 4 °C
- Fetal Calf Serum (Gibco) stored at -20 °C
- Fetal Calf Serum (Sigma) stored at -20 °C
- Glutamine solution 200 mmol/L (Gibco) stored at -20 °C
- 0.9% NaCl solution
- Neomycin sulphate (powder)
- Streptomycin sulphate (powder)
- Sodium Benzyl Penicillin (powder)
- PHA (Welcome)
- Trypan blue
- Hoechst solution 5 mg/100 ml
- Hanks Balanced Salt Solution (without Na bicarbonate or phenol red) – phosphate buffered saline may be used as alternative
- Citric acid [$(COOH)_3CH_2CH_2COH.H_20$]
- Disodium hydrogen phosphate ($Na_2HPO_4.2H_20$)
- Glycerol
- Reagent grade H_20
- Propyl alcohol

Preparation of solutions and media

1) Culture medium

To 500 ml modified Eagle's medium, add 50 ml (10%) fetal calf serum from the corresponding manufacturer. Prepare separate culture media from Gibco and Sigma to be used for two parallel cultures. Additionally, in the case of the Sigma medium, add 10 ml of the 200 mmol/L glutamine solution to the 500 ml modified Eagle's medium.

2) Antibiotics

Add 2 g neomycin, 2 g streptomycin and 2 g penicillin to 100 ml sterile 0.9% NaCl. Add 2.5 ml of this solution to 500 ml culture medium (final antibiotic concentration 100 units/ml). Prepare the antibiotic-containing culture medium separately for use only during the initial culture phase.

3) EBV medium

Thaw and grow an aliquot of the marmoset B95-8 cell line in a 75 cm^2 flask. Once sufficient cells are available, centrifuge 50 ml medium in a conical tube for 10 min at 168 g. Filter the supernatant through a 0.22 µm filter (thus removing marmoset cells) and add an equal quantity of fresh culture medium. This may be stored for 6 months at 4 °C. Caution: EBV medium (but not EBVTL) represents a source of potential infection with EBV to the operator. Demonstration of serum anti-EBV IgG before working with EBV medium is desirable. Studies have shown that 95% of adults are infected with EBV benignly for life (*in vivo*, EBV achieves true latency and is kept in check, but cannot be eradicated, by the immune system).

4) PHA

Dissolve 1 mg PHA in 5 ml reagent grade H_20. Make a 1 in 5 dilution with 0.9% NaCl. Filter though a 0.22 µm filter disc. Add 500 µl to 10 ml culture medium to a final concentration of 2 mg/L.

5) Trypan blue

Prepare a 2% solution in reagent grade H_20. Pour through filter paper. Take equal volumes of 2% trypan blue and 0.9% phosphate buffered saline, mix and centrifuge at 4000 g for 10 min. Aspirate 1% trypan blue ~ halfway from the bottom of the centrifuge tube to avoid debris. Mix 7 parts 1% trypan blue with 30 parts 3% EDTA / 0.9% phosphate buffered saline. The working solution (0.189% trypan blue) may be stored for 2 weeks at 4 °C.

6) Hoechst stain

Prepare by adding 1 ml of Hoechst solution to 99 ml Hanks Balanced Salt Solution to a final concentration of 0.5 mg/L. This is stored in a dark bottle at 4 °C. Do not filter the stain as this removes the fluorescent dye.

7) Mounting fluid: citric acid – disodium phosphate buffer

- Prepare a 0.1 mol/L citric acid solution by dissolving 1.05 g citric acid in 50 ml reagent grade H_20.
- Prepare a 0.2 mol/L disodium phosphate solution by dissolving 1.41 g disodium phosphate in 50 ml reagent grade H_20.
- Add 22.2 ml of the citric acid solution, 27.8 ml of the disodium phosphate solution to 45 ml of glycerol, pH to 5.5 and make up to 100 ml with reagent grade H_20. Note: the correct pH is vital for generating fluorescence with the Hoechst stain. Store at 4 °C.

Method

(Sterile technique with use of the tissue culture hood and fan, ethanol to clean hands and sterile equipment throughout essential)

- Centrifuge 10 ml whole heparinised blood for 5 min at 1400 xg. Draw buffy coat and plasma into a 10 ml pipette and mix.
- Layer plasma/ buffy coat onto 5 ml of Ficoll-hypaque.
- Centrifuge at 1400 xg for 20 min. Any residual red cells and neutrophils will fall through the Ficoll-hypaque gradient while some monocytes, platelets and lymphcytes will be found in a creamy layer between Ficoll and plasma. Remove lymphocytes from this intermediate layer. Avoid drawing up too much Ficoll in the process.
- Suspend lymphocytes in 5 - 8 ml culture medium and centrifuge at 170 xg for 10 min. Repeat once.
- If lymphocytes are being isolated for direct use in the FECH assay (i.e. without transformation) 0.9% saline may be used to wash in stead of culture medium. In this case, proceed to Appendix F and G by suspending the lymphocyte pellet in sonication buffer.
- Suspend washed lymphocytes in 5 ml EBV-containing medium and transfer to a 25 cm^2 flask. Add 0.25 ml PHA and incubate (with the flask in a vertical position) at 37 °C in a 10% CO_2 environment. The same incubation conditions are continued for the remainder of the culture process. Flasks should only be capped lightly to allow CO_2 to equilibrate with the bicarbonate buffer in the culture medium.
- After 3 days, remove 2.5 ml medium and add 2.5 ml fresh culture medium containing antibiotics.
- Assess cell growth every 3 - 4 days. Cells will tend to precipitate to the bottom of the flask. EBVTL concentration may thus be increased by removing medium. This is done if growth appears poor to improve the conditioning of the medium. Conversely, if abundant growth is present,

new medium (2 - 5 ml) may be added. In an intermediate situation, existing medium may be removed and an equal volume of fresh medium added.

- Once the culture is becoming established, place the 25 cm^2 flask in a horizontal position.
- Split the culture into 2 parallel cultures with different media. Antibiotics may be discontinued.
- Once culture growth allows, transfer 10 ml into a 75 cm^2 culture flask, add 10 ml of fresh medium and incubate the culture with the flask in a vertical position. Once this is established, double the culture volume by adding an equal volume of fresh medium and position 75 cm^2 flask horizontally.
- Abundant quantities of EBVTL should now be available for enzyme/RNA assay or freezing under liquid nitrogen at - 180 °C for later use.
- The entire transformation and culture process takes ~ 4 - 6 weeks.

Results

It is imperative that enzymes or RNA subjected to assay are derived from viable cells. Assay of dead or infected cells may result in spurious results.

1) Phase contrast microscopy

Under phase contrast microscopy, viable EBTVL may be seen as glossy structures of variable shape, usually arranged in clumps or rosettes. The phase contrast light generates a slight halo. In contrast, dead cells appear as uniformly darker, shrunken structures without a halo. A green filter improves the contrast effect.

2) Trypan blue exclusion test

Place a drop of an equal mixture of EBVTL in culture medium and 0.189% trypan blue on a slide, apply a cover slip, and examine under a microscope (preferably phase contrast) without a green filter. Viable cells do not take up trypan blue while dead cells do. A maximum of 5% blue (i.e. dead) cells should be seen. Avoid an undue delay between preparing the trypan blue/EBVTL mixture and examining the slide.

3) Hoechst fluorescent staining for *Mycoplasma* infection

Exclude *Mycoplasma* infection by placing a drop of EBVTL-containing culture medium on a slide, air drying, fixing with an acetic acid: methanol::1:3 (v/v) solution for 20 sec, and washing under tap H_20. Apply the Hoechst stain for 20 sec, wash under tap H_20, apply a cover slip with 1 drop of mounting fluid and examine under a fluorescent microscope. The Hoechst stain shows up nuclear material. *Mycoplasma* species, if present, will be seen as green dots in the EBVTL cytoplasm, around the nuclei. Bacterial nuclei may also be seen, around the EBVTL.

Storage of cells under liquid nitrogen

- Cells should only be stored once infection has been excluded.
- The freezing process is structured to allow a gradual temperature decline in order to prevent crystal formation and cell rupture, aiming for 1 °C per min.
- Allow cells to gather at the bottom of a 75 cm^2 flask and discard the supernatant, leaving only about 10 ml at the bottom of the flask.
- Transfer the 10 ml EBVTL-containing medium to a conical tube.
- Top up with culture medium to 15 ml and centrifuge for 10 min at 110 xg. Discard the supernatant, add 5 ml culture medium and repeat centrifugation.

- Again discard the supernatant and suspend EBVTL in 7 ml freezing medium consisting of Dulbecco's modified Eagle's medium with 20% Fetal Calf Serum and 10% glycerol.
- 1 ml aliquots are placed into cryotubes.
- Place cryotubes in the nalgene freezing container in the presence of 250 ml propyl alcohol at -80 °C for at least 4 h.
- Finally, the cryotubes may be transferred to the -180 °C freezer and stored under liquid nitrogen.
- Thawing, in contrast to freezing, is conducted rapidly by placing an EBVTL-containing cryotube in H_20 at 40 °C immediately after removal from the liquid nitrogen. Following this, the 1ml of EBVTL-containing medium is added to 5ml of culture medium which has been warmed to 37 °C and pre-equilibrated with CO_2 for a few h. After 3 days, the culture may be continued in the usual way.

APPENDIX F

Bradford (Bio-Rad) protein assay

(Bradford 1976, Bio-Rad Protein Assay package insert)

Principle

Binding of protein to Coomassie Brilliant Blue dye at a constant pH results in a shift in the absorbance from 465 nm to 595 nm. This results in the mixture becoming a deep blue colour. The dye binds to protonated amine groups of the protein in an acidic medium. This method is based on the 'protein error of indicators' principle which relates the hydrophobic interior of proteins to the change in indicator colour. The Beer-Lambert Law is used to calculate the concentration of the sample using a standard curve. It is well known that the Beer-Lambert Law breaks down at a high absorbance (e.g. absorbance > 1.2). Conversely, precision is compromised at an absorbance < 0.1. The standard curve is thus constructed to fall within the linear range. Samples are prepared or diluted appropriately to fall towards the centre of this curve where possible.

Specimen

EBVTL or lymphocyte sonicate in sonication buffer is used. However, this method may be used to determine the protein content of virtually any appropriately diluted fluid with sensitivity.

Five - 50 µl is needed per protein determination, depending on the dilutions made.

Equipment

- Spectrophotometer (Beckman DU 640)
- 2 Flasks
- Funnel
- Vortex mixer
- A selection of pipettes, tips and test tubes
- Cuvette (plastic is suitable)
- Filter paper (Whatman number 1)

Reagents

- Bio-Rad reagent (Bio-Rad Laboratories) containing dye, phosphoric acid and methanol
- Bovine serum albumin 1 mg/ml standard – stored in aliquots at -80 °C
- Reagent grade H_20

Method

Guard against residual glassware contamination by protein as this method is highly sensitive. "Standard" and "microassay" procedures are described in the Bio-Rad package insert. The method described here is a scaled-down version of the "standard" procedure, found to be most convenient.

1. Estimate the final volume of Bio-Rad reagent required.
2. Prepare the Bio-Rad reagent by diluting 1 in 5 with reagent grade H_20. Filter through filter paper placed in a funnel.

3. Prepare standard blank (reagent grade H_20) and 5 bovine serum albumin dilutions in a range of concentrations (as indicated below) in triplicate. The final volume in each tube is 50 µl.
4. Prepare sample blank (using sonication buffer as used in FECH enzyme assay) and sample dilutions in triplicate. The sample blank is diluted in the same way as the sample with H_20 (separate blanking for sample necessary to correct for any background absorbance from buffers present in sample and not in standard). The final volume in each tube is 50 µl.
5. To each blank, standard and sample add 2.5 ml diluted Bio-Rad reagent. Vortex, avoiding foaming, and allow to stand.
6. Read absorbance at 595 nm after 5 min and within 1 h. Blank on the standard blank and record absorbances thereafter.

Results

An example of standards, blanks and one sample (sample A) is presented in Table 9 showing dilutions, typical values obtained and standard curve construction (Figure 32) using Microsoft *Excel*.

Table 9: Example of data used to generate sample A protein concentration

Protein conc (mg/ml)	Vol (µl)	H_20 (µl)	Abs1	Abs2	Abs3	Mean abs	Dilution correction factor	Prot conc (mg/L)
Blanked Standards								
Blank	0	50	0			0		-
0.100	5	45	0.1561	0.1634	0.1538	0.1578		100
0.200	10	40	0.3047	0.3099	0.2942	0.3029		200
0.400	20	30	0.5115	0.5148	0.5123	0.5128		400
0.600	30	20	0.7051	0.6920	0.7187	0.7053		600
Sample								
Sample Blank	15	35	0.0094					-
Sample A	15	35	0.4389	0.4478	0.4458	0.4348	50/15	**1113**

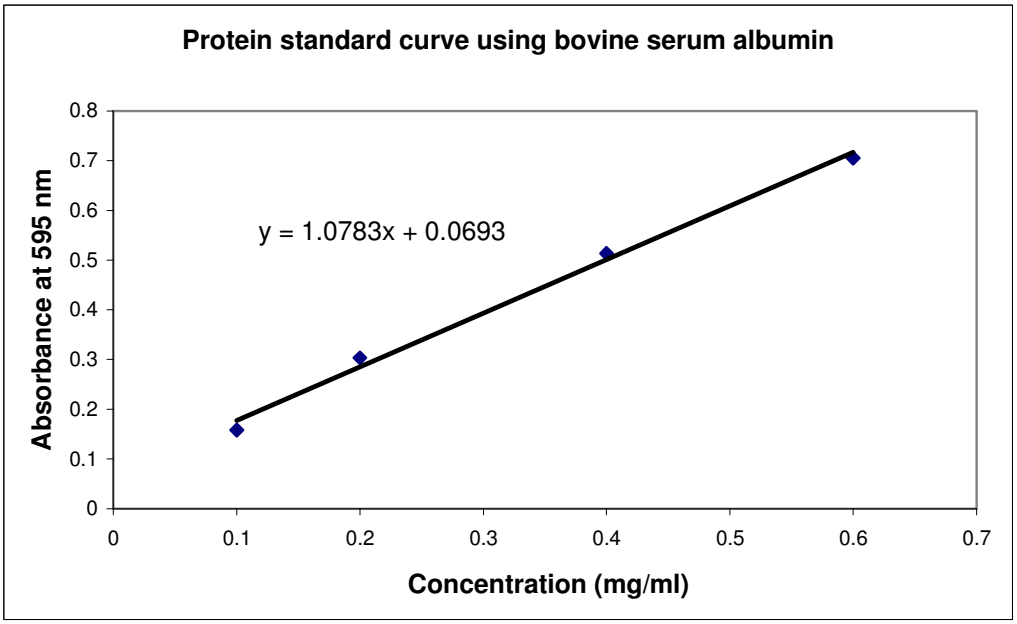

Figure 32: Protein standard curve and derived regression equation

Calculation

The regression equation is shown on the standard curve graph and the following may be derived for this standard curve:

Concentration = (absorbance/1.0783) – 0.0693

The sample is diluted in order to fall within the linear range on the standard curve and to make the final volume up to that of the standard. The initial, undiluted concentration of the sample is the desired parameter. Therefore, correction for sample dilution by means of a dilution correction factor is necessary.

Sample A protein concentration:

= (0.4348/1.0783 – 0.0693) x 50/15 = 1.113 mg/ml protein

= 1113 mg/L protein

APPENDIX G

FECH enzyme assay

(Li et al 1987, Rossi et al 1988, Gouya et al 2006)

Principle

An EBVTL or lymphocyte sonicate is used as source of FECH to quantify enzyme activity by measuring the formation of Zn meso fluorometrically per h per mg of protein at 37 °C.

Sample

EBVTL in tissue culture medium is used. Volume used will depend on EBVTL concentration but generally 10 ml is used. Lymphocytes may also be used: 10 ml of whole blood contains sufficient lymphocytes for assay. Lymphocytes are isolated as described in Appendix E.

Equipment

- Misonix sonicator 3000 (Lasec)
- Fluorescence spectrophotometer 650-10S (Hitachi Koki)
- Spectrophotometer (Beckman DU 640)
- Centrifuge
- Microcentrifuge
- Balance: 5 place (Sartorius Research)

- pH meter
- Magnetic stirrer
- Vortex mixer
- Water bath
- Timer
- A selection of pipettes, tips, 2 ml microcentrifuge tubes, glass tubes and beakers
- 15 ml conical tube
- Glass tubes
- Quartz or glass fluorimetry cell

Reagents

- Tris (Tris(hydroxylmethyl)aminomethane) ($(HOCH_2)_3CNH_2$: MW 121.1)
- Hydrochloric acid (0.1 N, 2.7 N, 5 N HCl solutions)
- Glycerol
- NaCl (0.9%)
- Triton X-100
- Palmitic acid ($CH_3(CH_2)_{14}$ COOH: MW 256.4)
- Mesoporphyrin IX dihydrochloride ($C_{34}H_{40}N_40_2.Cl_2$: MW = 639.62) (Frontier Scientific, catalogue number M566-9, 100 mg)
- Zn^{2+} mesoporphyrin IX ($C_{34}H_{36}N_4O_4Zn$: MW = 630.06) (Frontier Scientific, catalogue number M-40628, 25 mg)
- Zinc acetate Zn ($[CH_3COO]_2.2H_20$: MW 219.5)
- DMSO ($(CH_3)_2SO$)
- Methanol (CH_3OH)
- Reagent grade H_20

Preparation of solutions / buffers

1. Sonication buffer

A 50 mmol/L Tris buffer at pH 7.6 with 20% glycerol is prepared as follows:

- Dissolve 606 mg Tris in 60 ml reagent grade H_20
- pH to 7.6 with 5 N HCl
- Add 20 ml glycerol
- Add reagent grade H_20 to a final volume of 100 ml in a volumetric flask.

2. Enzyme sonicate

- Centrifuge suspension of EBVTL in culture medium in a conical tube at 170 xg for 10 min.
- Pour off culture medium. Suspend and mix pellet carefully in 10 ml 0.9% NaCl and centrifuge as before. Repeat once.
- Finally suspend the pellet in 800 µl sonication buffer.
- Cool lymphoblast suspension on ice.
- Sonicate suspension for 20 sec with a microprobe at 3 watt.
- Cool sonicate again on ice.

The sonicated enzyme preparation is stable at 4 °C for 24 h. In the case of heavy EBVTL growth, it is preferable to perform the protein assay (see Appendix F) prior to the enzyme assay. This allows appropriate sonicate dilutions to be made. The assay is linear up to 1000 mg/L protein (Rossi et al 1988) and 200 – 600 mg/L was used during the investigations described here.

The sonication buffer is used as blank during the enzyme assay.

3. Incubation buffer

A 250 mmol/L Tris solution with 1% Triton X-100 and 1.46 mmol/L palmitic acid is prepared as follows:

- Dissolve 1 ml Triton X-100 and 3029 mg Tris in 20 ml H_20 and mix well.
- Add 37.4 mg palmitic acid and sonicate liberally until macroscopically dissolved. Magnetically stir for 1hr. Dissolving the palmitic acid is slow and is aided by the high pH and Triton-X concentration before adjusting the pH and volume. The final reaction palmitic acid concentration is 0.76 mmol/L, including the palmitic acid in the reaction buffer and in the mesoporphyrin.
- Add reagent grade H_20 up to 80 ml and pH to 7.6 with 5 N HCl.
- Make up to a final volume of 100 ml with reagent grade H_20 in a volumetric flask.

4. Substrates

a. Mesoporphyrin

Prepare a 0.5 mmol/L solution as follows:

- Carefully weigh out 1 mg of mesoporphyrin and dissolve in 3127 µl incubation buffer. It is easier to weigh out an aliquot of ~ 1 mg, to note its exact mass, and to calculate the volume of buffer to add as follows:

Volume in µl = [(mass in mg)/ (639.62 x 0.5)] x 10^6

- Stir magnetically for 1 h covered by parafilm and tinfoil and verify visually that all mesoporphyrin has dissolved.
- Spectrophotometry may be used to quantitate the mesoporphyrin concentration. The millimolar extinction coefficient for

mesoporphyrin at 399 nm in 0.1 N HCl is 445 L/mmol/cm (Falk 1964):

- Add 980 µl 0.1 N HCl to 20 µl mesoporphyrin.
- Add 200 µl of the above to 1800 µl 0.1 N HCl.
- The total dilution is 1 in 500 (to a concentration of 1 µmol/L).

- Measure absorbance spectrophotometrically at 399 nm, blanking against 0.1 N HCl.

Concentration of mesoporphyrin = (absorbance x 500)/445

b. Zinc

A 1 mmol/L solution is prepared by dissolving 22 mg zinc acetate in 100 ml reagent grade H_20.

5. Stopping solution

Prepare a 30/70 (v/v) solution by adding 30 ml DMSO to 70 ml methanol in a fume hood. Store in a darkened glass bottle. Caution: DMSO is minimally toxic but may penetrate skin, carrying other compounds with it. Gloves are essential. Dispose of this solution in a chemical waste container.

6. Zn meso standard

- Prepare a 0.5 mmol/L solution as follows: carefully weigh out 1 mg of Zn meso and dissolve in 3174 µl stopping solution. It is easier to weigh out an aliquot of ~ 1 mg, to note its exact mass, and to calculate the volume of stopping solution to add as follows:

Volume in µl = [(mass in mg)/ (630.06 x 0.5)] x 10^6

- Stir magnetically for 10 min covered by parafilm and tinfoil.
- Although careful weighing and volume calculation as described above is essential in making up the Zn meso standard accurately, the final concentration of Zn meso is determined spectrophotometrically. For this purpose the mesoporphyrin extinction coefficient in 0.1 N HCl at 399 nm is used after first converting Zn meso to mesoporphyrin by acidification.
    - Use glass tubes for dilutions.
    - Add 50 µl Zn meso solution to 950 µl 2.7 N HCl (1 in 20 dilution).
    - Allow incubation for 10 min covered by parafilm and tinfoil.
    - Add 100 µl of the Zn meso/HCl solution to 2600 µl reagent grade H_2O (1 in 27 dilution).
    - Measure absorbance spectrophotometrically at 399 nm, blanking against 0.1 N HCl.

Concentration of Zn meso = (absorbance x 540)/445

Method

1) Assay

Perform the assay in triplicate. Use 2 ml microcentrifuge tubes (if possible, to aid mixing) and add the following:

Sonicate (diluted if appropriate; sonication buffer for blank)	200 µl
Incubation buffer	200 µl
Mesoporphyrin (0.5 mmol/L)	40 µl

- Preincubate in water bath at 37° C for 5 min.
- Add 20 µl zinc acetate (1 mmol/L) solution and mix.

- Continue incubation in a shaking waterbath at 37 °C for 60 min.
- Terminate the reaction by adding 1000 µl DMSO/methanol stopping solution, up to a final volume of 1460 µl.
- Centrifuge at 13 000 xg in a microfuge for 3 min.
- Transfer 1000 µl supernatant into a quartz or glass fluorimetry cell.
- Measure fluorescence using the following settings:
    - Slit width 5 nm
    - Sensitivity 1
    - Excitation 410 nm
    - Emission 580 nm
    - Fluorescence blanked on the stopping solution
- The stopping solution destroys enzyme activity (and aids porphyrin solubilisation) but does not prevent non-enzymatic autochelation of zinc by mesoporphyrin. Thus, undue delays after addition of the stopping solution until fluorescence measurement should be avoided.

2) Zn meso standard curve construction

- Use the 0.5 mmol/L (500 000 nmol/L) Zn meso solution to prepare a series of dilutions with the stopping solution.
- Use glass tubes.
- Add 100 µl Zn meso to 900 µl stopping solution = 50 000 nmol/L (1 in 10 dilution).
- Add 100 µl 50 000 nmol/L Zn meso to 900 µl stopping solution = 5000 nmol/L (1 in 10 dilution).
- Add 300 µl 5000 nmol/L Zn meso to 4700 µl stopping solution = 300 nmol/L (1 in 16.6 dilution).
- Prepare further dilutions as indicated in Table 10:

Table 10: Dilutions used for Zn meso standard curve

Volume of 300 nmol/L solution (µl)	Volume of stopping solution (µl)	Final Zn meso concentration (nmol/L)
1000	0	300
800	200	240
600	400	180
400	600	120
200	800	60
100	900	30
0	1000	0

- Record fluorescence in RFU.
- Plot RFU against concentration using Microsoft *Excel.*
- A regression equation is derived which allows fluorescence generated during the assay to be related to Zn meso formation.

Results

Typical values recorded during the standard curve construction (Figure 33) are shown in Table 11:

- The centre column shows the Zn meso concentration corrected to the Zn meso concentration as determined spectrophotometrically.
- In this case, the spectrophotometrically determined concentration of the primary Zn meso solution was found to be 0.48 mmol/L (as opposed to the concentration it was made up to of 0.5 mmol/L). The values in the centre column were derived by multiplying the concentration in the left column by (0.48)/ (0.50).

Table 11: Example of data used for Zn meso standard curve construction

Zn meso conc (nmol/L)	Corrected Zn meso conc (nmol/L)	Fluorescence (RFU)
0	0	0
30.0	28.8	133
60.0	57.6	242
120.0	115.2	504
180.0	172.8	745
240.0	230.4	955
300.0	288.0	1184

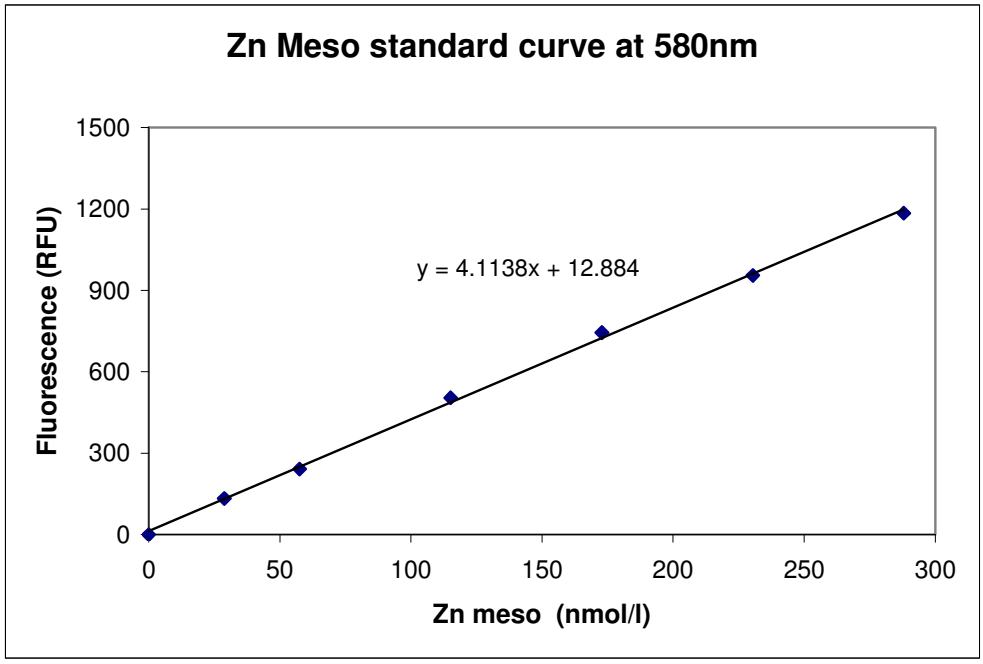

Figure 33: Zn meso standard curve and regression equation

- Example of fluorescence recorded after 1 h of FECH activity at 37 °C :
    - RFU blank = 140
    - RFU_1 sonicate = 600
    - RFU_2 sonicate = 615
    - RFU_3 sonicate = 627
    - Thus RFU_{mean} sonicate = 614

Calculation: example

$$\text{FECH activity} = \frac{\text{nmol Zn meso/L sonicate (nmol/L)}}{\text{protein sonicate (mg/L)} \times \text{time (h)}}$$

ΔRFU = RFU sonicate – RFU blank

= 474

Thus Zn meso formed per h = (474-12.884)/4.1138

= 112.1 nmol/L/h

But the sonicate enzyme activity has been diluted by 1460/200

= dilution factor of 7.3

Thus corrected Zn meso formed = 884.0 nmol/L/h

Protein in sonicate (determined via Bradford method, Appendix F)

= 720 mg/L

And incubation time = 1 h

Thus FECH activity at 37° C = 884.0 (nmol/L/h) / [720mg/L x 1 h]

= 1.23 nmol Zn meso/h/mg protein

APPENDIX H

DNA extraction

using Wizard® Genomic DNA Purification kit (Promega)

(Miller et al 1988, Wizard® Technical Manual)

Principle

Leukocytes are separated from whole blood by centrifugal pelleting after red cell lysis. After separation, the leukocyte nuclei are lysed, releasing DNA. Protein is removed by salt precipitation, the saturated salt solution driving protein out of aqueous solution. The negative charge on the phosphate backbone is capable of keeping DNA in solution under these conditions. The addition of isopropanol causes DNA to precipitate out by excluding water molecules. Finally, 70% ethanol is used to wash away residual salt while maintaining DNA in a precipitated state.

Specimen

Whole blood is used. Conventionally, EDTA anticoagulated samples are used for DNA/RNA studies. The package insert states that heparin and citrate are also acceptable anticoagulants. However, heparin is generally understood to interfere with the PCR and the use of heparin as an anticoagulant in this context was not verified here.

Starting volumes of 20 µl – 10 ml of whole blood may be utilised, provided that appropriate reagent volumes are added.

Equipment

- Vortex mixer
- Microcentrifuge
- Heating block
- A selection of microcentrifuge tubes, dedicated pipettes and filter tips
- Gene Quant II, RNA/DNA Calculator (Pharmacia Biotech)

Reagents

- Wizard® Genomic DNA Purification Kit (Promega) containing Cell Lysis Solution, Nuclei Lysis Solution, Protein Precipitation Solution and DNA Rehydration Solution
- Isopropanol ($CH_3CHOHCH_3$)
- 70% Ethanol (CH_3CH_2OH:H_20::70:30 (v/v))

Precautions

- In view of the sensitivity and the amplification inherent in a PCR reaction, avoidance of contamination is of paramount importance. Working in a DNA extraction area is advised. The most hazardous form of contamination is that of pre-PCR and PCR steps with PCR product.

Method

1. Allow samples to come to room temperature and mix.
2. Add 300 µl whole blood to 900 µl of Cell Lysis Solution in a microcentrifuge tube and mix by inversion.
3. Incubate for 10 min at room temperature.
4. Centrifuge at 16 000 xg for 2 min.
5. Discard supernatant.
6. If red cell contamination is visible in pellet, repeat steps 2-5. Haemoglobin partially inhibits PCR.
7. Vortex pellet.
8. Add 300 µl Nuclei Lysis Solution to the microcentrifuge tube and mix by inversion.
9. Add 100 µl Protein Precipitation Solution to the microcentrifuge tube and vortex for 20 sec.
10. Centrifuge at 16 000 xg for 3 min.
11. Transfer supernatant to a new tube containing 300 µl isopropanol. Mix by inversion. DNA will precipitate as visible strands.
12. Centrifuge at 16 000 xg for 1 min.
13. Discard supernatant.
14. Add 300 µl 70% ethanol to the microcentrifuge tube.
15. Centrifuge at 16 000 xg for 1 min.
16. Discard ethanol and evaporate DNA pellet to dryness for 15 min.
17. Add 100 µl DNA Rehydration Solution.
18. Cap the microcentrifuge tube and incubate for 1 h at 65 °C.
19. Store DNA extract at -20 °C.

DNA quantification

Use the Gene Quant spectrophotometer to quantitate DNA and ascertain DNA purity. This requires ~ 3 µl of DNA solution. A clean capillary tube is essential to obtain accurate results. Blank the instrument on DNA Rehydration Solution.

Nucleic acids have an absorption peak at 260 nm. An absorption coefficient exists (different for DNA and RNA), allowing quantitation. In contrast to DNA, protein has an absorbance peak at 280 nm. A 260:280 nm absorbance ratio of 1.7-2.0 is indicative of good DNA purity (> 80%). A value < 1.7 indicates protein contamination.

Other instruments used to quantify DNA, such as the Nanodrop ND 1000 (Inqaba), allows an additional measurement at 230 nm, resulting in a 260:230 nm absorbance ratio. A 260:230 nm absorbance ratio of 1.8 – 2.2 suggests DNA purity while a value below 1.8 may reflect the presence of impurities such as carbohydrates, salt or phenol which absorb at 230 nm (www.nanodrop.com).

APPENDIX I

Primer design

(Rybicki et al 2001)

Specificity in a non-probe based PCR reaction is critically dependent on primer selection. Primers bind to complementary sequences flanking the sequence to be amplified. The annealing temperature is the temperature at which the primer hybridises to its complementary sequence while the melting temperature (T_m) is that at which it dissociates.

ALAS2 exon 11 primers were designed using Primer Designer for Windows (Soft Packaging version 2, Scientific and Education Software). The sequence was tested using the BLAST (Basic Local Alignment Search Tool) function on NCBI (National Center for Biotechnology Information) Genbank (http://www.ncbi.nlm.nih.gov) to confirm forward and reverse primer specificity. The sequence complementary to the primer did not contain any single nucleotide polymorphisms (SNPs), as verified on Ensembl Human GeneView (http://www.ensembl.org).

General guidelines for primer design

1. Primer length = 17-28 base pairs. Below 17 the annealing temperature is too low and above 28 the benefit of added specificity plateaus.

2. Primer base pair composition = 50-60 % (G+C). This achieves optimal primer hybridisation.

3. The 3' end of the primers should be a G or C, or CG or GC to prevent "breathing" of ends and increase the efficiency of priming.

4. T_m may be calculated: $T_m = 4(G+C) + 2(A+T)\ ^{o}C$. A T_m between 55 and 80 ^{o}C is considered optimal. The T_m of the forward and reverse primer should optimally not differ by more than 3 °C.

5. The optimal annealing temperature will be between 50 and 60 °C and may be determined empirically.

6. Runs of 3 G or C bases at the 3' end may result in mispriming at GC rich sequences (due to stability of annealing) and should be avoided.

7. Complementarity at the 3' end between the forward and reverse primer may result in primer dimer formation in preference to product, and should be avoided.

8. If possible the sequence complementary to the primer should not contain SNP(s) as it may interfere with primer hybridisation. In the case of heterozygosity for a SNP this could result in preferential amplification of one allele (allelic drop-out).

APPENDIX J

PCR for *ALAS2* Exon 11

(GoTaq Flexi DNA Polymerase package insert)

Principle

The PCR amplifies a 417 bp fragment consisting of *ALAS2* exon 11 and flanking intronic sequences. Standard PCR methodology is used.

Sample

Extracted genomic DNA containing ~ 100 ng/µl DNA. Dilute (e.g. <30 ng/µl) template may be used but may result in no or weak amplification. Conversely, over concentrated (e.g. > 400 ng/ul) template may also not amplify.

Equipment

- Robocycler Gradient 40 Thermal Cycler (Stratagene)
- Vortex mixer
- Microcentrifuge
- A selection of microcentrifuge tubes, dedicated pipettes and filter tips

Reagents

- 5X Green GoTaq Flexi Buffer (Promega)
- $MgCl_2$ 25 mmol/L (Promega)
- GoTaq DNA Polymerase (Promega)
- Forward primer diluted to 25 µmol/L in nuclease free H_2O (IDT-Integrated DNA Technologies)
- Reverse primer diluted to 25 µmol/L in nuclease free H_2O (IDT-Integrated DNA Technologies)
- Deoxynucleotide triphosphates (dNTPs) – dATP, dCTP, dTTP, dGTP, 2.5 mmol/L of each in one solution (Promega)
- H_2O nuclease free (Sabax Water for Injection, Adcock Ingram)
- Mineral oil

Method

- Thaw reagents and DNA (except GoTaq DNA Polymerase which is liquid at -20 °C due to glycerol content; minimise its exposure to room temperature).
- Vortex and centrifuge reagents and samples. Brief centrifuging in between steps is a valuable adjunct in decreasing contamination and aiding mixing of reagents. All precautions and risks of contamination alluded to during the description of DNA extraction apply.
- Prepare the reaction mixture shown in Table 12 in a microcentrifuge tube. Increase proportionately depending on the number of samples processed. Include enough for a blank. Mix well.

Table 12: Reaction mixture for PCR reaction.

Number of reactions	Nuclease free H_20	Green Buffer	$MgCl_2$	Forward primer	Reverse primer	dNTP mix	Taq
1	32.8 µl	10 µl	3 µl	1 µl	1 µl	1 µl	0.2 µl

- Pipette 49 µl of the reaction mixture into each PCR microcentrifuge tube. Add 1 µl template, vortex briefly and pulse-centrifuge.
- Overlay with 1 drop of mineral oil (used to prevent evaporation since the thermal cycler does not have a heated lid).
- Transfer to the pre-heated Robocycler. Use a routine program:
  - Initial separation at 95 °C for 1 min — 1 cycle
  - Separation at 95 °C for 30 sec
  - Annealing at 52 °C for 30 sec — 35 cycles
  - Extension at 72 °C for 20 sec
  - Extension at 72°C for 7 min — 1 cycle
  - Cooling at 6°C for 5 min — 1 cycle

Results

PCR products are analysed by gel electrophoresis.

APPENDIX K

Polyacrylamide gel electrophoresis for PCR product visualisation

(Lo et al 2008)

Principle

Double stranded DNA is separated in polyacrylamide under non-denaturing conditions based on size, with high resolution ability. Polyacrylamide is formed by polymerisation of bisacrylamide and acrylamide. Polymerisation is aided by ammonium persulphate-induced free radical generation and catalysed by TEMED (see later). The phosphate backbone of DNA confers a negative charge and migration towards the anode occurs during electrophoresis. Fragment size is primarily a function of the number of base pairs. Shorter fragments travel faster. However, size is also influenced by conformation, e.g. as conferred by heteroduplexes. Ethidium bromide is a positively charged dye that intercalates with double stranded DNA and fluoresces under ultraviolet irradiation, allowing post electrophoresis visualisation of migrated PCR product.

Sample

Ten µl PCR product pipetted from below the mineral oil overlying the PCR reaction

Equipment

- Hoefer vertical electrophoresis unit SE600 Series (Amersham Pharmacia Biotechnology)
- Gel-doc: BTS-20M UVIband version 99 (UVItec)
- Mixing flasks and cylinder
- Selection of pipettes and tips
- Hamilton microsyringe

Reagents

- TEMED solution (tetramethylethylenediamine) $CH_3NCH_2CH_2N(CH_3)_2$
- Ammonium persulphate 10% $(NH_4)_2S_20_8$
- Acrylamide: bisacrylamide solution: 30% acrylamide (60 g) and 0.8% bisacrylamide (1.6 g) up to 200 ml with reagent grade H_20. Caution: acrylamide in the unpolymerised form is carcinogenic.
- 10X TBE buffer: 108 g Tris $((HOCH_2)_3CNH_2)$, 55 g boric acid and 9.3 g EDTA up to 1 L with reagent grade H_20
- Loading dye: 0.25 g bromophenol blue, 40 g sucrose and 4 ml 0.5 mol/L pH 8 EDTA ($C_{10}H_{16}N_2O_8$) solution up to 100 ml with reagent grade H_20
- Ethidium bromide solution. Add 100 µl 1 mg/ml ethidium bromide to 200 ml with reagent grade H_20. Caution: this compound is carcinogenic.
- 100 bp molecular weight marker (Promega). Make a 1:1 dilution of marker with loading dye.
- Reagent grade H_20

Method

1. Clamp 2 glass plates, separated by spacers, together on top of a gel casting stand. This needs to be done securely to prevent gel solution leakage during step 4.
2. Make 4 ml 10X TBE and 8 ml acrylamide: bisacrylamide solution up to 40 ml with reagent grade H_20 in a flask. The final acrylamide concentration is 6%. Add 40 µl TEMED and 400 µl ammonium persulphate and mix. Immediately proceed to step 3 to prevent polymerisation in the flask.
3. Pour the solution between the glass plates prepared in step 1.
4. Insert a 20-spacer comb into the top of the gel.
5. Allow the gel to set for at least 30 min.
6. Gently remove the comb.
7. Fit the top electrophoresis tank on top of the vertical glass-gel unit and fill the tank with 500 ml 1X TBE buffer (add 50 ml 10X TBE to 450 ml reagent grade H_20). Ensure that the electrode is covered by buffer.
8. Prepare samples/blank by adding 10 µl loading dye to 10 µl sample/blank.
9. Load prepared samples using a Hamilton microsyringe. Include 8 µl of 100 bp marker (1:1 dilution with loading dye).
10. Fill the bottom electrophoresis tank with 500 ml of 1x TBE. Carefully position the top tank/gel/glass plate unit into the bottom tank. Place lid on top electrophoresis tank. Connect the electrodes to power pack and run at 270 volt. The signal indicating “circuit complete” indicates that current is flowing through the system. Caution: electrical hazard. Allow the gel to run for ~ 1 h, until the loading dye is ~ 1 cm from the bottom of the gel.
11. Discontinue the electrical supply and remove the glass plate/gel unit. Stain in ethidium bromide for 10 min.

12. Rinse in tap H_2O. Transfer the gel to the Gel-doc photographing apparatus.
13. Photograph gel using ultraviolet light.

Results

A visible sample band on gel electrophoresis indicates amplification. Correlation with the molecular marker and knowledge of the amplicon size, allow confident PCR product identification. The 500 bp marker is brighter than the other marker bands. Absence of a sample band indicates failure of, or very weak, amplification.

Non-specific amplification (usually due to an inappropriate PCR annealing temperature) may be observed. Primer dimer formation, visible at the bottom of the gel due to its small size, may be seen in the blank as a normal phenomenon. No other bands should be seen in the blank lane, and if present, would indicate contamination.

In the case of heterozygosity, heteroduplexes may be observed proximal to the main PCR amplified band.

Amplification resolution on a 6% polyacrylamide gel is in the order of magnitude of a few base pairs. It may further be improved by loading less PCR product, running it for longer or using a higher polyacrylamide concentration.

If a particular mutation creates or abolishes a restriction enzyme site, pre-digestion of a PCR fragment followed by gel electrophoresis as described here, may be used to identify the mutation.

APPENDIX L

PCR product purification for sequencing

(GFX PCR DNA and Gel Band Purification Kit product booklet)

Principle

After confirmation of correct PCR amplification by gel electrophoresis, product is purified prior to sequencing. This excludes shorter DNA fragments (below 50 bp), buffer, primers, protein and dyes. DNA binds selectively to a silica membrane from which contaminants are washed, followed by elution of pure DNA.

Sample

Thirty five µl PCR product

Equipment

- Vortex mixer
- Microcentrifuge
- A selection of microcentrifuge tubes, dedicated pipettes and filter tips
- GFX Microspin Columns and Collection tubes (supplied with GFX PCR DNA and Gel Band Purification Kit, GE Healthcare)
- Gene Quant II, RNA/DNA Calculator (Pharmacia Biotech)

Reagents

(reagents supplied with GFX PCR DNA and Gel Band Purification Kit, GE Healthcare)

- Capture buffer type 2
- Wash buffer type 1
- Elution buffer type 6

Method

1. Add 500 µl Capture buffer type 2 and 35 µl PCR product to microcentrifuge tube, mix and pulse-centrifuge.
2. Place a Microspin column into Collection tube and pipette mixture from step 1 into the column.
3. Centrifuge at 16 000 xg for 2 min.
4. Discard flow through from Collection tube and replace the Microspin column.
5. Add 500 µl Wash buffer type 1 to the Microspin column and centrifuge at 16 000 xg for 2 min. Discard the flow through.
6. Repeat step 5 once.
7. Prepare a microcentrifuge tube by cutting the connection between the tube and lid. Label lid and tube. Place the Microspin column inside the microcentrifuge tube. Discard the Collection tube.
8. Add 30 µl Elution buffer type 6 to the center of membrane in the Microspin column. Incubate for 1 min.
9. Centrifuge at 16 000 xg for 1 min and discard the Microspin column.

10. Store eluate at -20 °C.
11. Quantitate the purified DNA using the Gene Quant spectrophotometer, blanking against Elution buffer type 6.

APPENDIX M

Preparation of samples and primers for sequencing

(Lo et al 2008)

Principle

The Sanger reaction is used to perform a unidirectional PCR using purified PCR product as template. A mixture of primer, dNTPs and fluorescently tagged ddNTPs (dideoxynucleotides – causing chain termination) creates sequences of varying length from which the sequence of the template may be deduced during capillary zone electrophoresis. Either forward or reverse sequences (or both, but not during the same reaction) may be obtained by using the appropriate primer. The Central DNA Sequencing Facility at the University of Stellenbosch has specific requirements for sample and primer preparation before submission.

Method

1. Dilute an aliquot of primer from 25 µmol/L as used during the initial PCR to 1.1 µmol/L. Prepare a clearly labelled microcentrifuge tube containing 10 µl primer and seal with parafilm.
2. Dilute or concentrate (by evaporation on a heating block) purified DNA to 8 ng/µl. Prepare a clearly labelled microcentrifuge tube containing 10 µl purified DNA and seal with parafilm.

APPENDIX N

Concluding letter to family EPP8

UNIVERSITY OF CAPE TOWN

Lennox Eales Porphyria Laboratories
UCT/MRC Liver Research Centre
Dept. of Medicine
K-floor, Old GSH Building
Observatory
7925
Tel: 27-21-406 6206
Fax: 27-21-448 6815
Email: Peter.Meissner@uct.ac.za

13th October, 2008

Dear Sir/Madam

You have participated in a number of studies relating to erythropoietic protoporphyria. We would like to thank you for your willingness to participate, your time and your encouragement.

After years of work by different investigators, both in South Africa and internationally, we have been able to find the porphyria-causing genetic mutation which is relevant to you and your family. A mutation is when a change occurs in the DNA sequence of a gene (there are a variety of potential reasons for such an occurrence), and can therefore be passed on to descendants.

Genes carry information required to produce all of the proteins required by the body, in a sequence of chemical units called 'base pairs'. The mutation we have discovered is a 4 base pair deletion in the gene coding for a protein called ALA synthase. This is a protein involved in haem biosynthesis – haem being required for many diverse functions in the body. ALA synthase is the first (of eight) enzymes in the haem synthetic pathway, and your family mutation leads to an 'overactive' ALA synthase enzyme.

Originally it was thought that your family, like the majority of families with erythropoietic protoporphyria (EPP), had a mutation in the ferrochelatase gene – the gene that encodes the last enzyme in the haem pathway. This is because the clinical presentation and the biochemical features (ie the porphyrin patterns) of EPP and this new type of porphyria are virtually identical.

The type of porphyria you have, we have termed 'X-linked Dominant Protoporphyria'. The ferrochelatase enzyme (although normal) is not able to cope with the increased quantity of porphyrins manufactured by the overactive ALA synthase enzyme. This leads to an accumulation of protoporphyrin in the red cells, and in some cases accumulation of protoporphyrin in the liver may lead to liver disease.

The mutation is carried on the X chromosome as a dominant condition, which means the daughter of an affected male will always inherit the gene mutation and the son of an affected male can never inherit the mutation. Both daughters and sons of an affected female have a 50% chance of inheriting the mutation. (The explanation for this lies in the fact that males carry one X and one Y chromosome, whereas females carry two X chromosomes.) It must be stressed that in the case of this particular mutation we are talking of the chances of inheriting the mutation in the ALA synthase gene – which does not necessarily correlate with the liver disease nor the severity of the condition – these are dependant on other factors which we don't fully understand, nor can we predict. This underscores our strong recommendations that you are regularly monitored by your physician for liver functions. As iron may play a role in this condition it is also advisable that iron levels be monitored and your physician may make some recommendations from time to time, based on these levels.

Please feel free to contact us at any time should you require further information or help. As a reference, the following scientific journal article describes the science behind this type of porphyria:

Whatley SD, Ducamp S, Gouya L, Grandchamp B, Beaumont C, Badminton MN, Elder GH, Holme SA, Anstey AV, Parker M, Corrigall AV, Meissner PN, Hift RJ, Marsden JT, Ma Y, Mieli-Vergani G, Deybach JC, and Puy H. C-Terminal Deletions in the ALAS2 Gene Lead to Gain of Function and Cause X-linked Dominant Protoporphyria without Anemia or Iron Overload. The American Journal of Human Genetics 2008; 83:1-7

Yours sincerely

Dr Carel Haumann
Registrar
Clinical Pathology NHLS AND UCT

Dr Mark Sonderup
Consultant
Department of Medicine UCT and Groote Schuur Hospital, UCT/MRC Liver Research Centre

Prof Peter Meissner
Head Porphyria Laboratories and co-Director UCT/MRC Liver Centre
HOD, UCT Division of Medical Biochemistry

References

Allen RC, Zoghbi HY, Moseley AB, Rosenblatt HM, Belmont JW. Methylation of Hpall and Hhal Sites near the polymorphic CAG repeat in the human androgen receptor gene correlates with X chromosome inactivation. American Journal of Human Genetics 1992;51:1229-1239

Allikmets R, Raskind WH, Hutchinson A. Mutation of a putative mitochondrial iron transporter gene (ABC7) in X-linked sideroblastic anemia and ataxia (XLSA/A). Human Molecular Genetics 1999; 8:743-749

Anderson KE, Sassa S, Bishop D, Desnick RJ. Disorders of heme biosynthesis: X–linked sideroblastic anaemia and the porphyrias. In: Scriver CR, Beaudet AL, Sly WS, Valle D (editors). The metabolic and molecular basis of inherited disease, 8th edition. New York: McGraw Hill, 2000:2961-3062

Anstey AV, Hift RJ. Liver disease in erythropoietic protoporphyria: insights and implication for management. Gut 2007;56(7):1009-1018

Aplin C, Whatley SD, Thompson P,Hoy T, Fisher P, Singer C, Lovell CR, Elder GH. Late-Onset Erythropoietic Porphyria Caused by a Chromosome 18q Deletion in Erythroid Cells. The Journal of Investigative Dermatology 2001;117(6):1647-1649

Astner I, Schulze JO, van den Heuvel J, Jahn D, Schubert WD, Heinz DW. Crystal structure of 5-aminolevulinate synthase, the first enzyme of heme biosynthesis, and its link to XLSA in humans. EMBO Journal 2005;24:3166-3177

Bharati A, Badminton MN, Whatley SD, O'Brien DV, Bell HK. Late-onset erythropoietic protoporphyria in association with haematological malignancy. Clinical and Experimental Dermatology 2006;31:668-670

Bird AG, Britton S, Ernberg I, Nilson K. Characteristics of Epstein-Barr virus activation of human B lymphocytes. Journal of Experimental Medicine 1981;154:832-839

Bishop DF, Kitchen H, Wood WA: Evidence for erythroid and nonerythroid forms of δ-aminolevulinate synthase. Archives of Biochemistry and Biophysics 1981;206:380-391

Bishop DF, Henderson AS, Astrin KH. Human delta-aminolevulinate synthase: assignment of the housekeeping gene to 3p21 and the erythroid specific gene to the X chromosome. Genomics 1990;7:207-214

Bottomley SS, Muller-Eberhard U. Pathophysiology of heme synthesis. Seminars in Hematology 1988;25:282-302

Bloomer J, Bruzzone C, Zhu L, Scarlett Y, Magness S, Brenner D. Molecular defects in ferrochelatase in patients with protoporphyria requiring liver transplantation. Journal of Clinical Investigation 1998;102:107-114

Bloomer JR, Hill HD, Kools AM. Heme synthesis in protoporphyria. Current Problems in Dermatology 1991;20:135-147

Bloomer JR, Morton KO. A radiochemical assay for haem synthase activity. Enzyme 1982,20:220-231

Bradford M. A rapid and sensitive method for the quantification of microgram quantities of proteins utilizing the principles of dye binding. Annals of Biochemistry 1976;72:248-254

Brancaleoni V, Di Pierro E, Tavazzi D, Cappelini MD. C – terminal deletions in the ALAS2 gene and X-linked dominant protoporphyria. Porphyrins and Porphyrias Abstracts 2009; Abstract P03

Camadro JM, Labbe P. Purification and properties of ferrochelatase from the yeast *Saccharomyces cerevisiae.* The Journal of Biological Chemistry 1988;263(24):11675-11682

Chen TR. Mycoplasma contamination detection in cell cultures using fluorescent Hoechst 33258 stain. Experimental Cell Research 1977; 104:255-256

Chen W, Dailey HA, Paw BH. Ferrochelatase forms and oligomeric complex with mitoferrin-1 and Abcb10 for erythroid heme biosynthesis. Blood 2010; 116(4): 628-630

Chu CY, Rana TM. Small RNAs: Regulators and guardians of the genome. Journal of Cellular Physiology 2007;213:412-419

Coceani F, Kelsey L, Seidlitz E, Marks GS, McLaughlin BE, Vreman HJ. Carbon monoxide formation in the ductus arteriosus in the lamb: implications for the regulation of muscle tone. British Journal of Pharmacology 1997;120:599-608

Cooperman SS, Meyron-Holtz EG, Olivierre-Wilson H, Ghosh MC, McConnell JP, Rouault TA. Microcytic anemia, erythropoietic protoporphyria, and neurodegeneration in mice with targeted deletion of iron-regulatory protein 2. Blood 2005;106:1084-1089

Cox TC, Bawden MJ, Martin A, May BK. Human erythroid 5-aminolevulinate synthase: promoter analysis and identification of an iron-responsive element in the mRNA. The EMBO Journal 1991;10:1891-1892

Cox TC, Sadlon TJ, Schwarz QP, Matthews CS, Wise PD, Cox LL, Bottomley SS, May BK. The major splice variant of human 5-aminolevulinate synthase-2 contributes significantly to erythroid heme biosynthesis. The International Journal of Biochemistry & Cell Biology 2004;36:281-295

Crooks DR, Ghosh MC, Haller RG, Tong WH, Rouault TA. Posttranslational stability of the heme biosynthetic enzyme ferrochelatase is dependent on iron availability and intact iron-sulfur cluster assembly machinery. Blood 2010; 115(4): 860-868

Dailey HA, Dailey TA, Wu CK. Ferrochelatase at the millennium: structures, mechanisms and [2Fe-2S] clusters. Cell Molecular Life Science 2000; 57:1909-1926

Dailey HA, Fleming JE. Bovine ferrochelatase. Kinetic analysis of inhibition by N-methylprotoporphyrin, manganese and haem. Journal of Biological Chemistry 1983;258:11453-11459

Dalyot N, Fibach E, Ronchi A, Rachmilewtiz EA, Ottolenghi S, Oppenheim A. Erythropoietin triggers a burst of GATA-1 in normal human erythroid cells differentiating in tissue culture. Nucleic Acids Research 1993;21(17):4031-4037

Day RS, Pimstone NR, Eales L. The diagnostic value of blood plasma porphyrin methyl ester profiles produced by quantitative TLC. International Journal of Biochemistry 1978;9(12):897-904

Deacon AC, Elder GH. Front line tests for the investigation of suspected porphyria. Journal of Clinical Pathology 2001;54:500-507

Deacon A, Whatley SD, Elder GH. Porphyrins and Disorders of Porphyrin Metabolism. In: Burtis CA, Ashwood ER, Bruns DE (editors). Tietz Fundamentals of Clinical Chemistry, 6th edition. St Louis: Saunders Elsevier, 2008:527-538

Eales L, Day RS, Pimstone NR. Protoporphyrin (proto)-determined hepatopathy in a South African jewish family. Annals of Clinical Research 1978;10:205-213

Elbert BL, Bunn HF. Regulation of the erythropoietin gene. Blood 1999;94: 1864-1877

Falk JR. Porphyrins and metalloporphyrins. Amsterdam: Elsevier, 1964:231-246

Ferreira GC. Ferrochelatase. International Journal of Biochemistry and Cell Biology 1999;31:995-1000

Finch C. Regulators of iron balance in humans. Blood 1994;84:1697-1702

Fingeroth, JD, Weiss JJ, Tedder TF, Strominger JL, Biro PA, Fearon DT. Epstein-Barr virus receptor of human B lymphocytes is the C3d receptor CR2. Proceedings of the National Academy Sciences of USA 1984;81:4510-4514

Furuyama K, Sassa S. Interaction between succinyl CoA synthase and the heme-biosynthetic enzyme ALAS-E is disrupted in sideroblastic anemia. Journal of Clinical Investigation 2000;105:757-764

Ganz T, Olbina G, Girelli D, Nemeth E, Westerman M. Immunoassay for human serum hepcidin. Blood 2008;112(10):4292-4297

Goldsmith JR, Landaw SA. Carbon monoxide and human health. Science 1968;162:1352-1359

Goodwin RJ, Kell WJ, Laidler P. Photosensitivity and acute liver injury in myeloproliferative disorder secondary to late-onset protoporphyria caused by deletion of a ferrochelatase gene in hematopoietic cells. Blood 2006;107:60-62

Gouya L, Martin-Schmitt C, Robreau AM, Austerlitz F, Da Silva V, Brun P, Simonin S, Lyoumi S, Grandchamp B, Beaumont C , Puy H, Deybach JC. Contribution of a Common Single-Nucleotide Polymorphism to the Genetic Predisposition for Erythropoietic Protoporphyria. The American Journal of Human Genetics 2006;78:1-14

Gouya L, Puy H, Robreau AM, Bourgeois M, Lamoril J, Da Silva V, Grandchamp B, Deybach JC. The penetrance of dominant erythropoietic porphyria is modulated by expression of wildtype *FECH*. Nature genetics 2002; 30: 27-28

Guo B, Phillips JD, Yu T, Leibold EA. Iron regulates the intracellular degradation of iron-regulatory protein 2 by the proteosome. The Journal of Biological Chemistry 1995;270(21):621-645

Handschin C, Lin J, Rhee J, Peyer AK, Chin S, Wu PH, Meyer UA, Spiegelman BM. Nutritional Regulation of Hepatic Heme Biosynthesis and Porphyrin through PGC-1α. Cell 2005;122:505-515

Harigae H, Furuyama K, Kimura A, Neriishi K, Tahara N, Kondo M, Hayashi N, Yamamoto M, Sassa S, Sasaki T. A novel mutation of the erythroid-specific δ-aminolaevulinate synthase gene in a patient with X-linked sideroblastic anaemia. British Journal of Haematology 1999; 106:175-177

Hart D, Piomelli S. Simultaneous quantitation of zinc protoporphyrin and free protoporphyrin in erythrocytes by acetone extraction. Clinical Chemistry 1981;27(2):220-222

Hastka J, Lasserre JJ, Schwarzbeck A, Strauch M, Hehlmann R. Zinc protoporphyrin in anemia of chronic disorders. Blood 1993;81:1200-1204

Heinemann IU, Jahn M, Jahn D. The biochemistry of heme biosynthesis. Archives of Biochemistry and Biophysics 2008;474:238-251

Hift RJ, Davidson BP, van der Hooft C, Meissner DM, Meissner PN. Plasma fluorescence scanning and faecal porphyrin analysis for the diagnosis of variegate porphyria: precise determination of sensitivity and specificity with detection of protoporphyrinogen oxidase mutations as a reference standard. Clinical Chemistry 2004;50:915-923

Holme SA, Worwood M, Anstey AV, Elder GH, Badminton MN. Erythropoiesis and iron metabolism in dominant erythropoietic protoporphyria. Blood 2007;110:4108-4110

Huang MLH, Becker EM, Whitnall M, Rahmanto YS, Ponka P, Richardson DR. Elucidation of the mechanism of mitochondrial iron loading in Friedreich's ataxia by analysis of a mouse mutant Proceedings of the National Academy of Sciences USA 2009; 106(38): 16381 - 16386

Hurley JH, Lee S, Prag G. Ubiquitin binding domains. Biochemistry Journal 2006;399:361-372

Hvidberg V, Maniecki MB, Jacobsen C, Højrup P, Møller HJ, Moestrup SK. Identification of the receptor scavenging hemopexin-heme complexes. Blood 2005;106:2572-2579

Ishikawa H, Kato M, Hori H, Ishimori K, Kirisako T, Tokunaga F, Iwai K. Involvement of heme regulatory motif in heme-mediated ubiquitinisation and degradation of IRP2. Molecular Cell 2005;19: 171-181

Israels LG, Israels ED. Heme synthesis and Porphyrin metabolism. In: Mechanisms in Hematology, 3rd edition. Winnipeg: Core Health Sciences Inc, 2002:123-131

Karr SR, Dailey HA. The synthesis of murine ferrochelatase *in vitro* and *in vivo*. Biochemistry Journal 1988;254(3)799-803

Keel S, Doty RT, Yang Z, Quigley JG, Chen J, Knoblaugh S, Kignsley PD, De Domenico I, Vaughn MB, Kaplan J, Palis J, Abkowitzi JL. A heme export protein is required for red blood cell differentiation and iron homeostasis. Science 2007;319:825-828

Key NS, Rank JM, Freese D. Hemolytic anemia in protoporphyria: possible precipitating role of liver failure and photic stress. American Journal of Hematology 1992;39:202-207

Killisch I, Steinlein P, Romisch K, Hollinshead R, Beug H, Griffiths G. Characterization of early and late endocytic compartments of the transferrin cycle: transferrin receptor antibody blocks erythroid differentiation by trapping the receptor in the early endosome. Journal of Cell Science 1992;103:211-232

Klausner RD, Rouault TA, Harford JB. Regulating the fate of mRNA: the control of cellular Iron metabolism. Cell 1993;72:19-28

Kubota T, Nonoyama S· Tonoki H, Masuno M, Imaizumi K, Kojima M, Wakui K, Shimadzu M, Fukushima Y. A new assay for the analysis of X-chromosome inactivation based on methylation-specific PCR. Human Genetics 1999;104:49-55

Lamola AA, Yamane T. Zinc protoporphyrin in the erythrocytes of patients with lead intoxication and iron-deficiency anemia. Science 1947;186: 936-938

Landefeld C, Whatley S, Rößler S, Habeck JO, Stauch Th, Beck JF, Kentouche K, Stölzel U. Blood transfusion related iron overload leading to highly significant biochemical and histological improvement of liver cirrhosis in a patient with X-linked Dominant Protoporphyria. Porphyrins and Porphyrias Abstracts 2009; Abstract 008 & P02

Langer EE, Haining RG, Labbe RF, Jacobs P, Crosby EF, Finch CA. Erythrocyte Protoporphyrin. Blood 1972;40:112-128

Lathrop JP, Timko MP. Regulation by heme of mitochondrial protein transport through a conserved amino acid motif. Science 1993; 259:522-525

Leimberg MJ, Prus E, Konijn AM, Fibach E. Macrophages function as a ferritin iron source for cultured human erythroid precursors. Journal of Cellular Biochemistry 2008;103(4):1211-1218

Li FM, Lim CK, Peters TJ. An HPLC assay for rat liver ferrochelatase activity. Biomedical Chromatography 1987;2:164-168

Lim HW. Pathophysiology of Cutaneous Lesions in Porphyrias. Seminars in Hematology 1989;26(2):114-119

Lo YMD, Chiu RWK, Wittwer CT, Kusukawa N. Nucleic Acids. In: Burtis CA, Ashwood ER, Bruns DE (editors). Tietz Fundamentals of Clinical Chemistry, 6th edition. St Louis: Saunders Elsevier, 2008:263-285

Lyoumi S, Abitbol M, Andrieu V, Henin D, Robert E, Schmitt C, Gouya L, de Verneuil H, Deybach JC, Montagutelli X, Beaumont C, Puy H. Increased plasma transferrin, altered body iron distribution and microcytic hypochromic anemia in ferrochelatase deficient mice. Blood 2007;109:811-818

Mahoney JJ, Vreman HJ, Stevenson DK, Van Kessel AL. Measurement of carboxyhemoglobin and total hemoglobin by five specialized spectrophotometers (CO-oximeters) in comparison with reference methods. Clinical Chemistry 1993;39:1693-1700

Maines MD. Zinc protoporphyrin is a selective inhibitor of heme oxygenase activity in the neonatal rat. Biochimica et Biophysica Acta 1981; 673:339-350

Mathews CK, van Holde KE. Metabolism of nitrogenous compounds. In: Biochemistry. Redwood City: The Benjamin/Cummings Publishing Company Inc, 1990:670-703

Marinkovic D, Zhang X, Yalcin S,1 Luciano JP, Brugnara C, Huber T, Ghaffari S. FOXO3 is required for the regulation of oxidative stress in erythropoiesis. Journal of Clinical Investigation 2007;117(8):2133-2144

Meissner P, Adams P, Kirsch R. Allosteric inhibition of human lymphoblast and purified PBG-deaminase by protoporphyrinogen and coproporphyrinogen. Journal of Clinical Investigation 1991;91:1436-1444

Meissner PN, Day RS, Moore MR, Disler PB, Harley E. Protoporphyrinogen oxidase and porphobilinogen deaminase in variegate porphyria. European Journal of Clinical Investigation 1986;16:257-261

Meyer UA, Schuurmans MM, Lindberg RLP. Acute Porphyrias: Pathogenesis of Neurological Manifestations. Seminars in Liver Disease 1998; 18(1): 43-52

Miller G, Lipman M. Release of infectious Epstein-Barr virus by transformed Marmoset Leukocytes. Proceedings of the National Academy of Sciences USA 1973;70(1):190-194

Miller IJ, Bieker JJ. A novel erythroid cell-specific murine transcription factor that binds to the CACCC element and is related to the Kruppel family of nuclear proteins. Molecular and Cellular Biology 1993;13:2776-2786

Miller SA, Dykes DD, Polesky HF. A simple salting out procedure for extracting DNA from human nucleated cells. Nucleic Acids Research 1988;16(3):1215

Nordmann Y. Erythropoietic protoporphyria and hepatic complications. Journal of Hepatology 1992;16:4-6

Nuez B, Michalovich D, Bygrave A, Ploemacher R, Grosveld F. Defective haematopoiesis in fetal liver resulting from inactivation of the EKLF gene, Nature 1995;375:316-318

Onaga Y, Ido A, Uto H, Hasuike S, Kusumoto K, Moriuchi A, Numata M, Nagata K, Hori T, Hayashi K, Tsubouchi H. Hypermethylation of the

wild-type ferrochelatase allele is closely associated with severe liver complication in a family with erythropoietic protoporphyria. Biochemical and Biophysical Research Communications 2004; 321:851-858

Peyssonaux C, Zinkernagel AS, Schuepbach RA, Rankin E, Vaulont S, Haase VH, Nizet V, Johnson RS. Regulation of iron homeostasis by the hypoxia-inducible transcription factors (HIFs). The Journal of Clinical Investigation 2007;117(7):1926-1932

Parker M, Corrigall AV, Hift RJ, Meissner PN. Molecular Characterisation of Erythropoietic Protoporphyria in South Africa. British Journal of Dermatology 2008;159(1):182-191

Philips JD, Kushner JP. Fast track to the porphyrias. Nature Medicine 2005;11(10):1049-1050

Piomelli S, Lamola AA, Poh-Fittzpatrick MF, Seamen C, Harber LC. Erythropoietic protoporphyria and lead intoxication: the molecular basis for difference in cutaneous photosensitivity. I. Different rates of disappearance of protoporphyrin from the erythrocytes, both in vivo and in vitro. Journal of Clinical Investigation 1975;56:1519-1527

Pitula JS, Deck KM, Clarke SL, Anderson SA, Vasanthakumar A, Eisenstein RS. Selective inhibition of the citrate-to-isocitrate reaction of cytosolic aconitase by phosphomimetic mutation of serine-711. Proceedings of the National Academy of Sciences USA 2004;101(30):10907-10912

Poh-Fitzpatrick MB. A plasma porphyrin fluorescence marker for variegate porphyria. Archives of Dermatology 1980;116(5):543-547

Poh-Fitzpatrick MB. Erythropoietic Protoporphyria. Seminars in Dermatology 1986;5:88-105

Ponka P. Tissue specific regulation of iron metabolism and heme synthesis: distinct control mechanisms in erythroid cells. Blood 1997;89:1-25

Ponka P, Beaumont C, Richardson DR. Function and regulation of transferrin and ferritin. Seminars in Hematology 1998;35:35-54

Ponka P, Neuwirt J, Borova J. The use of exogenous δ-aminolevulinic acid for the studies of the regulation of haem synthesis in rabbit reticulocytes. Biochimica et biophysica acta 1973;304(1):123-131

Ponka P, Schulman HM: Regulation of heme synthesis in erythroid cells: Hemin inhibits transferrin iron utilization but not protoporphyrin synthesis. Blood 1985;65(4):850-857

Porra RJ, Jones OT. Studies on ferrochelatase.1. Assay and properties of ferrochelatase from a pig-liver mitochondrial extract. Biochemical Journal 1963;87:181-185

Puy H, Gouya L, Deybach JC. Porphyrias. Lancet 2010; 375: 924-937

Rademakers LH, Koningsberger JC, Sorber CW, Baart de la Faille H, Van Hattum J, Marx JJ. Accumulation of iron in erythroblasts of patients with erythropoietic protoporphyria. European Journal of Clinical Investigation 1993;23:130-138

Risheg H, Chen FP, Bloomer JR. Genotypic determinants of phenotype in North American patients with erythropoietic protoporphyria. Molecular Genetics and Metabolism 2003;80:196-206

Rimington C, Cripps DJ. Biochemical and fluorescence-microscopy screening-tests for erythropoietic protoporphyria. Lancet 1965;1:624-626

Rodgers PA, Vreman HJ, Dennery PA, Stevenson DK. Sources of carbon monoxide (CO) in biological systems and applications of CO detection technologies. Seminars in Perinatology 1994;18:2-10

Rossi E, Costin KA, Garcia-Webb P. Ferrochelatase activity in human lymphocytes, as quantified by a new high-performance liquid-chromatographic method. Clinical Chemistry 1988;34(12):2481-2485

Rybicki EP. PCR Primer Design and Reaction Optimisation. In: Coyne VE, M James MD, Reid SJ, Rybicki EP (editors). Molecular Biology Techniques Manual. University of Cape Town, 3rd edition, 2001

Rufenacht UB, Gouya L, Schneider-Yin X. Systematic analysis of molecular defects in the ferrochelatase gene from patients with erythropoietic

protoporphyria. American Journal of Human Genetics 1998;62:1341-1352

Sadlon TJ, Dell'Oso T, Surinya KH, May BK. Regulation of erythroid 5-aminolevulinate synthase expression during erythropoiesis. The International Journal of Biochemistry & Cell Biology 1999;31:1153-1167

Sassa S. Modern diagnosis and management of the porphyrias. British Journal of Hematology 2006;135:281-292

Sassa S, Zalar GL, Poh-Fitzpatrick MB, Anderson KE, Kappas A. Functional evidence for a partial deficiency of ferrochelatase activity in mitogen-stimulated lymphocytes from a patient with erythropoietic protoporphyria. Journal of Clinical Investigation 1982;69:809-815

Schranzhofer M, Schrifrer M, Cabrera JA, Kopp K, Chiba P, Beug H, Mullner, EW. Remodelling the regulation of iron metabolism during erythroid differentiation to ensure efficient heme biosynthesis. Blood 2006;107:4159-4167

Shaw GC, Cope J, Li L, Corson K, Hersey C, Ackermann GE, Gwynn B, Lambert AJ, Wingert RA, Traver D, Trede NS, Barut BA, Zhou Y, Minet E, Donovan A, Brownlie A, Balzan R, Weiss MJ, Peters LL, Kaplan J, Zon LI, Paw BH. Mitoferrin is essential for erythroid iron assimilation. Nature 2006_a;440:96-100

Shaw GC, Langer NB, Wang Y, Li L, Kaplan J, Bloomer JR, Paw BH. Abnormal expression of Human Mitoferrin is associated with a variant of Erythropoietic Protoporphyria. Blood ASH Annual Meeting Abstracts 2006_b;108:Abstract 3

Smith A. Transport of tetrapyrroles: mechanisms and biological and regulatory consequences. In: Dailey HA (editor). Biosynthesis of Heme and Chlorophylls. New York: McGraw-Hill, 1990:435-490

Solis C, Martinez-Bermejo A, Naidich TP, Kaufmann WE, Astrin KH, Bishop DF. Acute intermittent porphyria: studies of the severe homozygous

dominant disease provide insights into the neurologic attacks in acute porphyrias. Archives of Neurology 2004;61(1):1764-1770

Sonderup M, Haumann C, Davidson B, Corrigall A, Meissner M. Response to intravenous iron therapy in two patients with X-linked dominant protoporphyria. Porphyrins and Porphyrias Abstracts 2009; Abstract 007

Surinya KH, Cox TC, May BK. Transcriptional regulation of the human erythroid 5-aminolevulinate synthase gene. Journal of Biological Chemistry 1997;26:585-594

Taketani S, Adachi Y, Nakahashi Y. Regulation of the expression of human ferrochelatase by intracellular iron levels. European Journal of Biochemistry 2000;267:4685-4692

Taketani S, Kakimoto K, Ueta H, Masaki R, Furukawa T. Involvement of ABC7 in the biosynthesis of heme in erythroid cells: interaction of ABC7 with ferrochelatase. Blood 2003;101(8):3274-3280

Taketani S, Tokunaga R. Rat liver ferrochelatase. The Journal of Biological Chemistry 1981;256(24)12748-12753

Theil EC. Iron-responsive element (IRE) family of mRNA regulators. Regulation of iron transport and uptake in animals, plants and microorganisms. Metal Ions in Biological Systems 1998;35:403-434

Thorley-Lawson DA. Epstein-Barr virus: exploiting the immune system. Nature Reviews Immunology 2001;1:75-82

Todd DJ. Erythropoietic protoporphyria. British Journal of Dermatology 1994; 131:751-766

van der Westhuyzen DR, Coetzee GA, Demasius IPC, Harley EH, Gevers W, Baker SG, Seftel HC. Low density lipoprotein receptor mutations in South African homozygous familial hypercholesterolemic patients. Arteriosclerosis 1984;4(3):238-247

Vreman HJ, Stevenson DK. Heme oxygenase activity as measured by carbon monoxide production. Annals of Biochemistry 1988;168:31-38

Whatley SD, Ducamp S, Gouya L, Grandchamp B, Beaumont C, Badminton MN, Elder GH, Holme SA, Anstey AV, Parker M, Corrigall AV, Meissner PN, Hift RJ, Marsden JT, Ma Y, Mieli-Vergani G, Deybach JC, Puy H. C-terminal deletions in the *ALAS2* gene lead to gain of function and cause X-linked dominant protoporphyria without anemia or iron overload. The American Journal of Human Genetics 2008;83:1-7

Weiss G, Houston T, Kastner S, Johrer K, Grunewald K, Brock JH. Regulation of cellular iron metabolism by erythropoietin: activation of iron-regulatory protein and upregulation of transferrin receptor expression in erythroid cells. Blood 1997;89(2):680-687

Zhao W, Kitidis C, Fleming MD, Lodish HF, Ghaffari S. Erythropoietin stimulates phosphorylation and activation of GATA-1 via the PI3-kinase/AKT signaling pathway. Blood 2006;107(3):907-915